SPRINGER BRIEFS IN MATERIALS

Giuseppe Chirico
Mykola Borzenkov
Piersandro Pallavicini

Gold Nanostars
Synthesis, Properties and Biomedical Application

Springer

SpringerBriefs in Materials

More information about this series at http://www.springer.com/series/10111

The SpringerBriefs Series in Materials presents highly relevant, concise monographs on a wide range of topics covering fundamental advances and new applications in the field. Areas of interest include topical information on innovative, structural and functional materials and composites as well as fundamental principles, physical properties, materials theory and design. SpringerBriefs present succinct summaries of cutting-edge research and practical applications across a wide spectrum of fields. Featuring compact volumes of 50 to 125 pages, the series covers a range of content from professional to academic. Typical topics might include • A timely report of state-of-the art analytical techniques • A bridge between new research results, as published in journal articles, and a contextual literature review • A snapshot of a hot or emerging topic • An in-depth case study or clinical example • A presentation of core concepts that students must understand in order to make independent contributions Briefs are characterized by fast, global electronic dissemination, standard publishing contracts, standardized manuscript preparation and formatting guidelines, and expedited production schedules.

Giuseppe Chirico • Mykola Borzenkov
Piersandro Pallavicini

Gold Nanostars

Synthesis, Properties and Biomedical Application

Springer

Giuseppe Chirico
Department of Physics
University of Milano-Bicocca
Milano, Italy

Mykola Borzenkov
Department of Physics
University of Milano-Bicocca
Milan, Italy

Piersandro Pallavicini
Department of Chemistry
University of Pavia
Pavia, Italy

ISSN 2192-1091 ISSN 2192-1105 (electronic)
SpringerBriefs in Materials
ISBN 978-3-319-20767-4 ISBN 978-3-319-20768-1 (eBook)
DOI 10.1007/978-3-319-20768-1

Library of Congress Control Number: 2015944064

Springer Cham Heidelberg New York Dordrecht London

Printed on acid-free paper

Springer International Publishing AG Switzerland is part of Springer Science+Business Media (www.springer.com)

Preface

Gold nanoparticles are nowadays used in high-technology applications such as organic photovoltaics, sensory probes, therapeutic agents, drug delivery in biological and medical applications, electronic conductors, and catalysis due to their unique properties. Among the various types of gold nanoparticles gold nanostars (GNS) feature two or more localized surface plasmon resonances (LSPR) that undergo thermal relaxation when irradiated. Moreover, at least one LSPR falls in the near-IR (NIR) range where tissues and blood are semitransparent making them attractive prospects for medicine and biology. The research groups at the Department of Chemistry (University of Pavia) and Department of Physics (University of Milano-Bicocca) have developed their own research field devoted to preparation, functionalization, and further application of these types of gold nanoparticles. In this brief we summarize the most essential information about GNS. Special emphasis has been given to the application of GNS and GNS-based systems to medicine and biology.

Milano, Italy — Giuseppe Chirico
Milano, Italy — Mykola Borzenkov
Pavia, Italy — Piersandro Pallavicini

Acknowledgments

The authors would like to express their gratitude to the all current and former members of corresponding research groups of the University of Milano-Bicocca and the University of Pavia for their strong support and cooperation.

Contents

About the Authors

Giuseppe Chirico is full professor in Applied Physics at the University of Milano-Bicocca. His main research interests are fluorescence correlation spectroscopy in solution and on cells, photon correlation spectroscopy, and metal nanoparticles for biomedical application.

Mykola Borzenkov received his Ph.D. in Organic Chemistry at Lviv Polytechnic National University (Lviv, Ukraine). At present time M. Borzenkov is a research assistant at Department of Physics at the University of Milano-Bicocca (Milan, Italy). His main research fields are synthesis and application of functional surface-active monomers, polymers of biomedical applications, synthesis, functionalization, and biomedical application of metal nanoparticles.

Piersandro Pallavicini is associate professor in General and Inorganic Chemistry at the University of Pavia. His main research interests are chemistry of nanoparticles and coordination compounds, fluorescent-labeled gold nanoparticles, and application of metal nanoparticles.

Introduction

Gold nanoparticles (GNP) are one of the most widely employed classes of metal nanoparticles due to a wide range of unique properties [1]. These include optical, electronic properties, and the possibility to be coated with diverse compounds providing the opportunities to be used in different technological applications [1–3]. The optical and electronic properties of gold nanoparticles are based on the presence of localized surface plasmon resonance (LSPR) and can be tuned by changing the size, shape, surface chemistry, or aggregation state of GNP [2]. Moreover, GNP can bind functional groups like amine and thiol groups, allowing surface modification and their use in biomedical applications [4, 5]. Therefore, different molecules such as drugs, siRNA, DNA, and proteins have been coupled with GNP for biomedical applications ranging from in vitro biosensing to in vivo cancer treatments [6]. The interactions of gold nanoparticles with cells have been developed and help now to engineer highly effective nanomaterial-based tools for diagnostics and therapeutics [7]. Plasmonic GNPs, whose extinction cross sections fall at near-infrared (NIR) frequencies, are excellent candidates as multifunctional agents for image-guided therapies based on localized hyperthermia. This is a noninvasive approach to cancer treatment, in which biological tissues are exposed to higher than normal temperatures to promote the selective destruction of abnormal cells [8]. For example, Halas et al. studied the feasibility of nanoshell-assisted photothermal therapy [9]. This technique takes advantage of the strong near-infrared absorption of gold nanoshells. This simple, noninvasive procedure showed great promise as a technique for selective photothermal tumor ablation.

The plasmonic behaviors of the gold nanostructures are strongly dependent on their surrounding media as it was shown in the previous publications [10–12].

Within different classes of existing GNP, nonspherical gold nano-objects have been the subject of hundreds of papers over last years. The anisotropy of nonspherical GNP is the source of the plasmon absorption in the NIR region in addition to plasmon absorption in the visible region. This NIR absorption is especially sensitive to the GNP shape and medium and can be shifted toward the part of the NIR region in which living tissue shows minimum absorption [3]. Moreover, a fluctuation in the

scattering polarization and intensity caused by gold nanoparticles anisotropy are also considered as important aspect in biosensing application.

Gold nanostars (GNS) and in general multibranched gold nano-objects have also received particular attention [13]. The key explanation of this is compared to the other shapes, nanostars can dramatically enhance the reflected light. GNS may hold the promise for new approaches in biomedical application, namely in medical diagnoses and sensing assays. Branched or star-shaped gold nanoparticles have been proposed for sensing applications on account of their huge surface-enhanced Raman spectroscopy (SERS) enhancement factors, and to a lesser extent as catalysts [14]. They feature two or more localized surface plasmon resonances with an intense band in the NIR range (650–1100 nm) and a weaker band at 500–550 nm [15]. It was shown that when laser irradiated at the resonance of the NIR band of the GNS exhibits excellent transduction of absorbed light into heat [16]. GNS may thus be excellent tools for nanomedicine, exploiting the 700–1000 nm transparent window of biological matter for through-tissue photothermal treatments [14]. Besides the photothermal therapy due to LSPR location of GNS the ability to attach a big range of molecules gives a promising opportunity to use them as nanosensors and targeted drug delivery platforms. Moreover, the ease of surface functionalization displayed by GNS would allow to change their charge and hydrophobicity and, therefore, enhance their efficiency for the treatment of superficial diseases [17].

It is worth to say that sensitivity of GNS can be further increased by linking GNS to other plasmonic nanoparticles and thereby inducing the creation of hot spots [18].

Neutral or slightly negative surface charge of GNS can be a key feature in reducing toxicology issues in their in vivo application and make them promising issues for application of hyperthermia therapy [17].

Therefore, this survey provides the most important information on GNS as promising biotechnological and biomedical tools. This review focuses on synthesis of GNS (Chap. 1) and functionalization with organic molecules, and physical properties of GNS including fluorescence quenching and Raman enhancement (Chap. 2). Moreover, the application of GNS for biofilms, nanosensing, thermal treatments, and delivery systems is described (Chap. 3). Finally, the information about interaction of GNS with cells is provided (Chap. 4).

References

1. Huang X, El-Sayed M (2010) Gold nanoparticles: optical properties and implementations in cancer diagnosis and photothermal therapy. J Adv Res 1:13–28
2. Daniel MC, Astruc D (2004) Gold nanoparticles: assembly, supramolecular chemistry, quantum-size-related properties, and application toward biology, catalysis, and nanotechnology. Chem Rev 104:293–346
3. El-Sayed IH, Huang X, El-Sayed M (2005) Surface Plasmon resonance scattering and absorption of anti-EGFR antibody conjugated gold nanoparticles in cancer diagnostics: application in oral cancer. Nano Lett 5:829–834

4. Jain S, Hirst DG, O'Sullvian JM (2012) Gold nanoparticles as novel agents for cancer therapy. Br J Radiol 85:101–113
5. Shukla R, Bansal V, Chaudhary M, Basu A, Bhonde RR, Sastry M (2005) Biocompatibility of gold nanoparticles and their endocytotic fate inside the cellular compartment: a microscopic overview. Langmuir 21:10644–10654
6. Saha K, Agasti SS, Kim C, Li X, Rotello VM (2012) Gold nanoparticles in chemical and biological sensing. Chem Rev 112:2739–2779
7. Xie N, Lin Y, Mazo M, Chiappini C et al (2014) Identification of intracellular gold nanoparticles using surface-enhanced Raman scattering. Nanoscale 6:12403–12407
8. van der Zee J (2002) Heating the patient: a promising approach? Ann Oncol 13:1173–1184.
9. O'Neal DP et al (2004) Photo-thermal tumor ablation in mice using near infrared-absorbing nanoparticles. Cancer Lett 209:171–176
10. Ye J, van Dorpe P (2012) Plasmonic behaviors of gold dimmers perturbed by a single nanoparticles in the gap. Nanoscale 4:7205–7211
11. Wen F et al (2012) Plasmon transmutation: inducing new modes in nanoclusters by adding dielectric nanoparticles. Nano Lett 12:5020–5026
12. Yang X et al (2014) Au nanoparticles on ultrathin MoS2 sheets for plasmonic organic solar cells. J Mater Chem A 2:14798–14806
13. Casu A, Cabrini E at al (2012) Controlled synthesis of gold nanostars by using zwitterionic surfactant. Chemistry 18:9381–9390
14. Rodriguez-Lorenzo L et al (2010) Surface enhanced Raman scattering using star-shaped gold colloidal nanoparticles. J Phys Chem C 114:7336–7340
15. Pallavicini P, Dona A et al (2013) Triton X-100 for three-plasmon gold nanostars with two photothermally active NIR (near IR) and SWIR (short-wavelength IR) channels. Chem Commun 49:6265–6267
16. Freddi S, Sironi L et al (2013) A molecular thermometer for nanoparticles for optical hyperthermia. Nanoletters 13:2004–2010
17. Chirico G, Pallavicini P, Collini M (2014) Gold nanostars for superficial diseases: a promising tool for localized hyperthermia? Nanomedicine 9:1–3
18. Shiohara A et al (2014) Plasmon modes and hot spots in gold nanostars-satellite clusters. J Phys Chem B. doi:10.1021/jp509953f

Chapter 1
Gold Nanostar Synthesis and Functionalization with Organic Molecules

Piersandro Pallavicini, Elisa Cabrini, and Mykola Borzenkov

Abstract This chapter is devoted to the synthesis and functionalization of gold nanostars. The physical-chemical characterization and singular features of gold nanostars with respect to other types of gold nanoparticles are provided. Various methods of GNS synthesis as well as of the functionalization of GNS with PEG, organic dyes, and bioactive compounds are discussed.

Keywords Gold nanostars • Seeded growth process • PEGylation • Fluorescence • Bioactive molecules

Before starting the review, Table 1.1 summarizes the information collected in this chapter.

1.1 Gold Nanoparticle Synthesis: Brief Introduction

A brief survey of the general techniques of GNP synthesis is required before we can analyze the different approaches to the gold nanostar synthesis.

The chemical reduction of transition metal salts in the presence of stabilizing agents with the subsequent generation of zerovalent metal colloids in aqueous or organic media is one of the most common and powerful synthetic methods in this field [1]. The simplest and by far the most commonly used protocol for the preparation of gold nanoparticles is the aqueous reduction of gold salt by sodium citrate at reflux [1, 2]. Generally, GNPs are synthesized in a liquid by reduction of chloroauric acid ($HAuCl_4$). During this process Au^{3+} ions are reduced to neutral gold atoms, the solution becomes supersaturated, and gold gradually starts to precipitate in the

P. Pallavicini • E. Cabrini
Department of Chemistry, University of Pavia, Viale Taramelli 12, Pavia 27100, Italy

M. Borzenkov (✉)
Department of Physics, University of Milano-Bicocca, Piazza Della Scienza 3, Milan 20216, Italy
e-mail: mykola.borzenkov@unimib.it

G. Chirico et al., *Gold Nanostars*, SpringerBriefs in Materials,
DOI 10.1007/978-3-319-20768-1_1

Table 1.1 Synthesis and functionalization of gold nanostars (summary of this chapter)

Synthesis of GNS	• In situ methods • Seed growth methods • Non-"seed-mediated" method • One-pot methods • Electron beam lithography technique
Functionalization of GNS	• PEGylation of GNS • Functionalization with dyes • Functionalization with DNA, proteins, aptamers, etc.

form of sub-nanometer particles [1, 3]. In general, the preparation process of GNP by chemical reduction contains two steps: (1) reduction using agents such as borohydrides, aminoboranes, hydrazine, formaldehyde, hydroxylamine, saturated and unsaturated alcohols, citric and oxalic acids, polyols, sugars, hydrogen peroxide, sulfites, carbon monoxide, hydrogen, acetylene, and monoelectronic reducing agents including electron-rich transition-metal sandwich complexes, and (2) stabilization by agents such as trisodium citrate dihydrate, sulfur ligands (in particular thiolates), phosphorus ligands, nitrogen-based ligands (including heterocycles), oxygen-based ligands, dendrimers, polymers, and surfactants [4]. The particle size depends on a large number of parameters; for example it can be controlled by the initial reagent concentrations [1, 3].

The preparation of GNP by reduction of $HAuCl_4$ and citrate-stabilized gold nanoparticles has been regarded as the most popular one for a long time, since their introduction by Turkevich [5]. The $HAuCl_4$ solution is boiled, and the trisodium citrate dihydrate is then quickly added under vigorous stirring. After a few minutes, the wine-red colloidal suspension is obtained, and the GNP size is about 20 nm [4, 5]. This technique was improved later by Frens, who obtained a broad size range of gold nanoparticles (from 15 to 150 nm) by controlling the trisodium citrate to Au ratio [2]. Nowadays the "in situ" Turkevich-Frens method has been further improved for reproducible preparation of citrate-stabilized gold nanoparticles [6–9].

The two-phase Brust-Schiffrin method, published in 1994, was the first method that allows to prepare the thiolate-stabilized gold nanoparticles via in situ synthesis using $NaBH_4$ as reduction agent, since it met great success [4, 10]. This method is performed in ambient conditions with relative high stability of the resulting GNPs. This method is suitable for obtaining particles in organic solvents. The GNPs are stabilized by relatively strong Au-S bonds and their diameters are in the 2–5 nm range, with the size much smaller than that of Turkevich [4]. Later this technique was improved by various research groups introducing thiolate-liganded gold nanoparticles [11–13].

The seed growth method is another popular technique for GNP synthesis. Compared with the in situ synthesis, the seed growth method enlarges the particles step by step, and it is easier to control the sizes and shapes of resulted gold nanoparticles. Therefore, this method is widely used in the most recent size- and shape-controlled GNP syntheses. Generally this process involves two steps. In the first step, small-size

AuNP seeds are prepared. In the second step, the seeds are added to a "growth" solution containing $HAuCl_4$ and the stabilizing and reducing agents. The newly reduced Au^0 grows on the seed surface starting from small gold crystals to form then large-size AuNPs. The reducing agents used in the second step are always mild ones that reduce Au^{3+} to Au^0 only in the presence of Au seeds as catalysts; thus the newly reduced Au^0 can only assemble on the surface of the Au seeds, and no new particle nucleation occurs in solution [4]. The initial procedures of preparation of GNP by seed growth were modified by El-Sayed using hexadecyltrimethylammonium bromide (CTAB) as the stabilizer instead of citrate [14]. These Au seeds with a diameter smaller than 4 nm were used to promote the narrow dispersity of GNP. GNPs with various shapes have been synthesized using the seed growth method [14].

1.2 Synthesis of Gold Nanostars

1.2.1 General Characterization of Gold Nanostars

As it has been already mentioned the optical properties of gold nanoparticles are of the great importance for application in various fields, especially for biomedical purposes. For anisotropic GNP it has been demonstrated that the presence of sharp edges and tips provides a very high sensitivity to local changes in the dielectric environment, as well as larger enhancements of the electric fields around the nanoparticles [15]. These features constitute the basis of LSPR- and surface enhancement Raman scattering (SERS)-based detections [16]. Hence, besides the main synthetic techniques described previously, an increasing number of synthetic routes are being developed, aiming at a simultaneous control of the size and shape of gold nanoparticles. Therefore, nonspherical gold nanoparticle synthesis has been the subject of numerous publications recently.

Among the various types, gold nanostars and in general multibranched gold nanoparticles have received much attention [17, 18]. Star-shaped GNPs have plasmon bands that are tunable into the NIR region, and the structure contains multiple sharp branches that act as "lightning rods" to greatly enhance the local EM field. The fabrication of gold nanostars has been driven by the interest on the LSPR response to the environment. This is particularly connected to GNS that display sharp tips and edges, where light can be highly concentrated [18, 19], and their structure is shown in Scheme 1.1. GNS colloids display two wide but distinct LSPR features including an intense band typically centered around 650–900 nm and a weaker band/shoulder located at ca. 500–600 nm [18]. When laser irradiated at the wavelength of their NIR band, GNS exhibit excellent transduction of absorbed light into heat [20]. Therefore, these types of gold nanoparticles could serve as effective tools for nanomedicine application. Moreover, nanostars display stronger SERS activity than spheres or even rods [21].

The following subchapter is devoted to the overview of different strategies of synthesis of different types of multibranched gold nanoparticles (see Scheme 1.1).

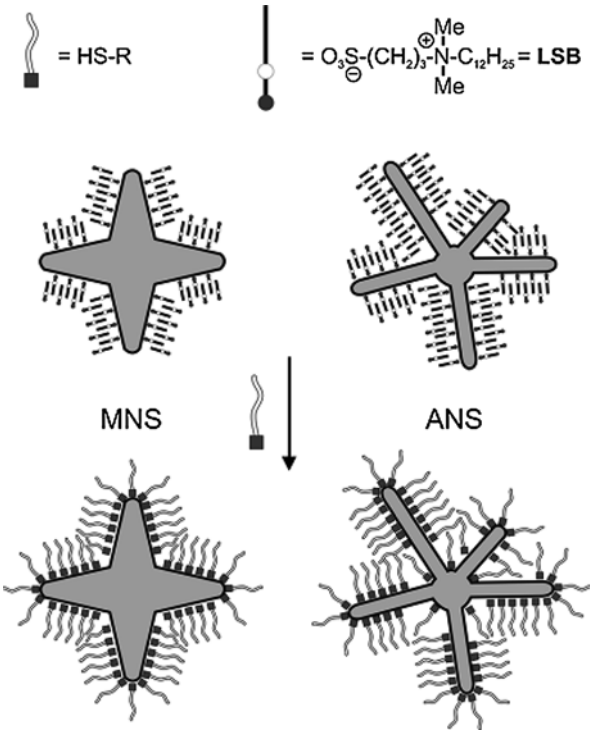

Scheme 1.1 The schematic structures of monocrystalline GNS (MNS) and penta-twinned asymmetric GNS (ANS) obtained by seed growth method assisted by the LSB surfactant. Protective surfactant and thiolated layers are also shown (reproduced from Casu et al. [17])

1.2.2 Synthesis of Gold Nanostars: An Overview of Synthetic Strategies

A wide variety of synthetic methods is available for the preparation of anisotropic gold nanoparticles with narrow size and shape distribution, and with specific branching degree. The choice of one or another of these preparative methods for star-shaped GNP depends on a number of relevant experimental parameters that determine the nucleation and growth steps of the particle synthesis, providing fine control over size and degree of branching of the nanoparticles [18, 22]. Both in situ and seed growth methods have been proposed during last 10 years for the synthesis of GNS. A recent review by Liz-Marzan et al. summarizes various synthetic approaches, optical properties, and application of GNS [18].

The most common method of GNS synthesis adopts seeded growth process, also widely employed for the synthesis of gold nanorods [14]. This process involves the reduction of chloroauric acid with ascorbic acid at ambient temperature on pre-synthesized gold nanoseeds and in the presence of surfactants (in most cases CTAB) [18, 23, 24]. These capping agents (surfactants or polymers) have preferential adsorption on certain crystalline facets of the metal seeds and have been claimed to trigger

the anisotropic growth process, through alteration of the growth rates along specific crystallographic directions [25]. It was shown for example that addition of $AgNO_3$ at different stages of nanocrystal growth increases the degree of control of the shape for penta-twinned gold nanoparticles [26]: penta-branched gold nanocrystals were obtained with sizes ranging from 70 to 350 nm and comprising single-crystalline tips with {111} outer faces. This study allowed not only to control the final nanostar morphology, but also to increase dramatically the yield of branched particles. In 2004 Murphy and coworkers studied the influence bromide ions by replacing CTAB with its chloride equivalent (CTAC) and adding different amounts of NaBr to achieve a better control over bromide concentration [24].

The nature of reducing agent was also studied. For example, in the paper published in 2006 in *Nanotechnology*, hydroxylamine sulfate was used in the preparation of polycrystalline-branched gold nanoparticles with sizes ranging from 47 nm up to 185 nm in a stepwise growth approach [27]. It has been reported that highly branched nanoparticles can be obtained upon addition of $HAuCl_4$ in the presence of 15 nm poly(vinylpyrrolidone) (PVP)-coated gold seeds, when the concentration of PVP in solution is high [28]. This process can be performed at room temperature in very short time. It was also observed that no significant changes in size and shape of nanostars were induced by changing the molecular weight of PVP. A simple one-step synthesis protocol for stable gold nanostars was recently reported [29], based on the reduction of a gold precursor in a basic environment using hydroxylamine as a reducing agent. These star-shaped gold nanostructures showed a higher amplification of the Raman scattering of rhodamine 6G molecules relative to spherical nanoparticles of the same dimension.

Khoury and Vo-Dinh reported in 2008 the controlled synthesis of high-yield gold nanostars ranging from 45 to 116 nm [30]. GNS were synthesized by extending the protocol reported by Liz-Marzan et al. [15], in order to enable size control of the stars from approximately 45 to 116 nm in size. This size range translates to tuning capabilities of the longitudinal plasmon peak in the NIR region from around 725 to over 850 nm. The authors used 20 nm PVP-coated gold seeds in ethanol and investigated the growth of GNS as a function of time during the synthesis by monitoring the spectrum of the GNS suspension and by imaging stars' morphological changes over time via TEM. As it was stated previously most nanostar synthesis requires the use of a surfactant (e.g., CTAB or PVP). In the paper published in *Nanotechnology* in 2012 [31] Khoury and coworkers presented a new, surfactant-free synthesis method of biocompatible gold nanostars with adjustable geometry that allows to tune the plasmon band into the near-infrared (NIR) region "tissue diagnostic window," which is most suitable for in vivo imaging [31]. Nanostars were prepared by a seed-mediated growth method within 1 min in high yield without the use of the toxic surfactant. To obtain nanostars of similar sizes and concentrations but of different geometries, authors investigated multiple factors, including pH, stirring speed, and concentration ratios of $AgNO_3$, ascorbic acid, $HAuCl_4$, and seed. In general, nanostars synthesized under lower pH, moderate vortexing speed, and ascorbic acid/$HAuCl_4$ ratio of 1.5–2 produced the most red-shifted plasmon.

Osinkina et al. reported a two-step approach for the fabrication of quasi-hexagonal ordered arrays of star-shaped gold nanoparticles for SERS spectroscopy by a combination of block-copolymer micelle nanolithography and electroless deposition [32]. Arrays of single-gold nanoparticles were fabricated by block-copolymer micelle nanolithography. Gold nanostars were prepared by incubating the samples in an aqueous solution of CTAB, gold (III) chloride hydrate, ascorbic acid, and silver nitrate. In a second paper published in 2013, GNS with tunable morphology were synthesized by a seed-mediated growth method using poly(diallyldimethylammonium chloride) as stabilizer [33]. The number and length of the branches of the nanostars can be controlled by adjusting the amount of silver nitrate. In a similar approach Chirea in a paper published in *Catalysts* in 2013 described gold nanostars (≈70 nm tip-to-tip distance) synthesized by seed-mediated method and covalently self-assembled on 1,5-pentanedithiol-modified electrodes [34]. The average core diameters and tip length of the GNS were 50 and 19 nm. These gold nanostars displayed two surface plasmon bands: a dominant broad feature at the edge of the visible range (≈837 nm). The cores produce instead a surface plasmon band at 545 nm. Kereselidze et al. developed the synthesis protocol for 180–300 nm GNS by means of a silver-seed-mediated method [35, 36]. Highly multibranched gold nanostars were also obtained at room-temperature synthesis assisted by deep-eutectic solvents (DES). DES is an ionic solvent composed of a mixture of quaternary ammonium salts with hydrogen donors, which shows a melting point much lower than that of the individual components. The advantages of DES-mediated synthesis are the high viscosity, polarity, thermal stability, ease of preparation, and low cost of the products. In addition, DES forms a highly structured "supramolecular" solvent, because of the extended hydrogen-bond network in the liquid state. The concentration of the ascorbate ions and the presence of water in the solution were found to have a profound influence on the formation of branches [37]. Stassi et al. investigated the relationship between the particle diameter, the protuberance size and shape, and the easiest and cost-effective reaction conditions. The corresponding gold nanostars were prepared by mild reduction of $HAuCl_4 \cdot 3H_2O$ with L-ascorbic acid in the presence of DES, prepared from choline chloride and urea in a 1:2 mixture.

Interesting methods of GNS synthesis were developed by Pallavicini et al. By replacing CTAB with the zwitterionic lauryl sulfobetaine (LSB) surfactant in the classical seed growth synthesis, monocrystalline gold nanostars and penta-twinned gold asymmetric nanostars were obtained instead of nanorods [17]. The main product under all synthetic conditions was asymmetric nanostars, which have branches with high aspect ratios, thus leading to LSPR absorptions in the 750–1150 nm range. The position of their LSPR absorption can be tuned up simply by regulating the concentration of reductant, the concentration of surfactant, or the concentration of the "catalytic Ag^+" cation. A growth mechanism that involves the direct contact of the sulfate moiety of LSB on the surface of the nano-object was proposed, thereby implying preferential coating of the {111} Au faces with weak interactions. Another benefit of using LSB surfactant instead of CTAB is that CTAB is cytotoxic and strongly bound to GNP. Therefore, the removal or substitution of

CTAB from GNP surface could be tricky or incomplete. In the next paper of the same research group published in 2013 five-branched gold nanostars were obtained using nonionic Triton X-100 surfactant in a seed growth synthesis [38]. The synthesized nanoparticles have the uncommon feature of two intense localized LSPRs in the NIR range 600–900 and 1100–1600 nm, besides the common visible LSPR ranges. Au nanoseeds were generated from $AuCl_4$ by means of $NaBH_4$ in the solutions of high surfactant concentration (0.05–0.15 M). The absorption spectra of growth solutions obtained in 0.05 M Triton X-100 and TEM images of resulted GNS are shown in Scheme 1.2.

Nehl et al. described the fabrication of GNS by a modified seed-mediated, surfactant-directed synthesis based on reduction of gold chloride [39]. This method was modified by means of different seed particles or by increasing the growth rate.

Feldmann and coworkers reported instead a water-based, non-"seed-mediated" GNS synthesis [40] method with high yield. This method allows to change the number and size of the spikes and the overall size of the particles, and hence to tune

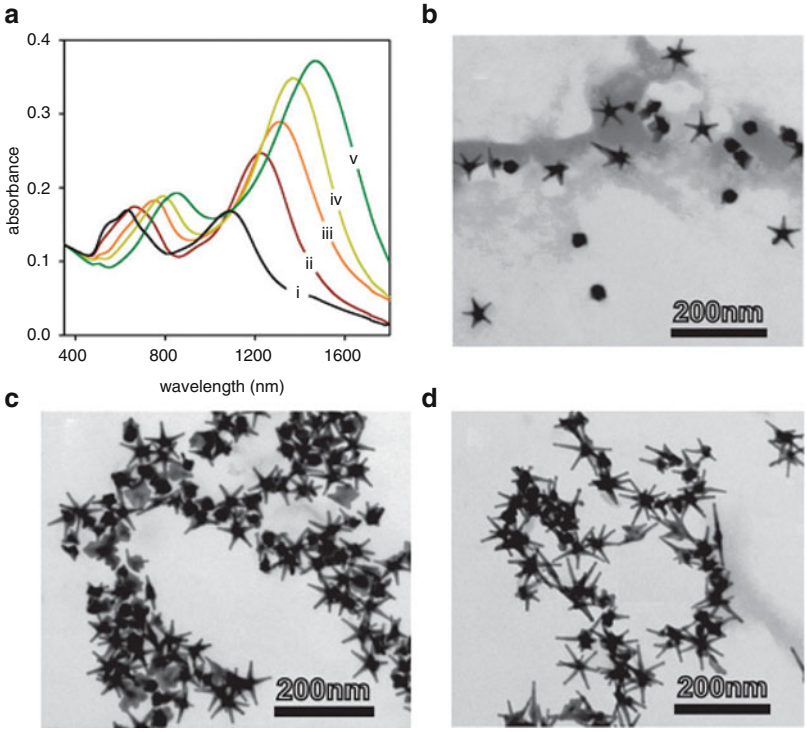

Scheme 1.2 (**a**) Absorption spectra of growth solutions obtained in 0.05 M od Triton X-100 and increasing concentration of ascorbic acid: (1) 1.576 10^{-3} M; (2) 1.773 10^{-3} M; (3) 2.364×10^{-3} M; (4) 2.758×10^{-3} M; (v) 3.152×10^{-3} M. (**b**) TEM image of GNS obtained from the solution of spectrum (1). (**c**) The same from the solution of spectrum (3). (**d**) The same from the solution of spectrum (5) (reproduced from Pallavicini et al. [38])

the localized surface plasmon resonances of the particles over the broad spectral range in the visible and NIR. CTAB was employed as the capping and growth-regulating agent.

One-pot methods of preparation of gold nanoparticles involve the direct preparation of the precursor solution in the presence of suitable reducing agents and surfactants at room temperature by means of a variety of reactant concentration and reaction times [18, 41]. Various one-pot syntheses to produce gold nanostars have been developed recently [15, 18]. These protocols are based on the use of the "green" chemical *N*-2-hydroxyethylpiperazine-*N*-2-ethanesulfonic acid used as reducing and stabilizing agent. Thus, three-dimensional branched nanocrystals with 1–8 tips as well as flower-like gold nanoparticles with twinned tips were obtained in high yield [42, 43]. Examples of one-pot method of preparation of GNS assisted by surfactants and capping agents were also reported: star-shaped gold nanoparticles were obtained by reduction with ascorbic acid in the presence of PVP [44]. However, in this case star-shaped nanoparticles (7 %) and tripod or regular triangular plates (4 %) were observed among a large amount of spherical particles (89 %) including distorted or aggregated ones. In a different approach polydisperse branched GNPs were obtained with high yield using hydrogen peroxide and sodium citrate as reducing agents in combination with bis(*p*-sulfonatophenyl) phenylphosphine dehydrate dipotassium as stabilizer [45]. Very recently Hegmann and coworkers described a simple one-pot silver-assisted synthesis of GNS that employs $AgNO_3$ and a mild reducing agent, ascorbic acid, in the presence of a lyotropic liquid crystal (LLC) template formed by Triton X-100 in water either in the hexagonal phase or the micellar phase [46]. The LLC template is found to assist in the formation of well-defined nanostars with long, twinned thorns and provides the necessary colloidal stability that prevents the final nanostars from irreversible aggregation. The length of the thorns on the nanostars can be tailored by controlling the Au/Ag ratio in the growth solution. By using aminosugars, a series of multipodal gold nanostructures has been obtained via a one-pot chemical reduction method in aqueous solution and at room temperature [47]. The size and shape of these nanoparticles were controlled either by adjusting the amount of reducing agent or by quenching the reaction at a given time.

Other alternative methods of preparation of GNS have been reported. Notably, an electrochemical method was implemented in a two-electrode cell in which the electrochemical reduction of $HAuCl_4$ was carried out in the presence of PVP and NaOH [48]. Basic values of pH were essential to produce branched gold nanoparticles. The shape control could also be achieved by using a template-directed synthesis, where the template comprised a three-dimensional porous lattice of uniform iron nanoparticles [49].

The fabrication of GNS arrays by means of electron beam lithography, in which the plasmon resonance energy can be tuned via the nanostar size from the visible into the NIR region, was also reported [50]. In a second publication of the same research group plasmonic nanostar-dimers, decoupled from the substrate, have been fabricated by combining electron-beam lithography and reactive-ion etching techniques [51]. The 3D architecture, the sharp tips of the nanostars, and the sub-10 nm gap size promote the formation of giant electric field in highly localized hot spots.

1.3 Functionalization and Coating Approaches of GNS

Gold nanoparticles are widely used as sensing, targeting, imaging, and delivery nanobioplatforms. For these applications, surface functionalization with suitable ligands is essential to ensure particle stability against aggregation and for targeting approaches [52, 53]. Various conjugation methods of gold nanoparticles with biomolecules have been developed for specific targeting, for drug delivery, and for sensing assays [53]. Finely tuned surface functionalization of the nanoparticles, which determines their interaction with the environment, is required [54]. These interactions ultimately affect the colloidal stability of the particles, and may yield to a controlled assembly or to the delivery of nanoparticles to a target. The surface of GNS can be functionalized similar to all other gold nanostructures. However, the high shape anisotropy adds specific features to their surface decoration. Thus, in this subchapter the functionalization approaches of GNS with various organic molecules are reviewed.

1.3.1 PEGylation of GNS

For various applications of gold nanoparticles, PEGylation is one of the most widely used functionalization strategies as it has numerous advantages. Polyethylene glycol (PEG) is known to reduce reticuloendothelial system uptake and increase circulation time versus uncoated counterparts, by reducing the nonspecific binding of proteins as well as their cytotoxicity [55]. PEGylation is now commonly used to coat different kinds of nanoparticles, in order to improve their stability under physiological conditions and biocompatibility [55]. PEG enhances in vitro stability of nanoparticles in saline buffers or culture media and it allows the coated nanoparticles to evade macrophage-mediated uptake and removal from systemic circulation in vivo [56]. PEG decoration is also advantageously employed for nanoparticle-specific functionalization, as many commercial PEGs carry α-function suitable for grafting on gold (typically a thiol) and remote ω-function (e.g., –OH, –COOH, $–NH_2$) that may be efficiently used for further chemical modification [57, 58].

A comprehensive study of PEGylated gold nanostars and PEGylated bipyramidal-like nanostructures was presented by Navarro et al. in 2012 [59]. The nanoparticles were prepared at high yield and their surface was covered with a biocompatible PEG polymer. The PEGylated gold nanoparticles were incubated with melanoma B16-F10 cells. Dark-field microscopy showed that the biocompatible gold nanoparticles were easily internalized and most of them localized within the cells. Jo et al. performed the PEGylation of GNS synthesized by seed growth with bifunctional *O*-[2-(3-mercaptopropionylamino)ethyl]-*O′*-methylpolyethylene glycol [60]. These PEGylated gold nanostars were further conjugated with aptamers for the targeting of prostate cancer cells. The PEGylation of GNS with (*O*-[2-(3-mercaptopropionylamino) ethyl]-*O′*-methylpolyethylene glycol for in vivo particle tracking and photothermal ablation was also reported [61].

Surface modification of gold nanostars by means of PEGs with terminated thiol group (PEG-SH) with different molecular weights prevents the aggregation of the nanoparticles, due to the amphiphilic characteristic of the polymer (it is soluble both in water and organic solvents) [62]. Pallavicini et al. coated the GNS synthesized in the presence of the LSB surfactant with PEG_{2000}-SH [17]. Upon coating the long and intermediate LSPR bands shifted to the red (10 nm and 5 nm, respectively) due to the substitution of LSB on GNS surface with PEG_{2000}-SH. These functionalized GNS have an exceptional stability in acidic and base media, PBS solution, and ISO-sensitest broth (a defined medium suitable for use in antimicrobial susceptibility). Noticeably, if not coated with PEG these nanoparticles aggregate both in PBS and ISO-sensitest broth media within a few minutes. Almost negligible variation of absorption intensity was observed if larger thiolated PEG is used. These PEGylated GNS can be stored either in water or organic solvents due to amphiphilic nature of PEG. During the storage in organic solvents the LSPR position of the long and intermediate band displays a red shift that correlates linearly with solvent refractive index. In a following paper by the same research group, GNS were prepared in the presence of surfactant Triton X-100 and were coated with PEG_{2000}-SH [37]. The just synthesized GNS were poorly stable and the addition of PEG_{2000}-SH at the end of the growth promoted the displacement of surfactant. The whole GNS surface was coated yielding the extremely stable PEGylated nanostars. They can be dried, handled as powder, and redissolved in water or solvents ranging from ethanol to toluene, with both LSPRs shifting to the red. Also these PEGylated GNS display a photothermal behavior on both the intermediate (NIR) and long (SWIR) LSPR.

Wang et al. reported a new therapeutic strategy using chlorin e6-PEG-functionalized gold nanostars (GNS-PEG-Ce6) to couple photodynamic therapy with plasmonic photothermal therapy under single continuous wave laser irradiation [63]. GNS were conjugated with thiol-PEG-amine through the Au-S bonds. The PEGylated GNS exhibited excellent dispersivity and stability in a range of solutions including ultrapure water, dimethylformamide, phosphate-buffered saline (PBS), and cell medium with serum. PEGylated GNS were easily purified by centrifugation and conjugated with Ce6 (a commonly used photosensitizer) by NHS-EDC reaction in DMF. For further conjugation of GNS with fluorescence probes for in vivo imaging, bifunctional SH-PEG-NH_2 was employed [64]. PEGylated gold nanostars have been tested as contrast agents for photoacoustic imaging of blood vessels in the brain [65]. Moreover, anticancer drugs (e.g., DOX) were loaded into PEG-coated gold nanostars. Systematic administration of DOX-loaded PEG-GNS followed by NIR irradiation showed greater antitumor activity in a xenograft model of breast cancer than free Dox, PEGylated GNS, or NIR laser alone [65].

1.3.2 Functionalization of GNS with Dyes

The modification of nanoparticles with various fluorescent dyes is widely used because of the potential use of these systems for photosensing, light harvesting, and biosensing applications [66–69]. The immobilization of dye molecules onto

nanoparticles induces dramatic changes in its optical properties for chemical and biological applications, including fluorescence quenching of small dye molecules on gold nanoparticles. This effect can be exploited, for example, for protein sensing approaches [70]. Complementary oligonucleotides for single-stranded DNA-linked metal nanoparticles or bar-coded metal nanowires and fluorescent-dye-doped nanoparticles have been developed for medical diagnostics and labeling.

The reason for this success is clear. Fluorescent organic dyes are widely used for the detection of nucleic acids, proteins, and saccharides [71, 72]. However, these dyes suffer from photobleaching and can only be detected through highly sensitive techniques. On the other hand, gold nanoparticles are not susceptible to photobleaching and their absorption and scattering cross sections are larger than those of conventional dyes. Numerous methods have been utilized for detecting GNPs such as colorimetric, scanometric, fluorescence, surface-enhanced Raman scattering and electrochemical techniques [73]. These unique aspects have permitted the development of novel GNP-based assays for molecular diagnostics which promise increased sensitivity and specificity, multiplexing capability, and short turnaround times [73]. But also the interactions between nanoparticles and organic dyes have gained considerable interest for biochemical assays because they provide additional parameters to modulate the quenching efficiency and the photostability over classical dye-quenching system. Gold is also particularly effective in quenching or enhancing fluorescence emission of organic compounds, depending on the mutual distance between these and the gold surface [74, 75]. The corresponding dyes could be conjugated with gold nanoparticles due to adsorption process resulting in formation of non-covalent bond, covalent bond, and ionic interaction of positively charged groups with negatively charged surfaces of particles [76]. The main disadvantage of such hybrid systems is that the surface exposure of the dyes promotes their photooxidation. Another approach consists in the decoration of GNP dyes via bifunctional spacers, such as PEG or carboxylic acids, with subsequent chemical interaction of dyes with proper functional groups [53, 77].

The gold nanoparticles conjugated with dye molecules are very attractive because they can be studied by fluorescence-based techniques in addition to electron microscopy. If gold nanoparticles can successfully enhance the fluorescent signal of dyes to a significant degree, they would be useful in many areas of biochemistry and biology. For instance, dye-labeled gold particles could track the movements of drugs in cells and could act as a kind of molecular probe. Moreover, fluorescent-labeled gold nanoparticles are really highly selective imaging probes also because in contrast to scattering probes, their detection is not limited by the Rayleigh scattering conditions.

Besides direct effect on the transition strength, the reason to conjugate GNS with organic dyes is their successful application in SERS and fluorescence resonance energy transfer (FRET) assays. These application fields are discussed in Chaps. 2 and 3.

The GNS functionalized with dyes are schematically shown in Scheme 1.3.

Regarding fluorescence, quenching and energy transfer depend critically on the dye-gold distance. Navarro et al. reported in 2013 the synthesis, functionalization, and photophysics of luminescent hybrid gold nanostars prepared using a layer-by-layer

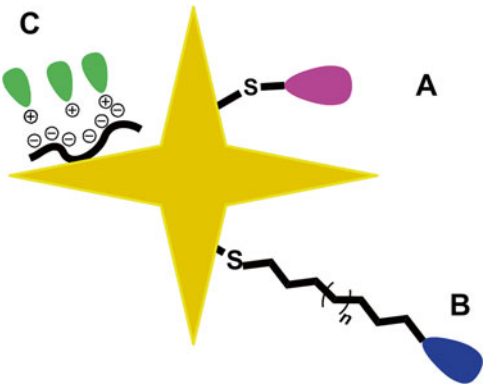

Scheme 1.3 Schematic representation of GNS functionalized with dyes via direct bounding (**A**), via bifunctional spacer (**B**), and through absorption onto surface (**C**)

(LbL) deposition method to tune the chromophore-to-particle distances, and studied the impact of the spectral overlap between the plasmon and the emission/absorption of the dyes on quenching [78]. Several luminescent dyes with different optical signatures were selectively adsorbed at the nanoparticle surface. The optimized systems, exhibiting the highest luminescence recovery, showed clearly that overlap must be as low as possible. The fluorescence intensities were quenched in close vicinity of the metal surface and revealed a distance dependence with almost full recovery of the emission when the dye was replaced by the 11 LbL layers, which corresponded to 15 nm distances evaluated on dried samples.

SERS-active probes were prepared by C. Khoury and Tuan Vo-Dinh by direct conjugation of p-mercaptobenzoic acid, a Raman-active dye, with synthesized GNS for potential use as SERS substrates in sensing [30]. In a more recent publication these authors presented a novel approach for the preparation of gold nanostar-functionalized substrates that show high sensitivity for chemical sensing based on surface-enhanced Raman spectroscopy [79]. Gold nanostars immobilized on a gold substrate via a Raman-silent organic tether serve as the SERS substrate, and facilitate the chemical sensing of analytes that can either be chemisorbed or physisorbed on the nanostars. For quantitative chemical detection based on SERS analysis, *p*-mercaptobenzoic acid is widely used as the model molecule. This is a Raman-active molecule with a relatively low-scattering cross section and *p*-mercaptobenzoic acid could be conjugated to GNS via its pendant thiol moiety as well as through π system interaction. In 2014 Khoury et al. presented also an effective method to distinguish intracellular from extracellular nanoparticles by selectively quenching the SERS signals from dye molecules absorbed onto star-shaped gold nanoparticles that have not been internalized by cells [80]. The conjugation of the fluorophores to the gold nanostars was achieved by first forming a cysteamine-Alexa 750 complex and then incubating it with PVP-capped GNS overnight. The dye-GNS conjugation efficiency was monitored through the observation of strong SERS signals from Alexa 750 at 789 nm [80].

An overview of recent developments and applications of surface-enhanced Raman scattering nanosensors has been published recently in *Nanomedicine and*

Nanobiotechnology [81]. The functionalization of GNS with different types of dyes and the properties of resulted systems were thoroughly discussed. For example, the functionalization of GNS with NAFTA6 dye, a derivative of 4-methoxy-1,8-naphthalimide bearing at the imide N-atom a long aliphatic chain with an SH terminal group, was reported [82]. In a second work, cyclic RGD peptide-modified GNS were subsequently labeled with a hydrophilic indocyanine green derivative (NIR fluorescent probe), to investigate the biodistribution of GNS and to assess the selective uptake of Au NS in tumors after attachment of cRGD [83]. The dye was activated with DCC and NHS before conjugation with cRGD-modified GNS. Vo-Dinh and coworkers reported in 2011 the synthesis and characterization of SERS label-tagged gold nanostars, coated with a silica shell containing methylene blue photosensitizing drug for singlet-oxygen generation [84]. The gold nanostars were tuned for maximal extinction in the NIR spectral region and tagged with an NIR dye (DTTC) for surface-enhanced resonance Raman scattering (SERRS). The use of an NIR dye further enhanced the SERS signal due to better spectral superposition. The protocol involving the silica coating was used by these authors to encapsulate the photosensitizer methylene blue in a shell around the nanoparticles as it is known that mesoporous silica shell can be used to encapsulate various dye molecules onto a metallic core. Methylene-blue-encapsulated nanoparticles showed a significant increase in singlet-oxygen generation as compared to nanoparticles synthesized without methylene blue.

In a different approach Melnikau et al. developed a hybrid system consisting of GNS and J-aggregates of the cyanine dyes and brought into evidence the coherent coupling between the localized plasmons of the metal component and the excitons of the J-aggregates through the Rabi splitting with the energy up to 260 meV [85]. J-aggregates were formed from the following two dyes: JC1 (5,5′,6,6′-tetrachloro-1,1′,3,3′-tetraethylimidacarbocyanine iodide) and S2165 2-[3-[1,1-dimethyl-3-(4-sulfobutyl)-1,3-dihydrobenzo[e]indol-2-ylidene]-propenyl]-1,1-dimethyl-3-(4-sulfobutyl)-1H-benzo[e] indolium hydroxide. Hybrid structures of gold nanostars and the J-aggregates of the JC1 dye were produced by the addition of the concentrated ethanol solution of the dye to an aqueous solution of gold nanostars in the presence of ammonia at pH 8. Interactions between nanostars and JC1 molecules of J-aggregates resulted in the formation of chain-like tightly bound agglomerates of gold nanostars interconnected by an organic matter.

It is worth noting that in 2009 a comparison study was published in which relevant photophysical properties of single-fluorescent molecules and single-SERS-active surface-coated gold nanostars tagged with the Raman reporter molecule 4-mercaptopyridine were compared for imaging purposes [86]. The nanostar-based SERS NP presented in this paper eliminates the traditional challenges of signal consistency and strength and demonstrates the viability of SERS probes for imaging applications. By comparing populations at the single-probe level, it was found that the count rate variance from a SERS NP is at least as good as that observed for fluorescent emission of Alexa Fluor 633. The preparation of gold nanostars modified with FITC-labeled chitosan was also reported later [87]. These modified GNS had a higher colloidal stability at physiological pH and they are more suitable mediators in cell photothermolysis due to the slower aggregation.

1.3.3 Other Examples of Functionalization of GNS

Functionalization of nanostructures GNS with biological molecules has many applications in biomedical imaging, clinical diagnosis, and therapy. A summary of the strategies of functionalization of GNS is shown in Scheme 1.4.

In most cases the functionalization of GNS aimed at the optimization of their intracellular delivery and photothermolysis efficiency. In order to increase the accumulation of nanoparticles at the tumor site and lower the side effects on normal tissues, many investigators have functionalized nanoparticles with ligands such as aptamer, peptide, and oligosaccharide for active tumor targeting. Moreover, besides the biological molecules, the functionalization of GNS with bifunctional spacers is also widely used for self-assembling monolayer formation and for further conjugation approaches.

The functionalization of gold nanoparticles, including GNS, with *peptides* is widely used. It was shown that *TAT-peptide*-functionalized gold nanostars enter cells significantly more than bare or PEGylated nanostars [88]. To fabricate stable constructs that resist aggregation in physiological environment and multiple washing

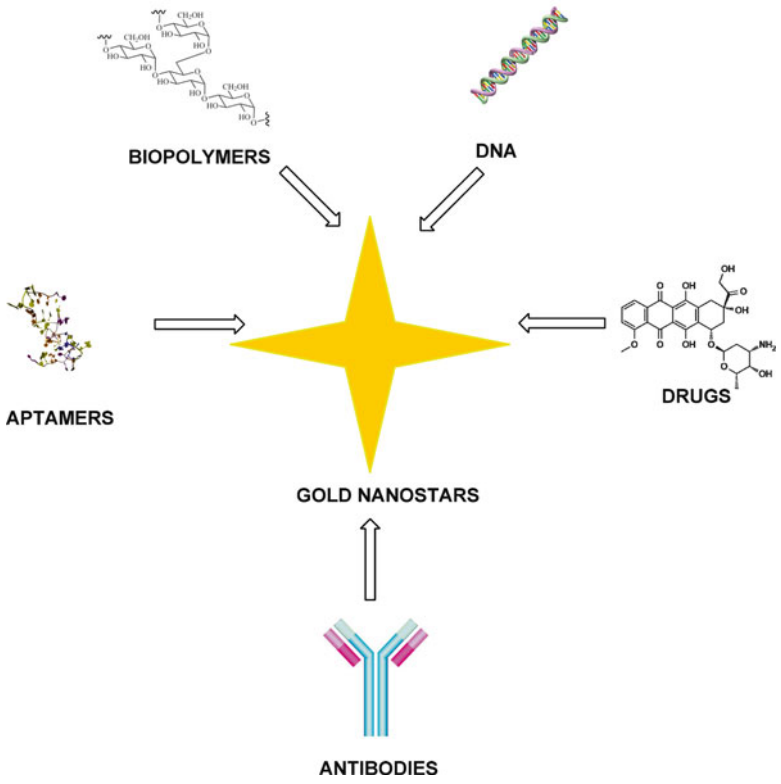

Scheme 1.4 General strategies of functionalization of GNS

cycles, GNS were decorated with cysteine-terminated TAT peptide and thiolated polyethylene glycol. The resulting constructs displayed enhanced intracellular delivery and efficient photothermolysis of TAT-modified nanostars and are considered promising agents in cancer therapy. *Biotin-functionalized* GNS were prepared by partial replacement of CTAB with biotinylated bovine serum albumin [89]. These functionalized GNS were used for detection of streptavidin. Nehl et al. bound mercaptohexadecanoic acid and *bovine serum* albumin to gold nanostars to create molecular sensors [38]. The observed shifts are consistent with the effects of these molecular layers on the surface plasmon resonances in continuous gold films. Vo-Dinh with coworkers presented the development of a theranostic system that combines Raman imaging and the photodynamic therapy effect [90]. The theranostic nanoplatform was created by loading the *photosensitizer*, *protoporphyrin IX*, onto a Raman-labeled gold nanostar. The co-decoration with a cell-penetrating peptide, TAT, enhanced intracellular accumulation of the nanoparticles and improved their delivery and efficacy. *TAT* conjugation was achieved by passive adsorption.

Aptamer-conjugated nanoparticles, especially gold nanoparticles, are promising for applications in bioanalysis and medical therapy, including early diagnosis and drug delivery. Novel valuable therapeutic complexes, namely *dual-aptamer*-modified gold nanostars, for the targeting of prostate cancers have been developed recently [60]. The aptamers were conjugated to PEGylated GNS via disulfide bonds. Nanoconstructs composed of nucleolin-specific aptamers and gold nanostars were actively transported to the nucleus and induced major changes to the nuclear phenotype via nuclear envelope invaginations near the site of the construct [91]. *AS1411 aptamers* containing thiol groups were grafted to GNS by capping molecule replacement, to create Apt–GNS nanoconstructs. To determine the number of aptamers attached to each GNS, the authors compared differences in fluorescence intensity of a solution of Cy5-labeled aptamer before and after conjugating the GNS. In an alternative application, highly selective, and reagent-free aptamer-based biosensor has been developed for quantitative detection of adenosine triphosphate [92]. The sensor contains a SERS probe made of gold nanostar-Raman label-SiO_2 core–shell nanoparticles in which the Raman label (malachite green isothiocyanate) molecules are sandwiched between a gold nanostar core and a thin silica shell [92]. The corresponding dye was chosen as the Raman label due to its nonfluorescent characteristic and its isothiocyanate (–N=*C*=S) group that can bind to the gold surface and is compatible with the SiO_2 encapsulation process as well. SiO_2 was employed as a protective layer because of its long-term stability and easy bioconjugation. These gold nanostars were finally functionalized with DNA. Firstly this process involved functionalization with 3-triethoxysilylpropyl succinic anhydride, and then the functionalization of DNA with carboxyl terminated constructs was carried out by the carbodiimide chemistry.

Dam et al. reported recently the design of a nanoconstruct that targets the ubiquitous protein nucleolin and that is largely independent of the cell phenotype [93]. Gold nanostars loaded with high densities of *nucleolin-specific DNA aptamer AS1411* produced anticancer effects in a panel of 12 cancer lines containing four representative subcategories. Thiolated AS1411 was attached to the AuNS surface via gold–sulfur

bonds in a 2-day "salt-aging" process. It was found that high loading densities of Apt on the AuNS increased the overall stability of aptamers in physiological environments, similar to other reports of nucleic acids on spherical gold particles.

The conjugation of *antibodies and RNA moieties* to gold nanoparticles is also widely used in a range of approaches. Liz-Marzan et al. developed an inverse sensitivity assay based on the detection of the plasmon resonance shift induced by the growth of silver crystals on the gold nanostars [94]. To control crystal growth the authors used the enzyme glucose oxidase (GOx), which generates hydrogen peroxide that reduces silver ions. Only when the enzyme is present at low concentration the reducing agent is in short supply and the crystal growth is slow, favoring the formation of a homogeneous silver coating on the gold nanostars with respect to single-silver nanocrystals. Once proved this inverse sensitivity mechanism, the GNS were modified with polyclonal antibodies against prostate-specific (rabbit) antigen and used as the label in a classical enzyme-linked immunoassay. This mechanism was demonstrated on polyclonal anti-PSA (rabbit) antibody.

Wege et al. described an RNA-directed bottom-up assembly procedure yielding bioinorganic hybrid nanostars with a central gold core and a surface-saturating number of virus-derived arms. These constructs are not gold nanostars but branched gold-based organic nano-objects with an exceptionally high and tunable ratio of the virus-based surface arms to the metal cores [95]. This was achieved by binding on the gold beads short oligonucleotides complementary for the initial sequence of the tobacco mosaic virus (TMV) *RNA*. The TMV RNA triggers the formation of the virus coat protein assembly in the peculiar rodlike shape of the TMV. The specificity of RNA hybridization to oligo-deoxynucleotides exposed on gold nanoparticles of different diameters allowed the simultaneous fabrication of star colloids with distinct predetermined arm-length distributions in single-batch processes [95].

Surface functionalization of GNS with ethylene glycol-modified Raman reporter derivatives Ra_1 and Ra_2 was adopted for both hydrophilic stabilization and subsequent biofunctionalization [96]. The two organic compounds Ra_1 and Ra_2 were synthesized from the Raman reporter molecule 5,5′-dithiobis(2-nitrobenzoic acid) by the formation of the corresponding amides with a short hydrophilic monoethylene glycol spacer (H_2N–MEG–OH for Ra_1) and a longer hydrophilic triethylene glycol spacer (H_2N–TEG–COOH for Ra_2), respectively. Bioconjugation of the SERS label to the anti-p63 antibody was achieved via activation of the COOH groups in Ra_2 using standard EDC/s-NHS chemistry.

In the paper published in 2009 a dynamic mode of optical contrast based on gyromagnetic imaging, in which gold nanostars with superparamagnetic cores are driven by a rotating magnetic field gradient to produce periodic variations in NIR scattering intensities, was presented [97]. These GNS were functionalized with oligoethyleneglycol-conjugated folic acid derivatives by in situ dithiocarbamate formation, followed by membrane dialysis.

For many purposes the functionalization with several species is also widely used. For example in previously cited paper gold nanostars were conjugated with *cyclic RGD* and NIR fluorescence probe or *anticancer drug* (*DOX*) to obtain multifunctional nanoconstructs [82]. Using tumor cells and tumor-bearing mice, these imaging nanoparticles demonstrated favorable tumor-targeting capability mediated by RGD

peptide binding to its over-expressed receptor on the tumor cells. The nanostars functionalized with RGD and DOX integrated targeting tumor, chemotherapy, and photo-thermotherapy into a single system. The synergistic effect of photothermal therapy and chemotherapy was demonstrated in different tumor cell lines and in vivo using S180 tumor-bearing mouse models. Gold nanostars have been assembled via electrostatically assisted *3-aminopropyltriethoxysilane* (APTES)-functionalized surface assembly method [98] to produce a substrate with SERS activity. The most attractive advantage of electrostatically assisted APTES-functionalized surface assembly method is that a substrate with a very homogeneous SERS signal and large area can be fabricated without sophisticated equipment. Plasmonic gold nanostars were also modified with a biopolymer *chitosan* [87]. The chitosan-modified nanostars dispersed in a medium with pH = 7.5 had higher stability than those of chitosan-capped nanorods because of the slower aggregation of GNS. At pH = 7.5 the chitosan-modified GNS formed aggregates with highly nonuniform sizes.

Wei et al. presented in 2012 a new surface-enhanced Raman spectroscopy platform suitable for gas-phase sensing based on the extended organization of *poly-N-isopropylacrylamide* (pNIPAM)-coated nanostars over large areas [99]. The authors reported the preparation of optically active gold nanostars coated with pNIPAM and their controlled assembly into highly ordered linear structures. Au-pNIPAM core–shell particles were prepared by precipitation polymerization of the monomer NIPAM in the presence of functionalized, spherical gold nanoparticles. pNIPAM-coated gold nanoparticles were dispersed in solution with PVP, and the solution was incubated overnight to allow diffusion of PVP to the Au surface. Nanostars were formed by adding to the resulted solution an aqueous solution of $HAuCl_4$.

A highly sensitive SERS-based sandwich immunoassay employed two derivatives of gold nanostars simultaneously [100]. One was densely packed self-assembled substrates of gold nanostars and the other was made of immune-labeled nanostar aggregates. 4-Mercaptobenzoic acid-labeled immune-labeled gold nanostar aggregates were obtained by successive Raman reporter replacement, aggregation, immune immobilization, and blocking. Gold nanostar multilayers were formed by the self-assembly between polyelectrolytes and gold nanostars through electrostatic interaction.

The GNS could also be decorated with mixed *lipid-polymer* coatings by exploiting thiol chemistry [101]. This multiple decoration would increase/modify their interaction with skin and enable the nanoparticles' drug delivery capabilities. Polymers capable of trapping and releasing drugs under temperature control obtained by NIR laser irradiation may in fact be employed for this purpose.

The integration of metal nanoparticles within cross-linked polymeric microgels, in a well-defined core–shell structure, offers unique possibilities in various fields due to the potential to introduce multiple functionalities by tailoring the properties of the inorganic and the organic components [102]. Recently the encapsulation of gold nanoparticles within pNIPAM (poly-*N*-isopropylacrylamide) microgels has been reported for different particle sizes, including nanostars. All strategies start from initial modification of the metallic surface with molecules containing vinyl groups, which serve as starting points for the polymerization and thus facilitate the

encapsulation. The resulted colloidal nanocomposites based on a metallic core and a pNIPAM shell preserve the main properties of both components, i.e., the optical response from the plasmonic nanoparticle and the thermosensitive behavior of the polymer shell [102]. The synthesis and application of such composites are described in an interesting highlight of Liz-Marzan et al. [103].

Esentruk and Walker produced *iron oxide-coated* gold nanostars by first synthesizing gold nanostars (ca 150 nm), and then introducing a PVP coating followed by reducing iron(II) and iron(III) salts on the nanoparticle (NP) surface [104]. Having both magnetic and plasmonic properties in one NP system makes these particles suitable for various bio-analytical applications such as biomolecule separation, sensing, and magnetic imaging.

A novel synthetic methodology for star-shaped *gold-coated magnetic* nanoparticles was reported in a paper published in 2014 in RCS Adv [105]. The coating was performed in two steps: formation of gold nuclei at the surface of magnetite nanoparticles followed by growth of the gold nuclei into a complete star-shaped shell. The star-shaped gold-coated magnetic nanoparticles thus obtained preserve the magnetic properties of the precursor magnetite nanoparticles; for example they can be easily separated with a magnet. In addition, the gold coating provides interesting optical properties while simultaneously allowing for biofunctionalization that may be advantageous for biological applications, such as (bio)detection via SERS. As a proof of concept, the GNS were modified with a capping agent terminated with a nickel(II)-nitrilotriacetate group that shows high affinity for histidine. The resulting star-shaped nanoparticles were used to selectively capture histidine-tagged maltose-binding protein from a crude cell extract. The performance of star-shaped gold-coated magnetic nanoparticles as SERS platforms was demonstrated through the detection of Raman-active dye (Astra Blue).

It has been already mentioned that a mesoporous *silica shell* can be used to encapsulate various dye molecules onto a metallic core. Vo-Dinh and coworkers developed and characterized label-tagged gold nanostars, coated with a silica shell containing methylene blue [84]. Silica encapsulation on GNS and their intracellular SERS detection were also reported by the same research group [106].

Gold nanostars due to a range of properties are promising platforms for applications in medicine and biology. The techniques used for their synthesis were reviewed in this chapter. Since for a variety of applications surface functionalization of GNS is essential, different functionalization approaches were also discussed here. The next chapter focuses on physical properties giving an explanation of righteous reinforced attention to these types of gold nanoparticles.

References

1. Zhou J, Ralston J, Sedev R, Beattie DA (2009) Functionalized gold nanoparticles: synthesis, structure and colloid stability. J Colloid Interface Sci 331:251–262
2. Frens G (1971) Controlled nucleation for the regulation of the particle size in monodisperse gold suspension. Nat Phys Sci 241:20–22

3. Hostetler M et al (1998) Alkanethiolate gold cluster molecules with core diameters from 1.5 to 5.2 nm: core and monolayer properties as a function of core size. Langmuir 14:17–30
4. Zhao P, Li N, Astruc D (2013) State of the art in gold nanoparticle synthesis. Coord Chem Rev 257:638–665
5. Turkevich J, Stevenson PC, Hillier J (1951) A study of the nucleation and growth process in the synthesis of colloidal gold. Discuss Faraday Soc 11:55–75
6. Kimling J et al (2006) Turkevich method for gold nanoparticle synthesis revisited. J Phys Chem 110:15700–15707
7. Pong BK et al (2007) New insights on the nanoparticles growth mechanism in the citrate reduction of gold (III) salt: formation of the Au nanowire intermediate and its nonlinear optical properties. J Phys Chem 111:6281–6287
8. Polte J et al (2010) Mechanism of gold nanoparticle formation in the classical citrate synthesis method derived from coupled in situ XANES and SAXS evaluation. J Am Chem Soc 132:1296–1301
9. Kumar S, Gandhi KS, Kumar R (2007) Modeling of formation of gold nanoparticles by citrate method. Ind Eng Chem Res 46:3128–3136
10. Brust M et al (1994) Synthesis of thiol-derivatised gold nanoparticles in a two-phase liquid-liquid system. J Chem Soc Chem Commun 7:801–802
11. Brust M et al (1995) Synthesis and reactions of functionalized gold nanoparticles. J Chem Soc Chem Commun 16:1655–1656
12. Templeton AC, Wuelfing WP, Murray WP (2000) Monolayer-protected cluster molecules. Acc Chem Res 33:27–36
13. Sardar R, Shumaker-Parry JS (2009) 9-BBN induced synthesis of nearly monodispersed ω-functionalized alkylthiol stabilized gold nanoparticles. Chem Mater 21:1167–1169
14. Mallick K, Wang ZL, Pal T (2001) Seed-mediated successive growth of gold particles accomplished by UV irradiation: a photothermal approach of size-controlled synthesis. J Photochem Photobiol A 140:75–80
15. Kumar SP et al (2008) High-yield synthesis and optical response of gold nanostars. Nanotechnology 19:015606
16. Burda C et al (2005) Chemistry and properties of nanocrystals of different shapes. Chem Rev 105:1025–1102
17. Casu A, Cabrini E et al (2012) Controlled synthesis of gold nanostars by using zwitterionic surfactant. Chemistry 18:9381–9390
18. Guerro-Martinez A et al (2011) Nanostars shine bright to you: colloidal synthesis, properties and application of branched metallic nanoparticles. Curr Opin Colloid Interface Sci 16:118–127
19. Alvarez-Puebla R, Liz-Marzan LM, Garcia De Abajo FJ (2010) Light concentration at the nanometer scale. J Phys Chem Lett 1:2428–2434
20. Freddi S, Sironi L et al (2013) A molecular thermometer for nanoparticles for optical hyperthermia. Nano Lett 13:2004–2010
21. Hrelesku C et al (2009) Single gold nanostars enhance Raman scattering. Appl Phys Lett 94:1–3
22. Gasser U, Weeks ER, Schofield A, Pusey PN, Weitz DA (2001) Real-space imaging of nucleation and growth in colloidal crystallization. Science 292:258–262
23. Kawamura G, Nogami M (2009) Application of a conproportionation reaction to a synthesis of shape-controlled gold nanoparticles. J Cryst Growth 311:4462–4466
24. Sau TK, Murphy CJ (2004) Room temperature, high-yield synthesis of multiply shapes of gold nanoparticles in aqueous solution. J Am Chem Soc 126:8648–8649
25. Kuo CH, Huang MH (2005) Synthesis of branched of gold nanocrystals by a seeding growth approach. Langmuir 21:2012–2016
26. Wu HL, Chen CH, Huang M (2009) Seed-mediated of branched gold nanocrystals derived from the side growth of pentagonal bipyramids and the formation of gold nanostars. Chem Mater 21:110–114
27. Zou H, Ying E, Dong S (2006) Seed-mediated synthesis of branched gold nanoparticles with the assistance of citrate and their surface-enhanced Raman scattering properties. Nanotechnology 17:4758–4764

28. Barbosa S et al (2010) Size tuning and sensing capabilities of gold nanostars. Langmuir 26:14943–14950
29. Minati L et al (2014) One-step synthesis of star-shaped gold nanoparticles. Colloids Surf A Physicochem Eng Asp 441:623–628
30. Khoury CG, Vo-Dinh T (2008) Gold nanostars for surface-enhanced Raman scattering: synthesis, characterization and optimization. J Phys Chem C 112:18849–18859
31. Yuan H, Khoury CG et al (2012) Gold nanostars: surfactant-free synthesis, 3D modelling, and two-photon photoluminescence imaging. Nanotechnology 23:075102
32. Osinkina L et al (2013) Synthesis of gold nanostar arrays as reliable, large-scale homogeneous substrates for surface-enhanced Raman scattering imaging and spectroscopy. J Phys Chem C 117(43):22198–22202
33. Li Y, Ma J, Ma Z (2013) Synthesis of gold nanostars with tunable morphology and their electrochemical application for hydrogen peroxide sensing. Electrochim Acta 108:435–440
34. Chirea M (2013) Electron transfer of gold nanostars assemblies: a study of shape stability and surface density influence. Catalysts 3:288–309
35. Kereselidze Z, Romero VH, Peralta XG, Santamaria F (2012) Gold nanostar synthesis with a silver seed mediated growth method. JoVE Bioeng. doi:10.3791/3570
36. Salinas K et al (2014) Transient extracellular application of gold nanostars increases hippocampal neuronal activity. J Nanobiotechnol 12:31
37. Stassi S et al (2012) Synthesis and characterization of gold nanostars as filler of tunneling conductive polymer composites. Eur J Inorgan Chem 16:2669–2673
38. Pallavicini P, Dona A et al (2013) Triton X-100 for three-plasmon gold nanostars with two photothermally active NIR (near IR) and SWIR (short-wavelength IR) channels. Chem Commun 49:6265–6267
39. Nehl CL, Liao H, Hafner JH (2006) Plasmon resonant molecular sensing with single gold nanostars. Proc SPIE 6323:63230G
40. Sau TK, Rogach AL, Döblinger M, Feldmann J (2011) One-step high-yield aqueous synthesis of size-tunable multispiked gold nanoparticles. Small 7:2188–2194
41. Xia Y, Xiong Y, Lim B, Skrabalak SE (2009) Shape-controlled synthesis of metal nanocrystals: simple chemistry meets complex physics? Angew Chem Int Ed 48:60–103
42. Xie J, Lee JY, Wang DIC (2007) Seedless, surfactantless, high-yield synthesis of branched nanocrystals in HEPES buffer solution. Chem Mater 19:2823–2839
43. Jena BK, Raj CR (2007) Synthesis of flower-like gold nanoparticles and their electrocatalytic activity towards oxidation of methanol and the reduction of oxygen. Langmuir 23: 4064–4070
44. Yamamoto M, Kashiwagi Y, Sakata T, Mori H, Nakamoto M (2005) Synthesis and morphology of star-shaped gold nanoplates protected by Poly(N-vinyl-2-pyrrolidone). Chem Mater 17:5391–5393
45. Hao E, Bailey RC, Scharz GC, Hupp JT, Li S (2004) Synthesis and optical properties of "branched" gold nanocrystals. Nano Lett 4:327–330
46. Umedevi S, Lee HC, Ganesh V, Feng X, Hegmann T (2014) A versatile, one-pot synthesis f gold nanostars with long, well-defined, thorns using a lyotropic liquid crystal template. Liquid Crystals 41:265–276
47. Moukarzel W, Fitremann J, Marty JD (2011) Seed-less amino-sugar-mediated synthesis of gold nanostars. Nanoscale 8:3285–3290
48. Zhou M, Chen S, Zhao S (2006) Preparation of branched gold nanocrystals by an electrochemical method. Chem Lett 35:332–333
49. Li Z, Li W, Camargo PHC, Xia Y (2008) Facile synthesis of branched Au nanostructures by templating against a self-destructive lattice of magnetic Fe nanoparticles. Angew Chem Int Ed 47:9653–9656
50. Chirumamilla M et al (2014) Plasmon resonance tuning in metal nanostars for surface enhanced Raman scattering. Nanotechnology 25:235303
51. Chirumamilla M et al (2014) 3D nanostars dimers with a sub-10-nm gap for single-/few-molecule surface enhanced Raman scattering. Adv Mater 26:2353–2358

52. Park G, Seo D, Chung IS, Song H (2013) Poly(ethylene glycol)- and carboxylate-functionalized gold nanoparticles using polymer linkages: single-step synthesis, high stability, and plasmonic detections of proteins. Langmuir 29:13518–13526
53. Tiwari PM et al (2011) Functionalized gold nanoparticles and their biomedical applications. Nanomaterials 1:31–63
54. Sperling RA, Parak WJ (2010) Surface modification, functionalization and bioconjugation of colloidal inorganic nanoparticles. Phil Trans R Soc A 368:1333–1383
55. Rahme K et al (2013) PEGylated gold nanoparticles: polymer quantification as a function of PEG lengths and nanoparticles dimensions. RSC Adv 3:6085–6095
56. Sanna V, Pala N, Sechi M (2014) Targeted therapy using nanotechnology: focus on cancer. Int J Nanomed 9:467–483
57. Kumar R et al (2013) Third generation gold nanoplatform optimized for radiation therapy. Transl Cancer Res 4:228–239
58. Manson J, Kumar D, Meenan BJ, Dixon D (2011) Polyethylene glycol functionalized gold nanoparticles: the influence of capping density on stability in various media. Gold Bull 44:99–105
59. Navarro JR et al (2012) Synthesis of PEGylated gold nanostars and bipyramids for intracellular uptake. Nanotechnology 46:465602
60. Jo H et al (2014) Ultra-effective photothermal therapy for prostate cancer cells using dual-aptamer modified gold nanostars. J Mater Chem B 2:4862–4867
61. Yuan H et al (2012) In vivo particle tracking and photothermal ablation using plasmon-resonant gold nanostars. Nanomed Nanotechnol Biol Med 8:1355–1363
62. Cennamo N et al (2013) Localized surface plasmon resonance with five branched gold nanostars in a plastic optical fiber for bio-chemical sensor implementation. Sensors (Basel) 13:14676–14686
63. Wang S et al (2013) Single continuous wave laser induced photodynamic/plasmonic photothermal therapy photosensitizer-functionalized gold nanostars. Adv Mater 25:3055–3061
64. Li W et al (2014) *In vivo* quantitative photoacoustic microscopy of gold nanostars kinetics in mouse organs. Biomed Opt Express 5(8):2679–2685. doi:10.1364/BOE.5.002679
65. Chen X, Wong STC (eds) (2014) Cancer theranostic. Academic, London
66. Nune SK et al (2009) Nanoparticles for biomedical imaging. Expert Opin Drug Deliv 6:1175–1194
67. Song Y, Zhu S, Yang B (2014) Bioimaging based on fluorescent carbon dots. RSC Adv 4:27184–27200
68. Zedler L et al (2012) Ruthenium dye functionalized gold nanoparticles and their spectral responses. RSC Adv 2:4463–4471
69. Narband N et al (2009) The interaction between gold nanoparticles and cationic and anionic dyes: enhanced UV-visible absorption. Phys Chem Chem Phys 44:10513–10518
70. Sironi L et al (2009) p53 Detection by fluorescence lifetime on a hybrid fluorescein isothiocyanate gold nanosensor. J Biomed Nanotechnol 5:683–691
71. Cordes DB et al (2005) Optical glucose detection across the visible spectrum using anionic fluorescent dyes and a viologen quencher in a two-component saccharide sensing system. Org Biomol Chem 3:1708–1713
72. Leung CH et al (2012) Luminescent detection of DNA-binding proteins. Nucleic Acids Res 40:941–955
73. Radwan SH, Azzazy HME (2009) Gold nanoparticles for molecular diagnostic. Expert Rev Mol Diagn 9:511–524
74. Yang PJ et al (2012) Quenching effects of gold nanoparticles in nanocomposites formed in water-soluble conjugated polymer nanoreactors. Polymer 53:239–946
75. Dulkeith E et al (2005) Gold nanoparticles quench fluorescence by phase induced radiative rate suppression. Nano Lett 5:585–589
76. Hutter E, Maysinger D (2013) Trends Pharmacol Sci 34:497–506
77. Conde J et al (2014) Revisiting 30 years of biofunctionalization and surface chemistry of inorganic nanoparticles for nanomedicine. Front Chem 2:48

78. Navarro JRG et al (2013) Tuning dye-to-particle interactions toward luminescent gold nanostars. Langmuir 29:10915–10921
79. Indrasekara AS et al (2014) Gold nanostar substrates for SERS-based chemical sensing in the femtomolar regime. Nanoscale 6:8891–8899
80. Xie N, Lin Y, Mazo M, Chiappini C et al (2014) Identification of intracellular gold nanoparticles using surface-enhanced Raman scattering. Nanoscale 6:12403–12407
81. Vo-Dinh T et al (2014) SERS nanosensors and nanoreporters: golden opportunities in biomedical application. Nanomed Nanobiotechnol. doi:10.1002/wnan.1283
82. Giorgetti E et al (2012) Tunable gold nanostars for surface enhanced Raman spectroscopy. Phys Stat Solidi B 249:1188–1192
83. Chen H et al (2013) Multifunctional gold nanostar conjugates for tumor imaging and combined photothermal and chemo-therapy. Theranostics 3:633–649
84. Fales AM, Yuan H, Vo-Dinh T (2011) Silica-coated gold nanostars for combined surface-enhanced Raman scattering (SERS) detection and singlet-oxygen generation: a potential nanoplatforms for theranostics. Langmuir 27:12186–12190
85. Melnikau D et al (2013) Strong plasmon-exciton coupling in a hybrid system of gold nanostars and J-aggregates. Nanoscale Res Lett 8:134
86. Allegeyer ES et al (2009) Optical signal comparison of single fluorescent molecules and Raman active gold nanostars. Nano Lett 9:3816–3819
87. Baginskiy I et al (2013) Chitosan-modified stable colloidal gold nanostars for the thermolysis of cancer cells. J Phys Chem 117:2396–2410
88. Yuan H et al (2012) TAT-peptide functionalized gold nanostars: enhanced intracellular delivery and efficient NIR photothermal therapy using ultralow irradiance. J Am Chem Soc 134: 11358–11361
89. Dondapati S et al (2010) Label-free biosensing based on single gold nanostars as plasmonic transducers. ACS Nano 4:6318–6322
90. Fales AM, Yuan H, Vo-Dinh T (2013) Cell-penetrating peptide enhanced intracellular Raman imaging and photodynamic therapy. Mol Pharm 10:2291–2298
91. Dam DH et al (2012) Direct observation of nanoparticles-cancer cell nucleus interactions. ACS Nano 6:3318–3326
92. Li M et al (2012) Detection of adenosine triphosphate with an aptamer biosensor based on surface-enhanced Raman scattering. Anal Chem 84:2837–2842
93. Dam DHM et al (2014) Grafting aptamers onto gold nanostars increases in vitro efficacy in a wide range of cancer cell types. Mol Pharm 11:580–587
94. Rodriguez-Lorenzo L et al (2012) Plasmonic nanosensors with inverse sensitivity by means of enzyme-guided crystal growth. Nat Mater 11:604–607
95. Eber FJ et al (2013) Bottom-up-assembled nanostar colloids of gold cores and tubes derived from tobacco mosaic virus. Angew Chem 125:7344–7348
96. Schutz M et al (2011) Hydrophilically stabilized gold nanostars as SERS labels for tissue imaging of the tumor suppressor p63 by immuno-SERS microscopy. Chem Commun 47:4216–4218
97. Wei Q et al (2009) Gyromagnetic imaging: dynamic optical contrast using gold nanostars with magnetic core. J Am Chem Soc 131:9728–9734
98. Su Q et al (2011) A reproducible SERS substrate based on electrostatically assisted APTES-functionalized surface-assembly of gold nanostars. ACS Appl Mater Interface 3:1873–1879
99. Mueller M et al (2012) Large-area organization of pNIPAM-coated nanostars as SERS platforms for polycyclic aromatic hydrocarbons sensing in gas phase. Langmuir 28:9168–9173
100. Pei Y et al (2013) Highly-sensitive SERS-based immunoassay with simultaneous utilization of self-assembled substrates of gold-nanostars and aggregates of gold nanostars. J Mater Chem B 1:3992–3998
101. Chirico G, Pallavicini P, Collini M (2014) Gold nanostars for superficial diseases: a promising tool for localized hyperthermia? Nanomedicine 9:1–3
102. Perez-Juste J, Pastoriza-Santos I, Liz-Marzan LM (2013) Multifunctionality in metal@microgel colloidal composites. J Mater Chem A 1:20–26

103. Caceres-Contreras R et al (2008) Encapsulation and growth of gold nanoparticles in thermo-responsive microgels. Adv Mater 20:1666–1670
104. Esentruk EN, Walker AR (2013) Gold nanosrars@iron oxide core-shell nanostructures: synthesis, characterization, and demonstrated surface-enhanced Raman scattering properties. J Nanopart Res 15:1364
105. Quaresma P et al (2014) Star-shaped magnetic@gold nanoparticles for protein magnetic separation and SERS detection. RSC Adv 4:3659–3667
106. Yuan H et al (2012) Spectral characterization and intracellular detection od surface-enhanced Raman scattering (SERS)-encoded plasmonic gold nanostars. J Raman Spectrosc 44:234–239

Chapter 2
Physical Properties of Gold Nanostars

Giuseppe Chirico, Piersandro Pallavicini, and Mykola Borzenkov

Abstract The most relevant applications of gold nanostars are based on their physical properties. These arise primarily from resonant oscillations of the conduction electrons of the nanoparticles called localized surface plasmon resonances (LSPR). In this chapter an introduction to the physical origin of the LSPR and the way the nano-environment affect them are provided. Finally the implication of the LSPR of gold nanostar surface-enhanced Raman scattering is also discussed.

Keywords Gold nanostars • Localized surface plasmon resonance • Surface-enhanced Raman scattering

GNS show a LSPR of the core and multiple LSPRs corresponding to the tips and core–tip interactions. The latter are polarization dependent and accompanied by large local electric field enhancements at the sharp ends of the tips [1]. The locally enhanced fields have been exploited to amplify Raman signals (SERS) allowing molecular detection at zeptomolar levels [2] and, very recently, have enabled the demonstration of SERS at the single-gold nanostar level [3]. As a consequence of the confined electric field enhancement at the tips, the spectral positions of the LSPRs of a nanostar are expected to depend strongly on the dielectric environment around the tips [4]. The coupling of propagating surface plasmons and localized surface plasmons leads to enhanced electromagnetic fields which can be exploited for surface-enhanced Raman scattering and fluorescence enhancement and opens wide routes for developing new sensors for in vitro and in vivo application, which are discussed in this chapter.

G. Chirico (✉) • M. Borzenkov
Department of Physics, University of Milano-Bicocca, Piazza Della Scienza 3, Milan 20216, Italy
e-mail: giuseppe.chirico@mib.infn.it; mykola.borzenkov@unimib.it

P. Pallavicini
Department of Chemistry, University of Pavia, Viale Taramelli 12, Pavia 27100, Italy

G. Chirico et al., *Gold Nanostars*, SpringerBriefs in Materials,
DOI 10.1007/978-3-319-20768-1_2

2.1 Brief Theoretical Introduction

Surface plasmons have attracted the attention of physicists, chemists, biologists, and material scientists for widespread use in areas such as electronics, optical sensing, biomedicine, data storage, and light generation. LSPR, associated with noble metal nanostructures, creates narrow spectral absorption and wide scattering peaks due to linear or nonlinear interaction with the EM field as well as strong electromagnetic near-field enhancements.

Recent developments in nanotechnology have provided new methods to control various properties of nanomaterials that can support surface plasmons for specific applications [5] and have offered new insights into the physics of these resonances. LSPR is an optical phenomena generated by a light wave trapped within conductive nanostructures or nanoparticles smaller than the wavelength of light. The phenomenon results from the interactions between the incident light and surface electrons in the conduction bands [6]. This interaction produces coherent localized plasmon oscillations with a resonant frequency that strongly depends on the composition, size, geometry, dielectric environment, and particle–particle distance of nanoparticles [5]. LSPR response arises from the electric field of the incident light driving surface conduction electrons collectively away from the metal nanoparticle lattice. A restoring force is provided by the Coulombic attraction between the negatively charged electron cloud and the positively charged metal lattice. Those wavelengths of light that couple most strongly to this resonance are absorbed and can be elastically re-emitted as scattered light from nanoparticles. The phenomena of LSPR is schematically shown in Scheme 2.1.

Mie theory, which was first described in 1908, can be used to understand LSPRs for spherical nanoparticles [7]. Mie described this effect by solving Maxwell's equations for a plane wave incident on a metal sphere surrounded by a dielectric medium, given the dielectric function of the metal. Mie theory provides an exact analytical solution for nanosphere LSPR in terms of a multipole expansion. For nanospheres whose diameters are less than about one-tenth the incident radiation

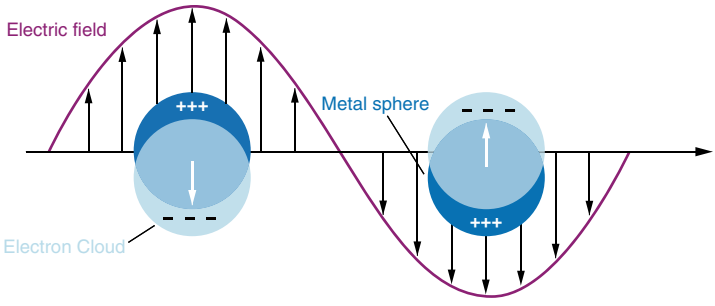

Scheme 2.1 The impinging light causes the electrons of the nanoparticle to delocalize forming an electric field opposite to the one of the wave. At specific frequencies, the electron oscillation is in resonance with the light wave and causes absorption

wavelength, only the dipole term in the expansion is significant, and the extinction simplifies to Eq. (2.1):

$$\sigma = \frac{18\pi V\varepsilon_m^{3/2}}{\lambda}\frac{\varepsilon_m}{\left(\varepsilon_1 + 2\varepsilon_m\right)^2 + \varepsilon_m^2} \tag{2.1}$$

where σ is the extinction cross section, V is the nanoparticle volume, λ is wavelength, ε_m is the dielectric constant of the medium, and $\varepsilon_1 + i\varepsilon_2$ is the complex dielectric function of the metal. The resonance condition is met when $\varepsilon_1(\lambda) = -2\varepsilon_m(\lambda)$, which occurs in the visible for gold and silver nanospheres. Indeed, for bulk metals ε_1 is typically small and negative [8]. This equation is valid only for spheres much smaller then wavelength of light.

For more complex geometries, however, one must employ more advanced electrodynamic numerical methods in order to correctly describe metal nanoparticle optical properties [6, 9]. Previous studies have shown the LSPR spectrum to be intimately related to the nanoparticle's size, shape, composition, and dielectric environment [10–12].

The theory of surface plasmons and LSPR is thoroughly discussed in two papers by Willets et al. [6] and Barnes et al. [13] appeared in 2007 and 2003. The oscillation frequency is critically determined by four factors: the density of electrons, the effective electron mass, and the shape and size of the charge distribution [14, 15]. Moreover, for a metal such as gold, the plasmon frequency is also influenced by the d-orbital electrons. Equation (2.1) indicates that in the dipole approximation, the position (λ_{max}) of the LSPR has no dependence on the size of gold nanospheres. The resonant condition is purely determined by the dielectric functions of the metal and the medium. However, for larger nanospheres where the higher multipoles become important, there is a modest red shift with size [15, 16]. Beyond this size, the resonance continues to shift but becomes significantly broadened. This broadening is due to both the different peak wavelengths of the higher multipoles and the radiative damping of the resonance as the scattering cross section rapidly increases [15].

The main solution to achieve broad LSPR tunability without sacrificing the linewidth of the resonance is to vary the gold nanoparticle shape. The LSPR tunability of gold nanorods, nanoshells, nanocages, and polyhedra is described in the literature [15–19]. We focus in this chapter on the LSPR tunability of branched gold nanoparticles, namely gold nanostars.

Due to Eq. (2.1) localized surface plasmon resonances that can be obtained in noble metal nanoparticles cause enhanced optical absorption and scattering that is tunable through the visible and near-infrared. Furthermore, these resonances create large local electric field enhancements at the nanoparticle surfaces, essentially focussing light at the nanometer scale.

In addition, the LSPR position depends on the dielectric properties of the local environment that surrounds the nanoparticles and the substrate, if any, on which the particles are supported [20–22]. These features have led to many biosensing applications and well-established techniques (such as ELISA) even on smooth thin gold

layers [23]. Later the similar studies were extended to nanoparticles as it was shown in the work by Messersmith et al. [22].

In addition to wavelength-selective photon absorption and scattering, an important consequence of LSPR excitation is the local electromagnetic field enhancement that lies at the heart of surface-enhanced spectroscopy [20]. Therefore, significant interest in understanding propagating and localized surface plasmons rose from the discovery of surface-enhanced Raman scattering (SERS) [6, 24]. For the rapid development of SERS during the last two decades, advances in nanofabrication and Raman instrumentation were equally important. Nowadays, scientists from a large range of disciplines—including chemistry, physics, and material and life sciences—are increasing our knowledge on SERS and only begin to fully exploit the huge potential of this technique in numerous uni- and multidisciplinary approaches [25]. In comparison to normal Raman spectroscopy, SERS additionally requires the presence of metal nanostructures as an integral component. The optical properties of metal nanostructures are the central topic of plasmonics [25, 26]. The enhancement takes place for molecules at the metal surface. Enhancement factors can be as high as $10^{14–15}$, which are sufficient to allow even single-molecule detection of Raman scattering [25]. The shape and size of the metal nanoparticles strongly affect the strength of the enhancement because these factors influence the ratio of absorption and scattering events [27]. The SERS effect is achieved when an analyte is absorbed onto or in close proximity to a prepared metal surface. The excitation laser produces surface plasmons on the metal surface that interacts with the analyte to greatly enhance its Raman emission.

2.2 LSPR of Gold Nanostars

Branched gold nanoparticles are generally not as highly monodisperse as those with other shapes. This may reflect in multiple bands in their spectra. In some cases well-defined peaks in the ensemble spectra can be observed [15]. With varying tip geometries and asymmetric shapes, one might expect branched nanoparticles to have complicated LSPR spectral features that are lost in ensemble measurements. To test this hypothesis, scattering spectra were measured for individual gold "nanostars" by single-particle spectroscopy [28]. With the aid of alignment marks, high-resolution electron micrographs of the individual nanostars were correlated with their scattering spectra. Typical single-particle spectra consisted of multiple peaks in the visible and near-infrared [15, 28]. To find if the spectral peaks corresponded to a specific tip, an analyzer was placed on the scattered light. By tracking the peak amplitudes as a function of analyzer angle, it was found that each spectral peak from a single nanostar was polarized in a different direction, and each such direction matched that of a tip on the star. Further evidence of the correlation between the structure and spectra of gold nanostars was provided through numerical simulation of nanostar optical properties by finite difference time-domain (FDTD) analysis [15, 29]. FDTD is a brute force method which solves Maxwell's equations repeatedly along a

time-evolving spatial grid, yielding information about the far-field extinction as well as the near-field enhancements at the nanoparticle surface. FDTD simulations were carried out on a structure modeled after an individual nanostar with a measured spectrum [28]. The spectral extinction determined by FDTD was in excellent agreement with the experimental observations. In addition, analysis of the near-field enhancements confirmed that the observed resonances are localized about a single tip on the nanostar [15, 28, 30]. In both reports, field enhancements of ca. 100–250 were found at the nanostar tips. These values are similar to those calculated for nanoparticle dimer junctions, though found in an open geometry, suggesting that the nanostars could be the basis for efficient SERS substrates [15, 31].

It has already been mentioned that despite the general observation that the optical response of GNS is dominated by LSPR tip mode, a finite contribution from the core plasmon has also been proposed in terms of plasmon hybridization, a concept originally developed for gold nanoshells, but which has also been applied to GNS in connection with FDTD simulations [29, 33]. The idea is that shorter wavelengths of the core mode allow the conduction electrons to adiabatically follow the lower frequency tip plasmon oscillations. This results in antenna effect, which is responsible for an increase in the extinction cross section (a factor of fourfold with respect to the individual tip plasmons), as well as in the respective electric field enhancements [33, 34].

LSPR of complex structures such as these branched gold nanoparticles can be understood in terms of the plasmon hybridization (PH) model [32]. Thus the nanostars can be broken down into the spherical core and the elongated tips, and the LSPR of each was found by FDTD [30]. Apart from determining the LSPR wavelength, the hybridization greatly increases the overall excitation cross section and field enhancements for the nanostar tips. This antenna effect of the nanostar core may be responsible for the relatively bright and narrow scattering spectra of nanostars in the single-particle measurements [29].

The combination of dielectric properties and chemical stability GNS made them ideal substrates to study LSPRs within visible and NIR range [30]. The outstanding advances in electron microscopy techniques have recently allowed to obtain experimental evidence for the spatial distribution of LSPRs using electron energy loss spectroscopy (EELS) in a scanning transition electron microscope (STEM) [33, 35]. This technique has been applied to map the low-energy plasmon mode in GNS, which in this case can be carried out for each individual branch, showing high localization of tips [2].

Pallavicini et al. obtained monocrystalline gold nanostars and penta-twinned gold asymmetric nanostars by replacing CTAB with LSB surfactant in classical seed growth synthesis [36]. The products of seed growth synthesis have been obtained by using six different concentrations of LSB in the seed growth solutions. Absorption spectra recorded over time revealed that spectral changes are complete in less than 30 min. No further changes were obtained after 48 h.

The general appearance of the final absorption spectra is a three-band profile that features a weak “short” band centered at 520–530 nm, an “intermediate” band of variable intensity that falls in the 690–720 nm range, and a “long” band, usually the

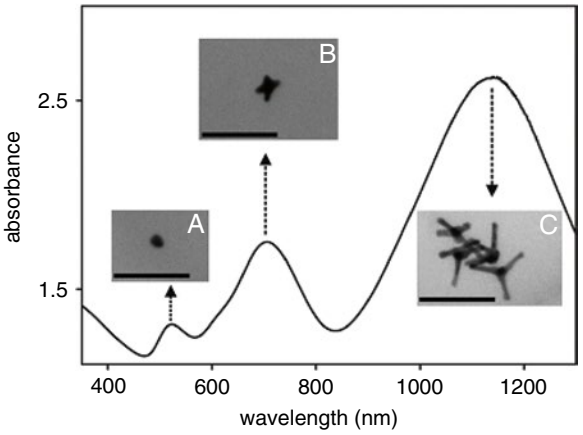

Fig. 2.1 UV/Vis absorption spectrum of a product solution [29] obtained in 0.1 M LSB. *Insets*: TEM images displaying the typologies of the objects that generate (*A*) short, (*B*) intermediate, and (*C*) long LSPR (dimension bar = 100 nm) (reproduced from Casu et al. [36])

most intense, that falls in the 750–1150 nm range (the intermediate bands appear as a shoulder of the long band if the latter falls near 750 nm). Figure 2.1 displays a representative spectrum.

The short band (A) is always found at the same wavelength range for gold nanostars and it has been attributed to a dipolar resonance localized at the central particle core [29]. The intermediate band owes itself to regular monocrystalline gold nanostars with large trapezoidal branches. The LSPR position can be controlled by means of multiple parameters such as LSB concentration, ascorbic acid concentration, and "catalytic" Ag^+ concentration. However, it was found that influence of $[Ag^+]$ on intermediate band of monocrystalline gold nanostars is poor; oscillation of the LSPR maximum was observed in the typical 690–720 nm range. It was found that for monocrystalline GNS and generally for branched nano-objects the LSPR position is proportional to the aspect ratio of branches, defined as the quotient of the branch length to its base width [37]. The long-wavelength band belongs to asymmetric nanostars that feature narrow long branches at higher aspect ratio. The authors demonstrated that, by controlling the aspect ratio in the synthetic conditions, the LSPR absorption maximum of the most abundant asymmetric GNS can be positioned in the 750–1150 NIR range.

In a more recent publication Pallavicini et al. described five-branched GNS obtained using Triton X-100 in seed growth synthesis [38]. They possessed uncommon feature of two intense LSPRs in the 600–900 and 1100–1600 nm range. Both LSPRs are able to convert laser irradiation into heat, offering two photothermally active channels in the NIR and SWIR ranges. The absorption spectra of these GNS showed three LSPRs in the 350–1800 nm range: a very weak one on a 530–560 nm (short band), an intense one in the 600–900 nm range (intermediate band), and the most intense in the 1100–1600 nm range (long band). At the reported surfactant concentration the position of the intermediate and long bands depends on the ascorbic acid concentration in the growth solution. The corresponding spectra are shown in Fig. 2.2.

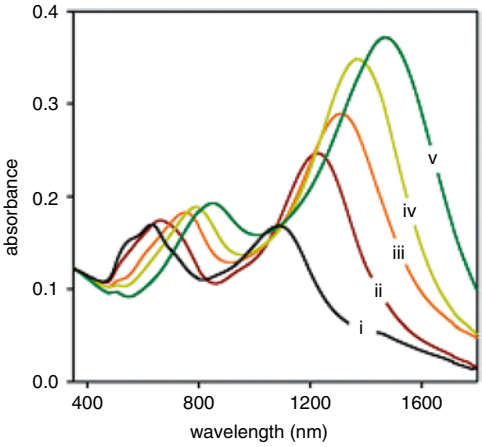

Fig. 2.2 Absorption spectra of growth solutions of GNS obtained in 0.05 M of Triton X-100 and increasing concentration of ascorbic acid: (i) 1.576×10^{-3} M; (ii) 1.773×10^{-3} M; (iii) 2.364×10^{-3} M; (iv) 2.758×10^{-3} M; (v) 3.152×10^{-3} M (reproduced from Pallavicini et al. [38])

While the short band is due to transversal LSPR to branches, the position of the intermediate and long LSPR is strictly connected to the increase of the length-to-width ratio (LWR) of branches. Therefore, for these GNS it was hypothesized that, since at least two branches are collinear, the longitudinal oscillation of the electrons along these aligned branches is responsible for the long LSPR. On the other hand, at least one branch forms an angle with all the other mutually aligned branches and therefore is not directly coupled to these. The electron oscillation along the length of these decoupled arms corresponds to a resonance at higher energy that corresponds to the intermediate LSPR band. Moreover, it was observed that a huge increase of concentration of ascorbic acid does not lead to further red shift of LSPRs but to their progressive merging into a large band spanning from 800 to 1800 nm due to the presence of multibranched objects, i.e., nanostars whose core and main branches bear sub-branches with many different lengths and widths, generating a polydisperse distribution of LWR.

For further application the GNS reported by Pallavicini et al. in refs. [36, 38] were PEGylated. PEGylation of GNS synthesized in the presence of LSB surfactant resulted in a red shift of the long and intermediate LSPR of 10 nm and 5 nm, respectively, due to the substitution of all LSB with PEG. GNS synthesized in the presence of Triton X-100 showed LSPR shifting to the red with the refractive index η (linear dependence of 175 nm and 580 nm per η unit for the intermediate and long LSPRs, respectively). All LSPRs are still photothermally active, i.e., convert efficiently radiation into heat. These GNS may thus, for instance, be used as tools for nanomedicine exploiting the 700–1000 nm transparent window of biological matter for through-tissue photothermal treatments against tumors or multidrug-resistant bacterial infections.

Nehl et al. fabricated GNS with a high yield by a modified seed-mediated, surfactant-directed method [39]. The single-particle spectra demonstrate that the plasmon resonances of single-gold nanostars are extremely sensitive to the local dielectric environment, yielding sensitivities as high as 1.41 eV photon energy shift per refractive index unit.

In the letter published in 2012 R. Rodriguez-Oliveros and J.R. Sanchez-Gil pointed out that gold nanostars are not only suitable for sensing application, but can also play the role of heat sources considerably more efficient than the nanospheres, as a result of the large extinction cross section at the LSPR [40]. By applying of the 3D Green's Theorem (surface integral equations) method for flexible-shape nanoparticles that the authors introduced the local electromagnetic field distribution on the surface of GNS at the LSPRs was calculated. From this the adsorption cross section was worked out, as needed to determine the steady-state temperature of GNS. In later publications the low energy of the LSPR of GNS was exploited to obtain hyperthermal effects from gold nanostars under NIR laser irradiation [41]. The detailed discussion of this phenomena is provided in Chap. 3 (Application of Gold Nanostars).

The LSPR features can be tailored even after synthesis. Gold nanostars can easily undergo reshaping into spherical particles by simply adding a small amount of CTAB. Such reshaping can be understood in terms of Ostwald ripening involving dissolution of weakly bound surface atoms from regions with high convex curvature and redeposition on concave areas. This process can be stopped at any time by adding silver ions, which block bromide and stabilize the surface. Because the localized surface plasmon resonance band of the nanostar colloid gradually changes during etching, stabilization of intermediate morphologies allows fine LSPR tuning, which can be exploited for plasmonic applications [42]. It was observed that when minute amounts of CTAB were added to PVP-capped GNS colloids, the GNS morphology was dramatically affected, eventually leading to complete loss of the sharp tips [42]. Control experiments showed that not only that reshaping occurs in the presence of Br^- ions, but also that the complementary presence of bromide and the surfactant chain of CTAB was essential to preferentially etch the highly curved tips. The process is slow enough, so that reshaping can be blocked at any stage, thus allowing a tight control over the morphology and fine-tuning of the LSPR tip mode in the colloid. The initially prepared GNS colloid displayed a well-defined LSPR band with a maximum absorbance at 781 nm (tip mode), together with a weaker shoulder around 545 nm corresponding to the core mode. The authors proposed a mechanism in which initial cleaning of PVP from the GNS surface allows CTAB adsorption on the tips, and causes the etching of weakly bound Au atoms from the sharp convex zones at tip ends. These released Au–CTAB complexes act as transporters and redeposit on more favorable adsorption sites at surface defects present in concave curvature areas where the tips join with the GNS core. The LSPR was in fact shifted to the green side of the spectrum. The reshaping process can be completely stopped by simply adding Ag^+ ions, which allowed to obtain GNS with any arbitrary intermediate morphology and LSPR wavelength.

It has already been shown that polyvinylpyrrolidone dispersed in DMF solvent medium acts as a unique candidate for realization of this 3D complex branched metal nanostructures even under normal conditions. Controlled addition of propanol to DMF brings about significant changes in the morphology of these gold nanostars visualized through gradual blue shifting of the LSPR from 920 to 600 nm [41]. Modified interaction between DMF and PVP due to addition of propanol

results in fine-tuning of LSPR and correlates with morphological changes. Cathodoluminescence spectroscopy and imaging under a high-resolution scanning electron microscope allowed to locally and selectively excite and investigate the plasmonic properties of a multibranched GNS on a silicon substrate [43]. This method allowed to map the local density of different plasmon modes associated with optical states from the nanostars with a spatial resolution down to a few nanometers, both in the spatial and spectral domain. FDTD numerical simulations were performed to support the experimental observations. The authors also investigated the effect of the substrate on the plasmonic properties of these complex-shaped nanostars. Moreover, the authors showed that local morphology, associated with substrate effects, leads to spectral changes in the plasmonic response of the nanostars. The relative position of the nanostar tips with respect to the substrate strongly modified the tip-substrate interaction, thus leading to spectral shifts of the tip of LSPR. Furthermore, the relative tip-core LSPR contributions were investigated as a function of the tip angular configuration. It was shown that spectra of nanostars with the tips pointed toward the electron beam are dominated by core LSPR. All together the experiments and the simulations results demonstrated that long tips in multibranched GNS could serve as efficient emitters at optical frequencies that can be precisely tuned by engineering the tip-substrate separation.

Liz-Marzan et al. developed the synthesis of GNS with well-defined optical response [44]. A systematic study was required to optimize the control over the specific morphology and more importantly over the size of the nanostars, since, for example, also the size of the core plays a critical role in the focalization of electric field at the tips. It has been demonstrated through FDTD calculations that the Au nanostar cores act as nanoantennae, enhancing the extinction cross section (a factor of 4) and the electric near field originating from the tip plasmon mode [30]. Thus, the authors systematically studied the effect of core size on nanostar formation, by using Au nanoparticles with diameters of 3, 15, and 30 nm as seeds [45]. Additionally, the influence of other parameters such as the seed composition, either a single-crystal Pt or polycrystalline Au seeds, the prereduction of Au^{3+} to Au^{+} before seed addition, and the reaction temperature were also investigated. The refractive index sensing capability of these nanoparticles was studied through two parameters, the absolute plasmon shift due to changes in the dielectric environment and the figure of merit (FOM). As it was mentioned before as a consequence of the confined electric field enhancement at the tips, the spectral positions of the LSPRs of gold nanostars are expected to depend strongly on the dielectric environment around the tips. In the paper published in *ACS Nano* in 2010 this dependency was characterized at the single-nanoparticle level and applied to the detection of biomolecular interactions [4]. In this study single-gold nanostars were located and investigated spectroscopically in a dark-field microscope equipped with a spectrometer coupled to a liquid-nitrogen-cooled CCD camera. The nanostars presented multiple LSPRs. In all cases the nanostars presented one weak and nearly-polarization-independent resonance at 540–560 nm which was ascribed as to the nanostar core. The longer wavelength resonances are polarization dependent and are attributed to the interaction between tips and core. It was noted that the peak around 610 nm presents a

weaker polarization dependency and then expected for a tip or core-tip interaction resonance. A possible explanation is the spectral superposition of tip or tip-core resonances that correspond to similar but differently oriented tips. To test the magnitude of the spectral shift of the LSPRs upon bulk changes in the refractive index, the spectra of individual nanostars were measured in air, water, and glucose solutions at different concentrations. The Liz-Marzan group quantified the shift of each peak with a four-peak (Lorentzian) fit of the spectrum. Since the spectral position of the resonances varies from one nanostar to another, in order to characterize the typical behavior of the nanostars, the shape of the resonances from different nanostars peaking between 650 and 750 nm was averaged. The average sensitivity was 218 nm/RIU. Considering the average fwhm of 43 nm for the resonances computed, the authors obtained a FOM for the sensitivity of 5, which is within the range of FOM values reported for Au nanostars, above that of Au bipyramids and much higher than those of other Au nanomorphologies (0.6 for spheres, 1.5 for nanocubes, 2.6 for nanorods) [28, 46].

In summary we have described briefly the features of LSPRs of gold nanostars in terms of the position of these resonances and possibilities of their fine control, which give wide opportunities to apply GNS as sensing platforms and hyperthermal treatment. These applications are discussed in Chap. 3. Another significant optical property of GNS, namely surface-enhanced Raman scattering (SERS), is discussed in next subchapter.

2.3 Surface-Enhanced Raman Scattering of GNS

The electromagnetic enhancement due to LSPRs is a major contributor to the phenomena of SERS [32, 47, 48]. SERS spectroscopy is considered as one of the most powerful analytical techniques for identification of molecules, since it provides their complete vibrational information of the molecular system under study. The Raman enhancement is the combined effect of the local increase in electric field when the molecule is illuminated by light at its resonant wavelength λ_{in} and the increase of the strength of the Raman dipole-emission transition at a longer wavelength λ_{out} [44, 49–51].

Because the focalization of the plasmonic electromagnetic field at the tips of gold nanostars gives rise to extraordinary field enhancements, compared to those in metallic spheres, nanostars are ideal candidates for application as single-particle SERS substrates. SERS enhancement factor can be calculated using boundary element method (BEM) [52]. Calculations for a gold nanoparticles with one or two tips, mimicking a nanostar, have shown not only that the enhanced electric field localized at the tips is indeed responsible for the SERS efficiency but also that enhancement factors at the tip resonance wavelength can even be higher than those for a sphere dimer, which has been long considered the paradigm SERS substrate, because of the formation of a “hot spot” at the gap between spheres due to plasmon

coupling [33, 53]. The enhancement is averaged over random positions of the sampled molecule on the particle surface and over random orientations of the excitation and emission dipoles [37].

Indeed, it was also observed that gold nanostars (though this applies to silver too) display stronger SERS activity than spheres or even rods. Nevertheless, it must be still considered and be taken into account that the large SERS signals only arise from the molecules that are attached to the tips, whereas those bound far from the tips experience much lower electromagnetic fields [54]. This large Raman signal amplification has allowed the observation of SERS from molecules absorbed onto GNS with no need for the formation of hot spots within nanoparticle aggregates, which makes this system extremely appealing for Raman imaging application [3, 55]. Therefore, as it was mentioned in Chap. 1 the limitations of fluorescent dyes experienced in some imaging techniques could be overcome by means of SERS from the single nanostars.

Hot spots can also be created via aggregation process between nanostars, resulting in even higher enhancement factors compared to those observed on aggregated spheres [56]. It should be noted that aggregation process leads to a random distribution of the hot spots, where the intensities of the enhanced near field vary significantly, depending on the specific morphological details at each site [57].

Liz-Marzan et al. calculated the enhancement ratio between the Raman signal for molecules attached to the particles and the signal for free-standing molecules (Eq. 2.2) [40]:

$$\mathrm{SERS} = \frac{\int_{\text{surface}} d^2\mathbf{s}\Gamma\left(\lambda_{\text{out}}\right)}{A\Gamma_0\left(\lambda_{\text{in}}\right)\Gamma_0\left(\lambda_{\text{out}}\right)}, \tag{2.2}$$

where the integral is extended over the surface of the particle, A is the area of the latter, $\Gamma(\lambda)$ is the wavelength- and position-dependent emission rate of a dipole at the particle surface, and $\Gamma_0(\lambda)$ is the emission rate for the same dipole in air. The excitation and observation wavelengths are λ_{in} and λ_{out}.

It should also be noted that the calculations were made for one particle with two tips: for particles containing a large number of tips a larger enhancement is to be expected [33].

The experimental demonstration of the high SERS activity that can be reached on GNS tips has been provided through controlled experiments where gold nanostars were uniformly assembled on a smooth gold film, previously decorated with a self-assembled monolayer of alkanethiols in which there was a low concentration of analyte (an aromatic dithiol) [2]. This configuration ensures that the nanostars selectively attach to the analyte through its free thiol group, and the attachment would occur at the tips because of steric reasons. The small gap formed between the tip and the film was found to give rise to field enhancements that are around two orders of magnitude larger than these in regular hot spots, and allowed quantitative single-molecule detection through “single-particle” SERS. This experiment is schematically shown in Scheme 2.2.

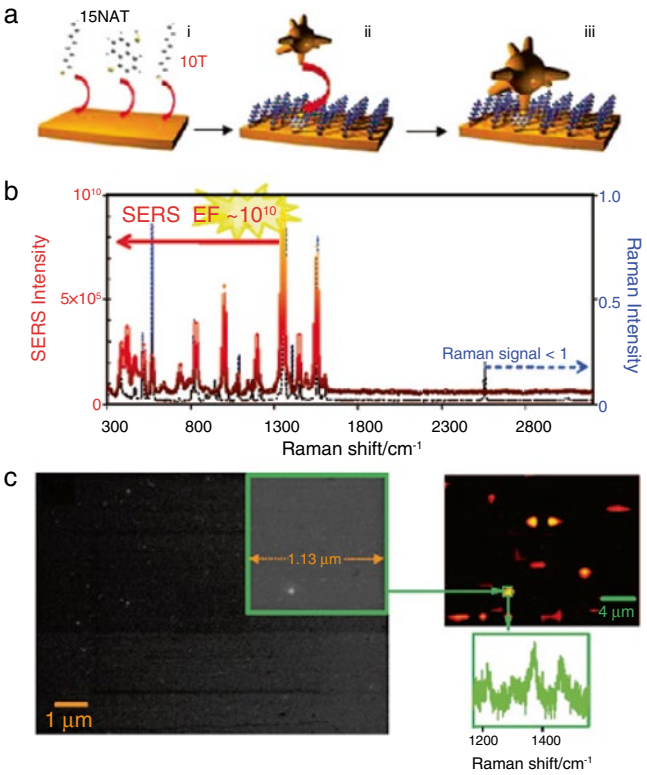

Scheme 2.2 (**a**) Sketch of deposition of single nanostars onto single molecules through thiol binding, exclusively onto 1,5-naphthalenedithiol (15NAT), which is also the optically active analyte, diluted in 1-octanethiol self-assembled monolayer. (**b**) Experimental bulk Raman spectrum of the concentrated solution of 15NAT and SERS spectrum of the same molecule located in the confined region between a nanostar and gold film, showing an overall enhancement factor larger then 10^{10}. (**c**) *Left*: SEM images of the nanostar/film system, showing less then 1 bound nanostar per μm^2. Right: SERS mapping of the same substrate and SERS spectrum collected within the *highlighted region* in the SEM image (reproduced from Guerrero-Martinez et al. [33])

Although this approach was initially restricted to SERS of molecules that can chemically react with the gold surface and the nanostar tip, analytical applicability of this sandwich configuration was later demonstrated by simply exploiting the confinement achieved by casting the probe molecules (with arbitrary chemical composition) on the gold substrate [33, 54]. The parallel detection of two different analytes was obtained on a similar system using long thorned wires rather than simple nanostars [58].

The controlled synthesis of high-yield gold nanostars of varying sizes, their characterization, and use in surface-enhanced Raman scattering measurements were reported by Khoury and Vo-Dinh [37]. The nanostar efficacy as substrates for SERS was correlated to the GNS size. As the overall star size increases (as measured

from TEM images), so does the core size, the number of branches, and branch aspect ratio. The number of branch tips per star surface area decreases with increasing size. The stars become more inhomogeneous in shape, although their yield is high and the overall size remains homogeneous. Variations in star size are also accompanied by shifts of the long plasmon band in the NIR region, which hints toward tuning capabilities that may be exploited in specific SERS applications. The measured SERS enhancement factors suggest an interesting correlation between nanostar size and SERS efficiencies, and were relatively consistent across different star samples, with the enhancement factor estimated as high as 5×10^3 for 52 nm nanostars excited at 633 nm.

In the paper published in 2013 Osinkina et al. presented a reliable and reproducible approach for the synthesis of gold nanostar arrays with high lateral order. The samples displayed a homogeneous SERS enhancement over an area of several hundreds of square micrometers [59]. The authors demonstrated also the applicability of this SERS-active platform for chemical imaging and spectroscopy by performing pH-sensitive Raman mapping of mercaptobenzoic acid (MBA) molecules that are adsorbed to the nanostar array. The SERS signals of MBA measured on the nanostar array were compared with the intensity of the Raman signal measured in bulk to determine the average enhancement factor (EF). The homogeneous EF of $\sim 10^5$ over an area of several hundreds of square micrometers illustrates the great potential of this nanostar substrate for label-free chemical analysis and spectroscopy.

Pei et al. developed in 2013 highly sensitive SERS-based sandwich immunoassay by combining two gold nanostar constructs: densely packed self-assembled substrates of gold nanostars and immuno-labeled nanostar aggregates [60]. Taking advantage of the electromagnetic field coupling between tips of adjacent individual nanostars, the self-assembled substrate of gold nanostars exhibited a better SERS performance than that of gold nanoparticles. On the other hand, the immuno-aggregates made of gold stars also showed an improved SERS activity compared to those made of gold nanoparticles. Thus, by combining the self-assembled substrates of gold nanostars and immuno-aggregates of gold nanostars, highly sensitive sandwich immunoassays were obtained. The experimental results show that there is a linear correlation between the concentration of antigens and the prominent peak intensity of SERS signals. In a paper published by Liz-Marzan et al. in 2014 gold nanostar monolayers were immobilized on transparent, flexible polydimethylsiloxane substrates and their refractive index sensitivity and SERS performance were studied [61]. These substrates exhibit high SERS activity toward thiolated and non-thiolated molecules.

Liz-Marzan et al. reported recently design, synthesis, and application of small highly bright, star-shaped SERS encoded single nanoparticles with the ability of providing an optical signal upon excitation with near-infrared light [62]. The resulted particles were colloidally stable and fully biocompatible and can be internalized into living cells for intracellular imaging. The optical efficiency of encoded nanostars versus nanospheres was probed by studying ultrathin films in a confocal micro-Raman system. Notably, samples exposed to nanostars showed a remarkable SERS intensity while basically no signal was obtained from those treated with

nanospheres even though the number of spheres internalized was considerably larger. Such efficiency difference is consistent with both the different LSPR energy between both types of encoded nanoparticles and with the field concentration at the apex of the tips of nanostars. It was also notable that, after mapping the samples, no visible signal of damage was observed in the films, indicating that NIR laser lines are an adequate source of light for long-term SERS experiments on biological samples.

As it has been shown, plasmonic gold nanostars offer a new platform for surface-enhanced Raman scattering. However, due to the presence of organic surfactant on the nanoparticles, SERS characterization and application of nanostar ensembles in solution have been challenging. Vo-Dinh et al. applied newly developed surfactant-free nanostars for SERS characterization and application [63]. The SERS enhancement factors of silver spheres, gold spheres, and nanostars of similar sizes and concentration were compared. Under 785 nm excitation, nanostars and silver spheres have a similar enhancement factor (EF), and for both the EF is much higher than that of gold spheres. Having plasmon matching the incident energy and multiple "hot spots" on the branches bring forth strong SERS response without the need to aggregate. Intracellular detection of silica-coated SERS-encoded nanostars was also demonstrated in breast cancer cells [63].

Hybrid materials formed by plasmonic nanostructures and J-aggregates provide a unique combination of highly localized and enhanced electromagnetic field in metal constituent with large oscillator strength and extremely narrow exciton band of the organic component. The coherent coupling of localized plasmons of the multispiked gold nanoparticles (nanostars) and excitons of JC1 dye J-aggregates results in a 260 meV Rabi [64]. The SERS spectrum of the hybrid nanostructures of gold nanostars and the JC1 J-aggregates showed identical features which are enhanced by more than an order of magnitude with respect to the conventional Raman spectrum of J-aggregates. Raman micromapping of hybrid gold nanostar/J-aggregate complexes dispersed over a glass slide directly demonstrates the strong enhancement of the Raman signal at the location of agglomerates.

Surface-enhanced Raman scattering spectroscopy performed with crystal violet as the probe molecule confirms continued strong SERS activity for gold nanostars after the iron oxide coating as it was reported by Esentruk and Walker [65]. Having both magnetic and plasmonic properties in one NP system makes these particles suitable for various bio-analytical applications such as biomolecule separation, sensing, and magnetic imaging. As discussed in detail in the next chapter, SERS offers unique advantages as an analytical tool with a high selectivity and sensitivity without matrix interference. For general understanding of the potentialities of SERS spectroscopy a couple of examples are discussed in this chapter. SERS-tagged silver/gold nanostars, coated with a silica shell encapsulating Nile blue A, were designed and used as potential platforms for SERS imaging [66]. For comparison and visualization of the nanoparticles, the samples were coated with a carbon layer and visualized in a scanning electron microscope. The authors demonstrated that SERS provides advantages over SEM. The nanoparticles can be visualized by SERS without coating of the samples. In addition, no vacuum is needed to image the nanoparticles, and the excitation laser line (633 nm) used applies a lower energy for

detection of nanoparticles than the electron beam of the SEM. A SERS-active gold nanostar layer on the surface of ITO glass slip has been prepared by a low-cost electrostatically assisted APTES-functionalized surface assembly method for SERS analysis [67]. The two-dimensional morphology of the SERS substrate was examined by scanning electron microscopy. Comparative analysis revealed that the optical characteristics and SERS efficiency of these substrates varied as a function of nanostar morphology. It was found that the substrate assembled with the longest branches of nanostars generated the best SERS efficiency, under the excitation source at 785 or at 633 nm. The potential use of these substrates in detection applications was also investigated by using Nile blue A and rhodamine 6G.

The SERS enhancement factor could be further increased by creating a core–satellite system in which metal nanoparticles are attached to a central metallic core. SERS measurements of core–satellite systems both using spherical nanoparticles and mixtures of nanorods and spheres were reported [68, 69]. Liz-Marzan et al. proposed that a core–satellite design comprising gold nanostar cores may offer a promising direction for the development of ultrahigh enhancing SERS substrates [70]. In this study they assembled core–satellite clusters comprising a central ∼65 nm gold nanostar surrounded by 12 nm spherical gold nanoparticles at different concentrations, which allowed to study the enhancing efficiency of this system. The results indicated that the hot spot formation is almost independent of GNS tip morphology and GNP size. The experimental results were confirmed by theoretical simulations based on a model that accurately reproduces the geometrical features of the real nanostructures. Therefore, it was proposed that this nanostar–satellite system has a great potential not only as a model system to better understand hot spot formation but also for applications such as sensing.

Summarizing this chapter, the LSPR of gold nanostars and their surface-enhanced Raman scattering are the key properties that allow a variety of possible applications of GNS as sensing platforms and for hyperthermal treatments. General biomedical applications of GNS-based platforms are provided in the next chapter.

References

1. Feng H et al (2007) Plasmon resonances of gold nanostars. Nano Lett 7:729–732
2. Rodríguez-Lorenzo L et al (2009) Zeptomol detection through controlled ultrasensitive surface-enhanced Raman scattering. J Am Chem Soc 131:4616–4618
3. Hrelescu C et al (2009) Single gold nanostars enhance Raman scattering. Appl Phys Lett 94:153113
4. Dondapati S et al (2010) Label-free biosensing based on single gold nanostars as plasmonic transducers. ACS Nano 4:6318–6322
5. Mulvaney P (1996) Surface plasmon spectroscopy of nanosized metal particles. Langmuir 12:788–800
6. Willets KA, Van Duyne RP (2007) Localized surface plasmon resonance spectroscopy and sensing. Annu Rev Phys Chem 58:267–297
7. Mie G (1908) Contributions to the optics of turbid media, especially colloidal metal solutions. Ann Phys 25:377–445

8. Comin A, Manna L (2014) New materials for tunable plasmonic colloidal nanocrystals. Chem Soc Rev 43:3957–3975
9. Sherry LJ et al (2005) Localized surface plasmon resonance spectroscopy of single silver nanocubes. Nano Lett 5:2034–2038
10. Haynes CL, Van Duyne RP (2001) Nanosphere lithography: a versatile nanofabrication tool for studies of size-depended nanoparticles optics. J Phys Chem B 105:5599–5611
11. Jensen TR et al (2000) Nanosphere lithography: tunable localized surface plasmon resonance spectra. J Phys Chem 104:10549–10556
12. Klar T et al (1998) Surface Plasmon resonances of in single metallic nanoparticles. Phys Rev Lett 80:4249–4252
13. Barnes WL, Dereux A, Ebbesen TW (2003) Surface plasmons subwavelength optics. Nature 424:824–830
14. Ghosh SK et al (2004) Solvents and ligand effects on the localized surface plasmon resonance (LSPR) of gold colloids. J Phys Chem B 108:13963–13971
15. Nehl CL, Hafner JF (2008) Shape-dependent plasmon resonances of gold nanoparticles. J Mater Chem 18:2415–2419
16. Noguez C (2007) Surface plasmons on metal nanoparticles: the influence of shape and physical environment. J Phys Chem 111:3806–3819
17. Oldenburg SJ et al (1998) Nanoengineering of optical resonances. Chem Phys Lett 288:243–247
18. Chen JY et al (2005) Gold nanocages: engineering their structure for biomedical applications. Adv Mater 17:2255–2261
19. Iglesias-Sanches A et al (2006) Synthesis and optical control of gold nanodecahedra with size control. Adv Mater 18:2529–2534
20. Malinsky MD et al (2001) Nanosphere lithography: effect of substrate on the localized surface plasmon resonance spectrum of silver nanoparticles. J Phys Chem 105:2343–2350
21. Hilger A et al (2000) Surface and interface effects in the optical properties of silver nanoparticles. Eur Phys J D Atom Mol Opt Phys 10:115–118
22. Messersmith RE et al (2013) Using the localized surface plasmon resonance of gold nanoparticles to monitor lipid membrane assembly and protein binding. J Phys Chem C 117: 26725–26733
23. Bantz KC et al (2011) Recent progress in SERS biosensing. Phys Chem Chem Phys 13:11551–11567
24. Albercht MG, Greighton GA (1977) Anomalously intense Raman spectra of pyridine at a silver electrode. J Am Chem Soc 99:5215–5217
25. Schlucker S (2014) Surface enhanced Raman spectroscopy: concept and chemical applications. Angew Chem 53:4756–4795
26. Shahbazyan TV, Stoskman MI (eds) (2014) Plasmonics: theory and application. Springer, London
27. Lu H et al (2011) Seed-mediated plasmon-driven regrowth of silver nanodecahedrons. Plasmonics 7:167–173
28. Nehl CL, Liao HW, Hafner JH (2006) Optical properties of star-shaped gold nanoparticles. Nano Lett 6:683–688
29. Bakr OM, Wunsch BH, Stellaci F (2006) High-yield synthesis of multi-branched urchin-like gold nanoparticles. Chem Mater 18:4894–4901
30. Hao F et al (2007) Plasmon resonance of gold nanostars. Nano Lett 7:729–732
31. Oubre C, Nordlander P (2005) Finite difference time-domain studies of optical properties of nanoshell dimers. J Phys Chem 109:10042–10051
32. Prodan E et al (2003) A hybridization model for the Plasmon responses of complex nanostructures. Science 302:419–422
33. Guerrero-Martinez A et al (2011) Nanostars shine bright to you: colloidal synthesis, properties and application of branched metallic nanoparticles. Curr Opin Colloid Interface Sci 16:118–127
34. Nelayah J et al (2010) Two-dimensional quasistatic stationary short range surface plasmons in flat nanoprisms. Nano Lett 10:402–407

35. Hao E et al (2004) Synthesis and optical properties of "branched" gold nanocrystals. Nano Lett 4:327–330
36. Casu A, Cabrini E et al (2012) Controlled synthesis of gold nanostars by using zwitterionic surfactant. Chem Eur J 18:9381–9390
37. Khoury CG, Vo-Dinh T (2008) Gold nanostars for surface-enhanced Raman scattering: synthesis, characterization and optimization. J Phys Chem C Nanometer Interfaces 112: 18849–18859
38. Pallavicini P, Dona A et al (2013) Triton X-100 for three-plasmon gold nanostars with two photothermally active NIR (near IR) and SWIR (short-wavelength IR) channels. Chem Commun 49:6265–6267
39. Nehl CL, Liao H, Hafner JF (2006) Plasmon resonant molecular sensing with single gold nanostars. Proc SPIE 6323:63230G–63231G
40. Oliveros-Rodriguez R, Sanchez-Gil A (2011) Gold nanostars as thermoplasmonic nanoparticles for optical heating. Optics express 20: 621–626 optical hyperthermia. Nano Lett 13: 2004–2010
41. Kedia A, Kumar PS (2013) Gold nanostars reshaping and plasmon tuning mechanism. AIP Conf Proc 232:1512
42. Rodriguez-Lorenzo L et al (2012) Reshaping and LSPR tuning of Au nanostars in the presence of CTAB. J Mater Chem 21:11544–11549
43. Das P et al (2013) Local electronic beam excitation and substrate effect on the plasmonic response of single gold nanostars. Nanotechnology 24:405704
44. Kumar PS et al (2008) High-yield synthesis and optical response of gold nanostars. Nanotechnology 19:1–5
45. Barbosa S et al (2010) Tuning size and sensing properties in colloidal gold nanostars. Langmuir 26:14943–14950
46. Chen H et al (2008) Shape- and size- dependent refractive index sensitivity of gold nanoparticles. Langmuir 24:5233–5237
47. Moskovits M (1985) Surface-enhanced spectroscopy. Rev Mod Phys 57:783–826
48. Dignam MJ, Moscovits M (1973) Influence of surface roughness on the transmission and reflectance spectra of adsorbed species. J Chem Soc Faraday Trans 2(69):65–78
49. Kneipp K, Kneipp H, Kneipp J (2006) Surface-enhanced Raman scattering in local optical fields of silver and gold nanoaggregates. From single-molecule Raman spectroscopy to ultrasensitive probing in living cells. Acc Chem Res 39:443–450
50. Guerrini L, Graham D (2012) Molecularly-mediated assemblies of plasmonic nanoparticles for surface-enhanced Raman spectroscopy applications. Chem Soc Rev 41:7085–7107
51. Lee SJ et al (2007) Surface-enhanced Raman spectroscopy and nanogeometry: the plasmonic origin of SERS. J Phys Chem 111:17985–17988
52. Myroshnychenko V et al (2008) Modelling the optical response of gold nanoparticles. Chem Soc Rev 37:1792–1805
53. Brus L (2008) Noble metal nanocrystals: plasmon electron transfer photochemistry and single molecule raman spectroscopy. Acc Chem Res 41:1742–1749
54. Rodriguez-Lorenzo L et al (2010) Surface enhanced Raman scattering using star-shaped gold colloidal nanoparticles. J Phys Chem C 114:7336–7340
55. Allgeyer ES et al (2009) Optical signal comparison of single fluorescent molecules and Raman active gold nanostars. Nano Lett 9:3816–3819
56. Esenturk NE, Walker ARH (2009) Surface-enhanced Raman scattering spectroscopy via gold nanostars. J Raman Spectrosc 40:86–91
57. Xu H et al (1999) Spectroscopy of single hemoglobin molecules by surface enhanced Raman scattering. Phys Rev Lett 83:4357–4360
58. Pazos-Perez N et al (2010) Growth of sharp tips on gold nanowires leads to increased SERS activity. J Phys Chem Lett 1:24–27
59. Osinkina L et al (2013) Synthesis of gold nanostar arrays as reliable, large-scale homogeneous substrates for surface-enhanced Raman scattering imaging and spectroscopy. J Phys Chem 117:22198–22202

60. Pei Y et al (2013) Highly-sensitive SERS-based immunoassay with simultaneous utilization of self-assembled substrates of gold-nanostars and aggregates of gold nanostars. J Mater Chem B 1:3992–3998
61. Shiohara A et al (2014) Solution processed/polydimethylsiloxane/gold nanostars flexible substrates for plasmonic sensing. Nanoscale 6:9817
62. Rodriguez-Lorenzo L et al (2011) Intracellular mapping with SERS-encoded gold nanostars. Integr Biol 3:922–926
63. Yuan H et al (2013) Spectral characterization and intracellular detection of surface-enhanced Raman scattering (SERS)-encoded plasmonic gold nanostars. J Raman Spectrosc 44: 234–239
64. Melnikau D et al (2013) Strong plasmon exciton coupling in a hybrid system of gold nanostars and J-aggregates. Nanoscale Res Lett 8:134
65. Esenturk NE, Walker ARH (2013) Gold nanosrars@iron oxide core-shell nanostructures: synthesis, characterization, and demonstrated surface-enhanced Raman scattering properties. J Nanopart Res 15:1364
66. Geerc C et al (2014) Visualisation of gold/silver nanostars in wood by surface enhanced Raman spectroscopy. In: Proceedings IRG annual meeting, IRG/WP 14-30653
67. Su Q et al (2011) A reproducible SERS substrate based on electrostatically assisted APTES-functionalized surface-assembly of gold nanostars. ACS Appl Mater Interface 3:1873–1879
68. Hoon KN, Joon LS, Moskovits M (2011) Reversible tuning of SERS hot spots with aptamers. Adv Mater 23:4152–4156
69. Yuling W, Kyuwan L, Irudayaraj J (2010) SERS aptasensor from nanorod-nanoparticle junction for protein detection. Chem Comm 46:613–615
70. Shiohara A et al (2015) Plasmon modes and hot spots in gold nanostars-satellite clusters. J Phys Chem B 119(20):10836–10843. doi:10.1021/jp509953f

Chapter 3
Applications of Gold Nanostars: Nanosensing, Thermal Therapy, Delivery Systems

Piersandro Pallavicini, Elisa Cabrini, Mykola Borzenkov, Laura Sironi, and Giuseppe Chirico

Abstract This chapter focuses on the most relevant applications of GNS in life science. The versatility of the GNS functionalization is combined with their optical properties to provide promising and prospective approaches in a variety of biomedical fields. Nanosensing assays, thermal treatments, and delivery systems based on GNS are discussed in this chapter.

Keywords SERS-based sensing • Hyperthermia • Photothermal effect • Smart delivery

Functionalized gold nanoparticles with controlled geometrical and optical properties are the subject of intensive studies and biomedical applications, including genomics, biosensors, immunoassays, clinical chemistry, laser phototherapy of cancer cells and tumors, and delivery platforms. In these fields targeted delivery of drugs, DNA, and antigens is coupled to optical bioimaging and the possibility to monitor cells and image details of tissues with the use of state-of-the-art detection systems [1]. Nonspherical gold nanoparticles are particularly interesting due to their capability to release locally heat with large efficiency when they are irradiated in the NIR region of the spectrum [2]. In addition their size and the shape anisotropy essentially determine the position and the amplitude of the NIR-localized surface plasmon resonance [3]. The shape of the gold nanostars (GNS), in particular, can be tuned from the shape of sea urchin to that of planar, highly regular penta-branched stars [4]. The NIR-localized surface plasmon resonance of GNS can be consequently tuned in a wide NIR range up to 1250 nm by varying the axial ratio of protruding branches and multiple LSPR band in the NIR can also be obtained [4]. The possibility to easily decorate the surface of GNS, in combination with their optical properties

P. Pallavicini • E. Cabrini
Department of Chemistry, University of Pavia, Viale Taramelli 12, Pavia 27100, Italy

M. Borzenkov (✉) • L. Sironi • G. Chirico
Department of Physics, University of Milano-Bicocca, Piazza Della Scienza 3, Milan 20216, Italy
e-mail: mykola.borzenkov@unimib.it; giuseppe.chirico@mib.infn.it

G. Chirico et al., *Gold Nanostars*, SpringerBriefs in Materials,
DOI 10.1007/978-3-319-20768-1_3

(LSPR and surface-enhanced Raman spectroscopy (SERS)), provides promising and prospective approaches of application in a variety of biomedical fields. The applications of GNS for sensing assays, thermal treatments, and target delivery are reviewed in this chapter.

3.1 Application of GNS for Sensing Assays

GNS can display tunable optical properties in the visible and NIR, which lead to strong electromagnetic field enhancement at their tips. Most of the applications of GNS for highly sensitive assays are based on the exploitation of LSPR and the correlated SERS signal. In particular, SERS provides a promising method for the detection of various biomarkers (DNA, RNA, protein, etc.) due to its high sensitivity, specificity, and capability for multiple analyte detection.

Firstly, we focus on SERS-based assays and start this review from a recently published example of the exploitation of the sensitivity of SERS-based chemical sensing [5].

In this work [5] the detection was obtained on GNS immobilized on a gold substrate via a Raman-silent organic tether. The GNS serve as the SERS substrate and facilitate the chemical sensing of analytes that can either be chemisorbed or physisorbed on the nanostars. Reported SERS substrates were capable of detecting chemisorbed 4-mercaptobenzoic acid at a concentration as low as 10 fM with a reproducible SERS enhancement factor of 10^9, and enable the semiquantitative multiplexed identification of analytes from mixtures in which they have been dissolved in variable stoichiometry. Moreover, also physisorbed analytes, such as crystal violet, could be detected with an excellent signal-to-noise ratio, hence serving as a versatile platform for the chemical identification of in principle any molecular analyte. In another more simple approach to SERS-based detection on GNS, Esenturk and Walker tested GNS for Raman enhancement using two target molecules, 2-mercaptopyridine and crystal violet [6]. They observed strong and reproducible enhancement of the Raman signal from 2-mercaptopyridine and crystal violet molecules in colloidal GNS solutions. Anisotropic, 3D nanostars produced much stronger enhanced Raman modes than nanospheres for both probe molecules. Although the Raman enhancement by nanostars and nanorods was similar for 2-mercaptopyridine at all studied concentrations of the molecule, it was significantly higher for nanostars compared to nanorods for crystal violet, in particular at low concentrations of the analyte.

A major breakthrough in online sensing was provided by Liz-Marzan et al., who immobilized GNS monolayers on transparent, flexible polydimethylsiloxane substrates, and studied their refractive index sensitivity and SERS performance [7]. They reported generalized application of GNS for ultrasensitive identification of molecules, based on both localized surface plasmon resonance and SERS. The applicability of such substrates for LSPR-based molecular sensing was demonstrated through the detection of a model analyte, mercaptoundecanoic acid. The authors further demonstrated SERS-based pesticide detection on fruit skin, by simply covering

the fruit surface at the contaminated site with the flexible plasmonic substrate. The transparency of the substrate allowed SERS detection through backside excitation, thereby facilitating practical implementation.

Gas-phase sensing could be obtained on a new SERS platform based on the deposition of ordered extended lines of poly-*N*-isopropylacrylamide (pNIPAM)-coated nanostars over large areas [8]. This system provided high and homogeneous SERS intensities, and simultaneously traps organic chemical agents as pollutants from the gas phase. pNIPAM-coated GNS were organized into parallel linear arrays. The optical properties of the fabricated substrates were investigated, and applicability for advanced sensing was demonstrated through the detection in the gas phase of pyrene traces, a well-known polyaromatic hydrocarbon.

Due to its excellent sensitivity, SERS has been capable also to achieve the single-molecule detection limit. Local pH environment has been identified to be a potential biomarker for cancer diagnosis since solid cancer is characterized by highly acidic environments [9]. An NIR SERS nanoprobe based on GNS for pH sensing was developed for future cancer detection. SERS spectrum of pH reporter under various pH environments was monitored and used for pH sensing. Furthermore, density functional theory (DFT) calculation was performed to investigate Raman spectra changes with pH at the molecular level. This study demonstrated that SERS is a sensitive tool to monitor minor molecular structural changes due to local pH environment for cancer detection.

Vo-Dinh et al. provided recently an overview of developments and applications of SERS nanosensors and nanoreporters in their laboratory for applications in biochemical monitoring, medical diagnostics, and therapy [10].

The SERS nanosensors can be used in various applications including pH sensing, protein detection, and gene diagnostics. The authors showed that GNS provide an excellent multimodality theranostic platform, combining Raman and SERS with two-photon luminescence imaging as well as photodynamic therapy, and photothermal therapy. The possibility to combine the spectral selectivity and the high sensitivity of the SERS process with the inherent molecular specificity of bioreceptor-based nanoprobes provides a unique multiplex and selective diagnostic modality. Several examples of optical detection using SERS in combination with other detection and treatment modalities are also discussed in this overview to illustrate the usefulness and potential of SERS nanosensors and nanoreporters for medical applications.

Khoury and Vo-Dinh investigated in 2008 the effect of the size of nanostars when they are used as substrates for SERS [11]. The measured SERS enhancement factors suggest an interesting correlation between the nanostar size and the SERS efficiencies, and were relatively consistent across different star samples, with the enhancement factor estimated as 5000 averaged over the 52 nm nanostars for 633 nm excitation. Solution-based SERS measurements were performed using the Raman-active dye *p*-mercaptobenzoic acid, demonstrating the use of this new nanostructure as a useful SERS-active substrate.

The Vo-Dinh research group investigated also the SERS enhancement factor (EF) of surfactant-free nanostars and applied the silica-coated SERS probe for intracellular detection [12]. The in vitro SERS detection was demonstrated by using

silica-coated SERS-encoded GNS incubated with BT549 breast cancer cells. SERS probes accumulated primarily in the cytoplasm, displaying a high SERS signal upon examination. The authors additionally confirmed that having a high EF without the need for aggregation, nanostars thus have a strong potential in sensing and imaging.

A more recent study of intracellular applications of GNS-SERS-based assay was reported by Liz-Marzan et al. These authors presented an effective method to distinguish intracellular from extracellular nanoparticles by selectively quenching the SERS signals from dye molecules adsorbed onto star-shaped gold nanoparticles that have not been internalized by cells [13]. A general method was presented to localize gold nanoparticles by means of the selective quenching of the SERS signals originating from dye-conjugated nanoparticles outside cells. This localization strategy would provide a mean for assessing the internalization efficiency of various cargos coupled with noble metal nanoparticles, such as DNA/RNA, proteins, or drugs, which are of major relevance when studying endocytosis.

Theoretical investigation of the LSPR resonances has also provided useful insights for subsequent sensing applications. Stable GNS were fabricated with tunable extinction properties from the visible spectral region up to 1800 nm, depending on the average values of core size and branch length [14]. Theoretical computations of the plasmonic properties of these nanoparticles have put into evidence the existence of hot spots located on the tips of the nanostars for wavelengths up to 1800 nm, which opens the way to the improvement of diagnostics in the IR region. Preliminary Fourier transform Raman experiments performed after functionalization with a fluorescent dye bearing end thiol groups seem to confirm the field-enhancing capability of the nanostructures at 1064 nm.

A SERS-active GNS layer on the surface of ITO glass slip has been prepared by a low-cost electrostatically assisted APTES-functionalized surface assembly method for SERS analysis [15]. It was found that the substrate assembled with the longest branches of nanostars generated the best SERS efficiency, whether the excitation source is 785 or 633 nm. The potential use of these substrates in detection applications was also investigated by using Nile blue A and rhodamine 6G. The detection limits are 5×10^{-11} M and 1×10^{-9} M, respectively, when using the 785 nm excitation source. Apart from this high enhancement effect, the substrate also showed extremely good reproducibility at the same time. The simplicity in the production of the GNS films compared to expensive lithographic methodologies, combined with the excellent reproducibility and high Raman EFs, provides an exceptionally cost-effective substrate for SERS analysis.

The first theranostic application of GNS appeared in 2013. Vo-Dinh et al. developed a non-construct that combines the possibility of Raman imaging and the photodynamic effect for medical therapy [16]. The theranostic nanoplatform was created by loading the photosensitizer, protoporphyrin IX, onto a Raman-labeled GNS. A cell-penetrating peptide, TAT, enhanced intracellular accumulation of the nanoparticles and improved their delivery and efficacy. The plasmonic GNS platform was designed to increase the Raman signal via the surface-enhanced resonance Raman scattering effect. Theranostic SERS imaging and photodynamic

therapy using this construct were demonstrated on BT-549 breast cancer cells. The TAT peptide allowed to use the GNS construct for effective Raman imaging and photosensitization after a 1-h incubation period. In the absence of the TAT peptide, nanoparticle accumulation in the cells was not sufficient to employ the Raman signal for imaging or to produce any photosensitization effect after the same incubation period.

Regarding the use of GNS-based SERS sensor of organic molecules, a simple, ultrasensitive, highly selective, and reagent-free aptamer-based biosensor has been developed for quantitative detection of adenosine triphosphate (ATP) using surface-enhanced Raman scattering [17]. The sensor contained a SERS probe made of gold nanostar@Raman label@SiO_2 core–shell nanoparticles in which the Raman-label (malachite green isothiocyanate, MGITC) molecules were sandwiched between a GNS core and a thin silica shell. Such a SERS probe brought enhanced signal and low background fluorescence, showed good water solubility and stability, and exhibited no sign of photobleaching. The aptamer labeled with the SERS probe was designed to hybridize with the cDNA on a gold film to form a rigid duplex DNA. In the presence of ATP, the interaction between ATP and the aptamer resulted in the dissociation of the duplex DNA structure and thereby removal of the SERS probe from the gold film, reducing the Raman signal. The response of the SERS biosensor varies linearly with the logarithmic ATP concentration up to 2.0 nM with a limit of detection of 12.4 pM.

Sensing of bio-molecules in biopsies was also reported by means of GNS-enhanced SERS spectroscopy. Schutz et al. presented biocompatible GNS stabilized with ethylene glycol-modified Raman reporter molecules [18]. The localization of the tumor suppressor p63 was obtained in prostate biopsies after immuno-staining with the SERS labels for optical microscopy.

Hybrid nanoparticles composed of gold and silver or iron oxide have been developed and applied to bio-sensing. Star-shaped hybrid nanoparticles have been obtained by growing a star-shaped gold coating onto a magnetic core and have been tested for biodetection via magnetic separation and via SERS [19]. A capping agent terminated with a nickel-nitrilotriacetate group showing high affinity to histidine was used to modify the surface of nanoparticles. The resulting star-shaped construct nanoparticles were used to selectively capture histidine-tagged maltose-binding protein from a crude cell extract. The performance of star-shaped nanoparticles as SERS platforms was instead demonstrated through the detection of the Raman-active dye Astra Blue.

Always in the field of hybrid gold nanoconstructs, we cite the fabrication of ultrasensitive SERS substrates based on high-density GNS assemblies on silver films with tailored surface plasmons. On these substrates multiple field enhancements from particle-film and interparticle plasmon couplings are expected and lightening rod effected of sharp tips of nanostars contributes to the enormous values of the Raman enhancement that has been described [20]. The authors showed that the interparticle and particle-film plasmon couplings of high-density GNS on metal and dielectric films can be tuned through the interparticle separation to provide maximum SERS effects. The authors observed also that the SERS enhancement factor of

GNS on a metal film as a function of interparticle separation followed a broken power law function, where the EF increases with the interparticle separation for the strong interparticle coupling range below an interparticle separation ≈0.8 times the GNS size, but decreased for the weak interparticle coupling range (for an interparticle separation of >0.8 times the GNS size). Finally, the use of tailored plasmonic substrates as ultrasensitive SERS chemical sensors with an attomole level of detection capability of 2,4-dinitrotoluene, a model compound of nitroaromatic explosives, was demonstrated.

We move now to sensors purely based on LSPR. In these constructs we can single out strong and weak coupling regions.

In general LSPR-based sensing provides a label-free technology for sensing. As an example, streptavidin molecules were detected upon binding to individual, biotin-modified GNS through the spectral shifts in the localized surface plasmon resonances [21]. The authors characterized this dependency at the single-nanoparticle level. Concentrations as low as 0.1 nM produced a shift of the tip-related plasmon resonances of about 2.3 nm (5.3 meV).

The exploitation of the dependence of the refractive index on the LSPR position is quite common for GNS, as it is for thin gold layers. In a paper published in 2013 a refractive index sensor based on LSPR in a plastic optical fiber (POF) was presented and experimentally tested [22]. LSPR was obtained by exploiting five-branched GNS obtained using Triton X-100 in a seed growth synthesis. As it was discussed in Chaps. 1 and 2 these GNS have the uncommon feature of three localized surface plasmon resonances. The strongest LSPRs fall in two ranges, one in the 600–900 nm range (LSPR 2) and the other one in the 1100–1600 nm range (LSPR 3), both sensible to refractive index changes. Due to the extremely strong attenuation (>10^2 dB/m) of the employed POF in the 1100–1600 nm range, only LSPR 2 can be exploited for refractive index change measurements, useful for biochemical sensing applications. Optical sensor system based on LSPR is shown in Scheme 3.1.

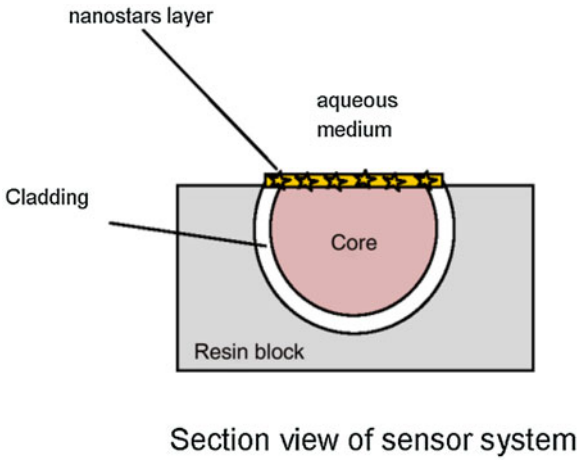

Scheme 3.1 Optical sensor system based on LSPR in POF (reproduced from Cennamo et al. [22])

The proposed device is based on the excitation of localized surface plasmons at the interface between the medium to be tested and a nanostar layer deposited on the fiber core. The sensing device has been characterized by exploiting a halogen lamp to illuminate the optical fiber and observing the transmitted spectra, normalized to the spectrum transmitted when the outer medium is air. The experimental results indicated that the configuration exhibits good performance in terms of sensitivity.

Later this method was applied for selective detection and analysis of trinitrotoluene in aqueous solution [23]. LSPR was excited in five-branched GNS, suspended in molecularly imprinted polymer specific for trinitrotoluene, which assures the selectivity. This sensing layer was deposited directly on the exposed plastic optical fiber core. The sensor showed better performance than a similar one proposed previously, in which surface plasmon resonance was excited in thin gold layer at the surface of plastic optical fiber. In the GNS sensor the sensitivity was $8.5\,10^4$ nm/M, three times higher than in the gold layer sensor. Nehl et al. described the application of single star-shaped gold nanoparticles for LSPR-based sensing [24]. The single-particle spectra demonstrated that the LSPR of single GNS are extremely sensitive to the local dielectric environment, yielding sensitivities as high as 1.41 eV photon energy shift per refractive index unit. To test their properties as molecular sensors, single-nanostar spectra were monitored upon exposure to alkanethiols and proteins known to bind gold surfaces. The observed shifts were consistent with the effects of these molecular layers on the surface plasmon resonances in continuous gold films. The obtained results suggested that LSPR sensing with single nanoparticles is analogous to the well-developed field surface plasmon resonance sensors, and would push the limits of sensitivity. The new GNS-based sensor developed at Imperial College London and the University of Vigo, Spain, can detect concentrations that are at least ten times lower than the existing ultrasensitive tests [25]. The scientists of these two groups presented a signal-generation mechanism that redefines the limit of detection of nanoparticle sensors by inducing a signal that is larger when the target molecule is less concentrated. The key step to achieve this inverse sensitivity is to use an enzyme that controls the rate of nucleation of silver nanocrystals on plasmonic transducers. The authors demonstrated the outstanding sensitivity and robustness of this approach by detecting the cancer biomarker prostate-specific antigen down to 10^{-18} g ml^{-1} (4×10^{-20} M) in whole serum.

3.2 Application of GNS for Thermal Therapy

Hyperthermia (also called thermal therapy or thermotherapy) is a type of medical treatment in which body tissue is exposed to high temperatures (up to 45–47 °C). Research has shown that high temperatures can damage and kill cancer cells, usually with minimal injury to normal tissues [26]. By killing cancer cells and damaging proteins and structures within cells, hyperthermia may shrink tumors [27]. Cells, either cancer or healthy, heated to temperatures in the range of 41–47 °C

begin to show signs of apoptosis, while by increasing temperatures above 50 °C one induces necrosis [28, 29].

Hyperthermia alone does not provide the standard of efficacy and selectivity that are required to be adopted as a cancer therapy. However, gold nanoparticles are optimal adjuvant therapies since they are known to enhance the efficacy of X-ray in tumor irradiation resulting in tumor heating and ablation [30]. Moreover, they absorb light and have been explored since long time as a method of heating [30]. For example, spherical gold nanoparticles with a peak absorption at 530 nm have been irradiated with a 514 nm laser to kill cells in vitro [31]. However, spherical GNPs absorb only visible light, so are generally poor choices for tissue heating since the penetration of UV and visible light in tissues is limited. The optimal wavelength for best tissue penetration is ~800 nm (NIR) [30]. Nonspherical gold nanoparticles are suitable prospects in this sense due to their capability to locally release heat efficiency when irradiated in NIR region where tissues are transparent [3]. It has already been mentioned that NIR plasmon resonance of GNS can be tuned in a wide NIR range up to 1250 nm [4]. Therefore, a brief overview of application of GNS for thermal treatment is made in this subchapter.

The large absorption cross sections make GNS good candidates to be used as heat sources. The presence of LSPR in NIR region reduces the flow of the impinging beam needed to heat nanoparticles, which makes more unlikely damaging of non-cancerous cells.

Rodriguez-Oliveros and Sanchez-Gil theoretically studied GNS as efficient thermal heaters at their corresponding LSPRs [32]. The authors showed that the photothermal properties of the GNS, resulting from their symmetry and geometrical dimensions, are excellent for a variety of optical heating applications. Additionally, the red shift of the LSPR induced by the increase in the number and/or sharpness of GNS tips opens the way to the use of a wide range of frequencies in the visible and near-IR regions. All their theoretical studies confirmed that GNS are promising materials for photothermal cancer application.

Nanostars, with their small core size and multiple long thin branches, exhibit high absorption cross sections that are tunable in the near-infrared region with relatively low scattering effect, making them efficient photothermal transducers [33].

The research group led by Vo-Dinh demonstrated particle tracking and photothermal ablation both in vitro and in vivo [33]. Using SKBR3 breast cancer cells incubated with bare nanostars, they observed photothermal ablation within 5 min of irradiation (980 nm continuous-wave laser, 15 W cm^{-2}). On a mouse injected systemically with PEGylated nanostars for 2 days, extravasation of nanostars was observed and localized photothermal ablation was demonstrated on a dorsal window chamber within 10 min of irradiation (785 nm continuous-wave laser, 1.1 W cm^{-2}).

Thermal therapy is also very effective in antimicrobial treatment. Regarding the specific issues of GNS in this field Pallavicini et al. grafted monolayers of GNS on mercapto-propyl-trimethoxysilane-coated glass slides [34], and showed that in these monolayers the GNS LSPR can be tuned in the 700–1100 nm range. Upon laser excitation of the NIR LSPR, an efficient photothermal response was observed, inducing local hyperthermia and efficient killing of *Staphylococcus aureus* biofilms

under laser irradiance at intensity values significantly lower than the maximum permissible exposure of skin. Chen et al. conjugated uniform GNS with cyclic RGD peptide and NIR fluorescence probe or anticancer drug (DOX) to obtain two multifunctional nanoconstructs [35]. These nanoparticles have favorable tumor-targeting capability mediated by RGD peptide binding to its overexpressed receptor on the tumor cells, both in vitro and in vivo. The multi-therapeutic analogue, Au-cRGD-DOX, integrates targeting tumor, chemotherapy, and photo-thermotherapy into a single system. The synergistic effect of photothermal therapy and chemotherapy was demonstrated in different tumor cell lines and in vivo using S180 tumor-bearing mouse models. The viability of cancer cells was only 40 % after incubation with Au-cRGD-DOX and irradiation with NIR light.

The direct monitoring of the temperature around gold nanoparticles is essential to test their therapeutic efficiency. For this reason a number of methods have been proposed [36, 37]. Regarding GNS, groups at the University of Milano-Bicocca and at the University of Pavia developed an all-optical method to measure the temperature of gold (nanorods and nanostars) and magnetite nanoparticles under NIR and radiofrequency excitation by monitoring the excited state lifetime of rhodamine B that lies ≈20 nm from the nanoparticle surface [38]. It was shown that GNS are ≈3 and ≈100 times more efficient in inducing localized hyperthermia with respect to gold nanorods and magnetite nanoparticles. The scheme of gold nanorods and GNS decorated with polyelectrolytes and temperature-sensitive dye is sketched in Scheme 3.2 together with temperature increase profile.

It is worth to mention that photothermal therapy is affected by the weakness of inducing thermotolerance in cancer cells, mediated by heat-shock proteins (HSPs) [39, 40]. These proteins have been known to play a significant role in enabling the survival of cancer cells in high-temperature conditions [40, 41]. Therefore, a synergistic approach in which photothermal therapy is combined with another therapeutic

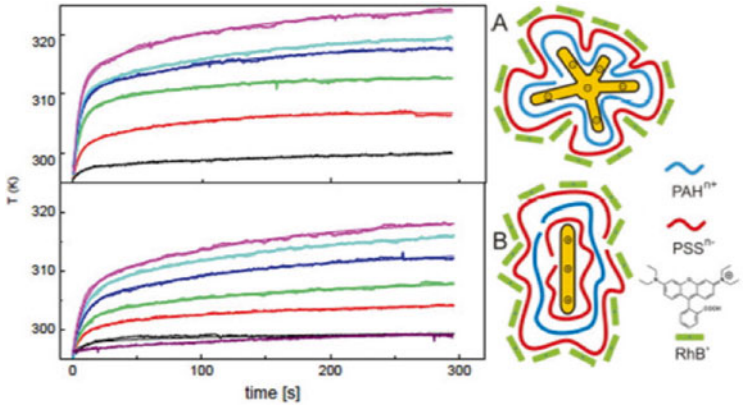

Scheme 3.2 Gold nanoparticles decorated with polyelectrolytes and dye and the temperature increase profile with polyelectrolytes and dye and the temperature increase profile under irradiation (reproduced from Freddi et al. [38])

modality is needed to overcome the limitations [40]. Chen and coworkers demonstrated that photosensitizer-coated GNS could induce a synergistic photodynamic/photothermal effect under single-laser irradiation [42].

To induce both photodynamic and photothermal effect by single NIR-CW laser, they adapted the localized surface plasmon resonance of GNS to fit the absorption of the photosensitizer chlorin e6 (Ce6). Ce6-incorporated GNS efficiently killed cancer cells in vitro upon single-laser irradiation (671 nm) compared to free Ce6-alone phototherapy.

For in vivo experiments, MDA-MB-435 tumor-bearing mouse model was intratumorally injected with the Ce6-incorporated GNS and irradiated with a single-CW laser at 4 h post-injection. The coordinated photothermal/photodynamic therapy obtained with the Ce6-incorporated GNS significantly reduced tumor growth compared to either therapeutic modality alone. It was also demonstrated in this study that synergic effect of the combined photothermal/photodynamic therapy could be modulated by adjusting the irradiation times due to photostability difference between GNS and photosensitizers.

Reduced thermotolerance can be achieved also by increasing thermal efficiency of the GNS in terms of their internalization in cells. GNS modified with a biopolymer chitosan with such improved properties were reported [43]. An in vitro photothermolysis experiment on J5 cancer cells showed that energy fluences of 23 mJ/cm^2 are necessary to cause complete death of J5 cells incubated with 4 μg/mL chitosan-capped GNS. The more uniform cellular uptake in comparison to other gold nanoparticles, like gold nanorods, allowed to use lower energy fluence for cell photothermolysis.

A stepwise fabrication of GNS-Raman reporter-photosensitizer conjugate for cancer treatment was reported in a recent paper [44]. The efficacy of such constructs as multimodal nanoprobes for SERS imaging and photodynamic/photothermal treatment of cancer was examined.

Multifunctional hybrid nanomaterials with enhanced therapeutic efficiency for externally triggered, image-guided therapy are highly attractive for nanomedicine. In a recently published paper a novel class of multifunctional hybrid nanopatches comprised of graphene oxide and GNS for enhanced photothermal effect and image-guided therapy was demonstrated [45]. The hybrid nanopatches with tunable LSPR into the NIR therapeutic window (650–900 nm) were realized using a biofriendly method that obviates the need for toxic shape-directing agents. It appears that the amphiphatic nature and the large surface area of graphene oxide enable it to serve as a soft, flexible, and biocompatible intracellular carrier for the in situ-grown plasmonic nanostructures and provide long-term biocompatibility with extremely low cytotoxicity. The photothermal transduction capabilities of graphene oxide, GNS, and graphene oxide-GNS constructs were compared. The temperature measurements of the solutions of these compounds indicated a rapid increase for the nanopatches within 2 min of laser irradiance (laser power density (0.75 W cm^{-2})) to 54.4 °C, while the same for GNS alone and for graphene oxide alone was found to be 50 and 30 °C, respectively, under the same irradiation conditions.

To monitor the therapeutic efficiency of these nanohybrids a live/dead cell assay was performed following the irradiation of the cells with 808 nm wavelength laser. As opposed to individual plasmonic nanostructures that act as nanoscale heaters, the unique nanopatch-like morphology of the hybrid construct with high density of GNS serves as a heating patch, which enhanced efficiency of local destruction of SKBR-3 cells due to their local destruction after intracellular colocalization. The perfect match of the LSPR wavelength of the GNS with the excitation of laser wavelength maximizes the photothermal effect of the nanopatch. Complete cell death occurred at ultralow laser power irradiation (0.75 W cm^{-2}) after only 2 min of laser exposure.

It should be noted that even though GNS have a remarkable photothermal transduction capability evidenced by the temperature measurements of the nanoparticle solutions, their negligible cellular uptake in the absence of surface modifications and aggregation outside the cells resulted in their poor therapeutic effect.

Jo et al. developed novel valuable therapeutic complexes, namely dual-aptamer-modified GNS, for the targeting of prostate cancers, including PSMA(+) and PSMA(−) cells [46]. The synthesized probes were subsequently analyzed for cytotoxicity tests, cell uptake, and in vitro photothermal therapy. The homogeneously well-fabricated nanostars presented high selectivity to prostate cancer cells and extremely high efficiency for therapy using an 808 nm laser under an irradiance of 0.3 W cm^{-2}, which is lower than the permitted value for skin exposure (0.329 W cm^{-2}). In another paper [47], bioconjugated GNS were tested as antigen-targeted photothermal agents for cancer treatment. GNS were biofunctionalized with nanobodies, the smallest fully functional antigen-binding fragments evolved from the variable domain, the VHH, of a camel heavy chain-only antibody [45]. These nanobodies bind to the HER2 antigen which is highly expressed on breast and ovarian cancer cells. Laser irradiation studies revealed that HER2-positive SKOV3 cells exposed to the anti-HER2-targeted GNS were destroyed after 5 min of laser treatment at 38 W cm^{-2} using a 690 nm continuous-wave laser.

3.3 GNS as Targeted Delivery Platforms

Recent advances in nanotechnology and biology are fostering the development of nanoparticles with specific functional properties that address the shortcomings of traditional disease diagnostic and therapeutic agents [48, 49]. These nanoconstructs act as excellent drug carriers (tailored drug uptake and release, low immunogenicity, etc.), offering improved efficacy for disease treatments and reduced side effects [48, 50].

The therapeutic potential of gold nanoparticles as drug-delivery carriers is primarily due to their tunable characteristics such as size, stability, and biocompatibility [51, 52]. Recently, publications from various laboratories have shown that GNS functionalized with drug molecules have a substantially increased therapeutic performance [53–56]. In these systems, drug molecules can be released from the

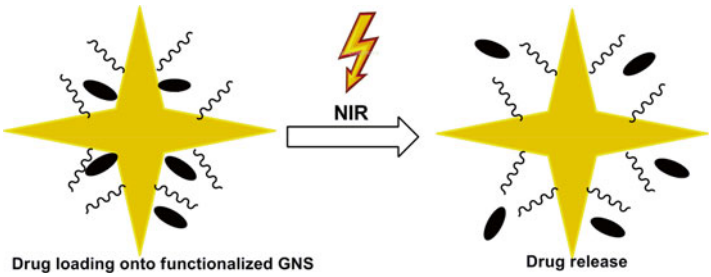

Scheme 3.3 Pictorial sketch of functionalized GNS for drug delivery

surface of GNP by desorption through ligand-exchange processes or the protonation of thiol groups at low pH [51, 57]. The increased surface volume of the star-shaped nanoparticles allows more drug to be attached and therefore potentially delivered to the target cells. However, size, shape, surface charge, and protein corona severely affect the nonspecific cellular uptake of nanoparticles, making GNS surface functionalization a key feature for the fabrication of successful delivery systems.

In this subchapter the application of GNS for targeted delivery is discussed. The schematic representation of GNS-based platforms for drug delivery is shown in Scheme 3.3.

Researchers at Northwestern University in the USA have shown that GNS can be used to carry drugs directly into the nucleus of a cancer cell [58]. This approach could be particularly useful in cases where tumors lie fairly close to the skin's surface, such as some breast cancers. In two publications Odom et al. [58, 59] studied a nanoconstruct composed of GNS loaded with the single-stranded DNA aptamer AS1411, which shows a high binding affinity for nucleolin. Nucleolin, the most abundant nucleolar phosphoprotein presents in the nuclei of normal cells, but overexpressed in the cytoplasm and plasma membranes of cancer cells [58], acts as a shuttle that carries the nanostars to the perinuclear region, where they release their drug payload. This nanoconstruct induced major changes in the nuclear phenotype through nuclear envelope invaginations near the site of the construct. Nuclear invaginations were more prominent when AS1411 aptamers were released from GNS by femtosecond laser pulses [59].

Femtosecond laser excitation of the aptamer–GNS at the localized surface plasmon resonance wavelength promoted the aptamer release by breaking its chemical bond with the gold nanoparticle. It was also shown that the release of the aptamer from the GNS at perinuclear locations not only increased the number of nuclear envelope folds but also resulted in higher apoptosis signals and cell death. This study has brought into evidence a clear correlation between drug-induced changes in nuclear phenotypes and increased therapeutic efficacy that can provide new insight into nuclear-targeted cancer therapy.

Vo-Dinh et al. demonstrated that plasmonics-active theranostic GNS can be a versatile nanoplatform for brain tumor imaging and controlled delivery of GNS into tumor in preclinical settings [60]. GNS could be delivered beyond the tumor

vasculature and deep into the tumor parenchyma. By focusing ultrafast pulsed laser irradiation through in vivo cranial window in mice preinjected with PEGylated GNS, the authors demonstrated for the first time a proof-of-concept plasmonics-enhanced optically modulated and image-guided brain tumor microvascular permeabilization and showed a highly spatial selective delivery of GNS into the tumor parenchyma with minimal off-target distribution. The authors envision a strong translational potential of plasmonics-active theranostic GNS for brain tumor molecular imaging and image-guided plasmonics-enhanced cancer therapy.

To achieve successful and selective photothermolysis, GNS need to be delivered sufficiently to the designated target cells without compromising cell viability. In general, NP size, shape, surface charge, and coating (e.g., protein corona, polymer, antifouling layer) all affect their cellular delivery. Scientists have tried numerous methods to increase the uptake of NP. One of the most efficient ways to do this is achieved by surface coating with cell-penetrating peptides (CPPs) [61].

Moreover, with a high absorption-to-scattering ratio in the NIR and multiple sharp edges favorable for heat generation, GNS efficiently transduce photon energy into heat for hyperthermia therapy. To date, most photothermolysis studies utilize laser irradiation higher than the maximal permissible exposure (MPE) of skin per ANSI regulation. Therefore, there is a strong need to design a more efficient photothermal transducer for pulsed lasers (e.g., GNS) with optimized cellular uptake.

As stressed by Vo-Dinh et al. apart from the great potential of gold nanoparticles for photothermal therapy, their intracellular delivery has to be optimized [62]. Therefore, the researchers demonstrated that TAT-peptide-functionalized GNS enter cells significantly more than bare or PEGylated GNS. The cellular uptake mechanism involves actin-driven lipid raft-mediated macropinocytosis, where particles primarily accumulate in macropinosomes and may also leak out into the cytoplasm.

Since induced angiogenesis is a major hallmark of malignant tumor, cyclic Arg-Gly-Asp (RGD) peptide-conjugated plasmonic GNS (RGD-GNS) were also prepared in order to specifically target $a_v\beta_3$ integrin overexpressed on tumor neovasculature, enabling highly sensitive angiography and photothermal therapy [63]. For the first time the authors used hemispherical photoacoustic imaging to volumetrically map the tumor angiogenesis quantitatively, offering deeper imaging depth with homogeneous resolution over existing optical imaging techniques for early diagnosis of tumor angiogenesis. This study suggests that the photoacoustic angiography with plasmonic RGD-GNS can be applied as a triple functional platform for tumor diagnosis, photothermal therapy, and treatment monitoring.

Liz-Marzan et al. in the paper published in 2014 presented seed-mediated growth of reduced graphene oxide-GNS nanocomposites and their application for anticancer drug (DOX) loading and release [64]. SERS applications of the constructs to probe DOX loading and pH-dependent release were successfully demonstrated, showing promising potential for drug delivery and chemotherapy.

Vo-Dinh et al. in 2011 reported the synthesis and characterization of surface-enhanced Raman scattering label-tagged GNS, coated with a silica shell containing methylene blue-photosensitizing drug for singlet oxygen generation [65]. To demonstrate the potential of these nanoconstructs as theranostic agents, in vitro PDT study

was performed. Methylene blue-encapsulated nanoparticles showed a significant increase in singlet oxygen generation as compared to nanoparticles synthesized without it. This increased singlet oxygen generation provided a cytotoxic effect on BT549 breast cancer cells upon laser irradiation.

Another important issue is to understand the effects that nanoparticles may have on cell function. Identifying these effects and understanding the mechanism through which nanoparticles interfere with the normal functioning of a cell are necessary for any therapeutic or diagnostic application. For this reason GNS were applied to acute mouse hippocampal slices while recording the action potentials from single neurons in the CA3 region [66]. The results showed that CA3 hippocampal neurons increase their firing rate by 17 % after the application of GNS. The increase in excitability lasted for as much as 50 min after a transient 5-min application of the nanoparticles. Further analyses of the action potential shape and computational modeling suggested that nanoparticles block potassium channels responsible for the repolarization of the action potentials, thus allowing the cell to increase its firing rate.

In this chapter the most important applications of GNS were briefly discussed. The next chapter is devoted to application of GNS as imaging agents and to the interaction of GNS with cells.

References

1. Dykman LA, Khlebstov NG (2011) Gold nanoparticles in biology and medicine: recent advances and prospects. Acta Nat 3:34–55
2. Zagar TM et al (2010) Hyperthermia combined with radiation therapy for superficial breast cancer and chest wall recurrence: a review of randomized data. Int J Hyperthermia 26:612–617
3. Huang X et al (2006) Determination of the minimum temperature required for selective photothermal destruction of cancer cells with the use of immunotargeted gold nanoparticles. Photochem Photobiol 82:412–417
4. Chirico G, Pallavicini P, Collini M (2014) Gold nanostars for superficial diseases: a promising tool for localized hyperthermia? Nanomedicine 9:1–3
5. Indrasekara ASDS et al (2014) Gold nanostars substrates for SERS-based chemical sensing in the femtomolar regime. Nanoscale 6:8891–8899
6. Esenturk NE, Walker ARH (2009) Surface-enhanced Raman scattering spectroscopy via gold nanostars. J Raman Spectrosc 40:86–91
7. Shiohara A et al (2014) Solution processed/polydimethylsiloxane/gold nanostars flexible substrates for plasmonic sensing. Nanoscale 6:9817
8. Mueller M et al (2012) Large-area organization of p-NIPAM coated nanostars as SERS platforms for polycyclic aromatic hydrocarbons sensing in gas phase. Langmuir 28:9168–9173
9. Liu Y et al (2014) Plasmonic gold nanostar for biomedical sensing. Proc SPIE 8957:895703-1
10. Vo-Dinh T et al (2015) SERS nanosensors and nanoreporters: golden opportunities in biomedical application. Wiley Interdiscip Rev Nanomed Nanobiotechnol 7:17–33
11. Khoury CG, Vo-Dinh T (2008) Gold nanostars for surface-enhanced Raman scattering: synthesis, characterization and optimization. J PhysChem C Nanometer Interfaces 112:18849–18859
12. Yuan H et al (2013) Spectral characterization and intracellular detection of surface-enhanced Raman scattering (SERS)-encoded plasmonic gold nanostars. J Raman Spectrosc 44: 234–239

13. Xie H et al (2014) Identification of intracellular gold nanoparticles using surface-enhanced Raman scattering. Nanoscale 6:12403–12407
14. Giorgetti E et al (2012) Tunable gold nanostars for surface enhanced Raman spectroscopy. Phys Stat Solidi 249:1188–1192
15. Su Q et al (2011) A reproducible SERS substrate based on electrostatically assisted APTES-functionalized surface-assembly of gold nanostars. ACS Appl Mater Interface 3:1873–1879
16. Fales AM, Yuan H, Vo-Dinh T (2013) Cell-penetrating peptide enhanced intracellular Raman imaging and photodynamic therapy. Mol Pharm 10:2291–2298
17. Li M et al (2012) Detection of adenosine triphosphate with an aptamer biosensor based on surface-enhanced Raman scattering. Anal Chem 84:2837–2842
18. Schutz M et al (2011) Hydrophilically stabilized gold nanostars as SERS labels for tissue imaging of the tumor suppressor p63 by immuno-SERS microscopy. Chem Commun 47: 4216–4218
19. Quaresma P et al (2014) Star-shaped magnetic@gold nanoparticles for protein magnetic separation and SERS detection. RSC Adv 4:3659–3667
20. Lee J (2014) Tailoring surface plasmons of high-density gold nanostars assemblies on metal films for surface-enhanced Raman spectroscopy. Nanoscale 6:616–623
21. Dondapati SK et al (2010) Label-free biosensing based on single gold nanostars as plasmonic transducers. ACS Nano 4:6318–6322
22. Cennamo N et al (2013) Localized surface plasmon resonance with five-branched gold nanostars in a plastic optical fiber for bio-chemical sensor implementation. Sensor 13: 14676–14686
23. Pesavento M et al (2014) A new approach for selective optical fiber sensor based on localized surface plasmon resonance of gold nanostars in molecularly imprinted polymer. Adv Biol Chem Eng Mater Sci 14:71–75, Proceedings of BBE '14
24. Nehl CL, Liao H, Hafner JF (2006) Plasmon resonant molecular sensing with single gold nanostars. Proc SPIE 6323:63230G–63231G
25. Rodriquez-Lorenzo L et al (2012) Plasmonic nanosensors with inverse sensitivity by means of enzyme-guided crystal growth. Nat Mater 11:604–607
26. van der Zee J (2002) Heating the patient: a promising approach? Ann Oncol 13:1173–1184
27. Hildebrandt B et al (2002) The cellular and molecular basis of hyperthermia. Crit Rev Oncol Hematol 43:33–56
28. Milleron RS, Bratton SB (2007) 'Heated' debates in apoptosis. Cell Mol Life Sci 64: 2329–2333
29. Wust P et al (2002) Hyperthermia in combined treatment of cancer. Lancet Oncol 3:487–497
30. Hainfeld JF et al (2014) Gold nanoparticle hyperthermia reduces radiotherapy doses. Nanomed Nanotechnol Biol Med 10:1609–1617
31. El-Sayed HI, Huang X, El-Sayed MA (2006) Selective laser photo-thermal therapy of epithelial carcinoma using anti-EGFR antibody conjugated gold nanoparticles. Cancer Lett 239: 129–135
32. Rodriguez-Oliveros R, Sanchez-Gil JA (2012) Gold nanostars as thermoplasmonic nanoparticles for optical heating. Opt Express 20:621–626
33. Yuan H et al (2012) In vivo particle tracking and photothermal ablation using plasmon-resonant gold nanostars. Nanomedicine 8:1355–1363
34. Pallavicini P et al (2014) Self-assembled monolayers of gold nanostars: a convenient tool for near-IR photothermal biofilm eradication. Chem Commun 50:1969–1971
35. Chen H et al (2013) Multifunctional gold nanostar conjugates for tumor imaging and combined photothermal and chemo-therapy. Theranostics 3:633–649
36. Shao J et al (2013) Photothermal nanodrugs: potential of TNF-gold nanospheres for cancer theranostics. Sci Rep. doi:10.1038/srep01293
37. Zharov V et al (2006) Photothermal nanotherapeutics for selective killing of bacteria targeted with gold nanoparticles. Biophys J 90:612–627
38. Freddi S et al (2013) A molecular thermometer for nanoparticles for optical hyperthermia. Nano Lett 13:2004–2010

39. Lepock JR (2003) Cellular effects of hyperthermia: relevance to the minimum dose for thermal damage. In J Hyperthermia 19:252–266
40. Oh J, Yoon H, Park J (2013) Nanoparticle platforms for combined photothermal and photodynamic activity. Biomed Eng Lett 3:67–73
41. Gibbons NB (2000) Heat-shock proteins inhibit induction of prostate cancer cells apoptosis. Prostate 45:58–65
42. Wang S et al (2013) Single continuous wave laser induced photodynamic/plasmonic photothermal therapy using photosensitizer-functionalized gold nanostars. Adv Mater 25:3055–3061
43. Baginskiy I et al (2013) Chitosan-modified stable colloidal gold nanostars for the thermolysis of cancer cells. J Phys Chem 117:2396–2410
44. Raghavan V et al (2014) Gold nanosensitisers for multimodal optical diagnostic imaging and therapy of cancer. J Nanomed Nanotechnol 5:6
45. Nergiz SZ et al (2014) Multifunctional hybrid nanopatches of graphene oxide and gold nanostars for ultra efficient photothermal cancer therapy. Appl Mater Interfaces. doi:10.1021/am504795d
46. Jo H et al (2014) Ultra-effective photothermal therapy for prostate cancer cells using dual aptamer-modified gold nanostars. J Mater Chem B 2:4862–4867
47. Van de Broek B et al (2011) Specific cell targeting with nanobody conjugated branched gold nanoparticles for photothermal therapy. ACS Nano 5:4319–4328
48. Veiseh O, Jonathan WG, Zhang M (2010) Design and fabrication of magnetic nanoparticles for targeted drug delivery and imaging. Adv Drug Deliv Rev 62:284–304
49. Ferrari M (2005) Cancer nanotechnology: opportunities and challenges. Nat Rev Cancer 5:161–171
50. Torchilin VP (2006) Multifunctional nanocarriers. Adv Drug Deliv Rev 58:1532–1555
51. Park C et al (2009) Ceclodextrin-covered nanoparticles for targeted delivery of an anti-cancer drug. J Mater Chem 19:2310–2315
52. Han G, Ghosh P, Rotello VM (2007) Functionalized gold nanoparticles for drug delivery. Nanomedicine 2:113–123
53. Podsiadlo P et al (2008) Gold nanoparticles enhance the anti-leukemia action of a 6-mercaptopurine chemotherapeutic agent. Langmuir 24:568–574
54. Alexander CM et al (2014) Multifunctional DNA-gold nanoparticles for targeted doxorubicin delivery. Bioconjug Chem 25:1261–1271
55. Kumar A, Zhang X, Liang X (2013) Gold nanoparticles: emerging paradigm for targeted drug delivery system. Biotechnol Adv 31:593–606
56. Li N et al (2014) Polysaccharide-gold nanocluster supramolecular conjugates as a versatile platform to the targeted delivery of anticancer drugs. Sci Rep 4, PMC3933908
57. Paciotti GF (2004) Colloidal gold: a novel nanoparticles vector for tumor directed drug delivery. Drug Deliv 11:169–183
58. Dam DH et al (2012) Direct observation of nanoparticles-cancer cell nucleus interaction. ACS Nano 6:3318–3326
59. Dam DH et al (2012) Shining light on nuclear-targeted therapy using gold nanostars constructs. Ther Deliv 3:1263–1267
60. Yuan H et al (2014) Plasmonics-enhanced and optically modulated delivery of gold nanostars into brain tumor. Nanoscale 6:4078–4082
61. Patel L, Zaro J, Shen WC (2007) Penetrating peptides: intracellular pathways and pharmaceutical perspectives. Pharm Res 24:1977–1992
62. Yuan H et al (2012) TAT-peptide functionalized gold nanostars: enhanced intracellular delivery and efficient NIR photothermal therapy using ultralow irradiance. J Am Chem Soc 134: 11358–11361
63. Nie L et al (2014) Plasmonic nanostars: in vivo volumetric photoacoustic molecular angiography and therapeutic monitoring with targeted plasmonic nanostars. Small 10:1441
64. Wang Y, Polavarapu L, Liz-Marzan L (2014) Reduced graphene oxide supported gold nanostars for improved SERS sensing and drug delivery. Appl Mater Interfaces 6:21798–21805

65. Fales AM, Yuan H, Vo-Dinh T (2011) Silica coated gold nanostars for combined SERS detection and singlet oxygen generation: a potential platform for theranostics. Langmuir 27(19):12186–12190
66. Salinas K et al (2014) Transient extracellular application of gold nanostars increases hippocampal neuronal activity. J Nanobiotechnol 14:31

Chapter 4
Interactions of Gold Nanostars with Cells

Laura Sironi, Mykola Borzenkov, Maddalena Collini, Laura D'Alfonso, Margaux Bouzin, and Giuseppe Chirico

Abstract Unique optical properties, chemical stability, ease of synthesis, and wide functionalization possibilities make GNP attractive candidates for use in biomedical research including chemical sensing, biological imaging, drug delivery, and cancer treatment. In particular, the strong two-photon luminescence of GNP coupled to a specific targeting makes them ideal candidates as contrast agents. To this aim, the interaction with cells and their cellular tracking are important issues for successful application of GNP to biomedical purposes. Properties of gold nanoparticles, namely gold nanostars, as contrast agents and interaction of GNS with cells are highlighted in this chapter.

Keywords Cellular uptake • Intracellular tracking • Contrast agents • Bioimaging

4.1 Intracellular Tracking of Gold Nanoparticles

Rapid advances in molecular biology and genetic engineering provide an unprecedented opportunity for delivery of drugs and genes to intracellular targets [1, 2]. Current intracellular delivery systems are classified as being either viral or non-viral in origin [1]. Viruses are efficient in delivery. However they suffer from poor safety profiles [1, 3]. Non-viral delivery systems, albeit not as efficient as viruses, have the promise of safety and reproducibility in manufacturing [4]. To enhance delivery of drugs and genes to intracellular targets using non-viral delivery systems, it is necessary to have a detailed understanding of the transport process and identify ways of overcoming the cellular barriers [1, 5].

Gold nanoparticles are known to be taken up by cells spontaneously whereby their intracellular distribution depends on many factors such as particle charge, surface modification, particle size and shape, as well as experimental procedures involving concentration and exposure time [6]. Indeed, for biomedical applications,

L. Sironi • M. Borzenkov • M. Collini • L. D'Alfonso • M. Bouzin • G. Chirico (✉)
Department of Physics, University of Milano-Bicocca, Piazza Della Scienza 3, Milan 20216, Italy
e-mail: mykola.borzenkov@unimib.it; giuseppe.chirico@mib.infn.it

G. Chirico et al., *Gold Nanostars*, SpringerBriefs in Materials,
DOI 10.1007/978-3-319-20768-1_4

surface functionalization of gold nanoparticles is an essential step for any specific targeting of pathological tissues and to allow them to selectively interact with cells or biomolecules [1]. Additionally, for systemic applications, long-circulating nanoparticles are desired both for passive targeting to tumors and inflammatory sites [1] or for specific targeting. Different cellular mechanisms are involved in particle uptake such as phagocytosis and pinocytosis [6]. The latter facilitates the uptake process through small membrane-bound vesicles, called endosomes [6, 7]. Following internalization, membrane-bound vesicles encapsulating the particles mature and eventually fuse with lysosomes [6]. Intracellular gold nanoparticles are trapped inside membrane-bound vesicles of the endocytosis pathway [8]. Trapped in endocytosis vesicles, particles get transported through cells via the common cellular transport mechanisms that relies on the kinesin or dynein molecular motors moving along microtubules that form the intracellular filament network [6, 9]. Studies revealed that average velocities strongly depend on the size of attached cargo that is transported by these motors [10].

With recent achievements in the fabrication of functionalized GNP, which have controllable properties and are decorated with targeting molecules, the endocytosis of such GNPs has become crucial for successful biomedical applications [11]. GNP uptake has employed various cell lines in vitro and GNP of various sizes, shapes, and structures (nanospheres, nanorods, nanoshells, nanocages, nanostars, etc.) [11].

Gold nanoparticles have been considered as potential issues to become versatile biomarkers. For further use of GNP labeled with functionalized molecules, their visualization in biological systems by routine laboratory tools such as light microscopy is urgent.

Nanoparticle contrast agents for molecular targeted imaging have widespread interest in diagnostic applications with cellular resolution, specificity, and selectivity for visualization and assessment of various pathological processes. Single-particle tracking is an important tool to investigate dynamic biological processes by following the movement of individual labeled molecules with high spatial and temporal resolution [12]. Forty nanometer gold nanoparticles are efficient light scatters which have long been used as probes in single-particle tracking application [12, 13]. Moreover, the tracking of individual gold nanoparticles with a spatial resolution of ≈1.5 nm at 25 μs temporal resolution in vivo was demonstrated [14]. As it has already been discussed in previous chapters, excellent optical properties of gold nanoparticles result from the resonant excitation of collective oscillations of the particles' free electrons, known as localized surface plasmons, which cause large optical cross sections at their respective resonance wavelengths. In addition, GNPs are not only very radiant but also display an extreme photophysical stability. Gold nanoparticles do not blink or bleach unlike many fluorescent dyes or quantum dots [12].

Gold nanoparticles can also be treated in order to reduce the cellular toxicity. This fact together with the strong light absorption contributes to make them ideal contrast agents for photoacoustic imaging [15]. On the other hand, gold nanospheres maximally absorb in the visible light region (520 nm), but plasmon coupling following nanosphere endocytosis by cells leads to peak broadening [15].

The unique properties of GNS provide wide opportunities to use as delivery, sensing, and photothermal agents. From an imaging perspective, gold nanoparticles have shown great promise for their use in computed tomography and photoacoustic imaging. Gold nanostars and other gold nanoparticles have recently been examined as contrast agents for biomedical imaging because of their brightness at near-infrared wavelengths, which can penetrate through tissue better than visible light.

Therefore understanding the biodistribution and transport kinetics and the toxicity of gold nanoparticles is vitally important for biological, medical, and pharmacological applications. The following paragraphs focus on GNS as contrast agents and on their interaction with cells.

4.2 GNS Constructs as Contrast Agents for Imaging Applications

For further use of GNP labeled with functionalized molecules, the possibility of visualizing them inside biological systems by means of routine laboratory tools such as light microscopy is crucial.

Nanoparticle-based contrast agents for molecular targeted imaging have in fact widespread interest in diagnostic applications with cellular resolution, due to their specificity and selectivity for visualization and assessment of various pathological processes.

A particularly relevant application of GNS is in the field of microstructural analysis of biomaterials and tissues in ex vivo or in vivo conditions through optical imaging. As it has already been mentioned in previous chapter there are two contributions to the optical properties of the GNS: absorption and scattering.

While GNS with high absorption contribution are more convenient for photothermal or photoacoustic approaches, GNS with high scattering cross section are better for dark-field or Raman-based techniques.

GNS with LSPR in NIR region display greatly enhanced two-photon photoluminescence (TPL). Vo-Dinh and coworkers reported the synthesis of GNS with adjustable geometry particularly suitable for in vivo imaging [16]. The synthesized nanostars showed an extremely strong two-photon photoluminescence process which is confirmed by the quadratic dependence of the luminescence signal up to excitation power (10 mW). The broad-emission spectrum observed by Vo-Dinh et al. implies that TPL from nanostars may originate from electron-hole recombination as it was found in case of nanorods [16, 17], with two cascade excitation processes with a relative delay of only 50–100 ps. The quadratic dependence was not seen on 60 nm gold and silver nanosphere solutions under similar conditions. It was also shown that for higher values of the excitation power the dependence became close to linear. This could be explained by the competition between linear decay and the upconversion for the depletion of the intermediate excited state [18]. Notably, the concentration-normalized emission intensity at 800 nm of nanostar solutions was found to be 1.1×10^4 greater than that of rhodamine B, making the strong

two-photon action cross sections (TPACS) of nanostars more than a million GM units [16].

Gold nanostars can also be applied as strong contrast agents in TPL imaging in biological samples. For this purpose Vo-Dinh et al. reported TPL imaging of wheat-germ agglutinin (WGA)-functionalized gold nanostars on BT549 cancer cells [16], fixed with paraformaldehyde for imaging. The broad-emission spectrum from nanostars resulted in a balanced emission on the red, green, and blue channels resulting in a white color on the reconstructed images. GNS emitted strongly without photobleaching under low laser power (4 mW), which is in the typical working range for organic fluorophores. Unlike gold nanostars, a signal from WGA-coated spheres was observed only under much stronger excitation power.

Tracking of gold spherical nanoparticles in vivo is essential for preclinical studies but was considered as a difficult issue. For fluorescence microscopy one typically needs to label the nanoparticles with organic dyes that are largely quenched by energy transfer to the gold nanoparticles when their mutual distance is <3–4 nm [16]. The labeling of spherical gold nanoparticles requires then the delicate tuning of the distance between the surface of metal nanoparticles and the fluorophores [19]. Alternative techniques able to visualize gold spherical nanoparticles are dark-field and differential interference contrast microscopy. These can visualize gold nanoparticles in cells but not available in tissue.

On the contrary, imaging and tracking of gold nanostars are possible without the need of fluorophores due to strong two-photon action cross sections (TPACS) that is maintained also when the GNS are internalized in cells and in tissues as it has been demonstrated on nude mice [16, 20]. Within 5 min from the injection, PEGylated GNS traveled along the blood vessel where the tissue vasculature became clearly visible at rather low excitation power with minimal tissue autofluorescence background. Due to the high TPACS of nanostars, tracking the motion of PEGylated nanostars in blood vessels was also possible.

In medicine novel techniques with high specificity, such as positron emission tomography (PET), require probe labeling and offer low spatial resolution. Photoacoustic microscopy (PAM) is an emerging imaging modality that combines both rich optical absorption and high ultrasonic resolution in a single-imaging modality [21–23] and it is based on the use of highly absorbance nanoparticles. PAM provides in vivo functional imaging information at clinically relevant penetration depths [21]. Under irradiation of non-ionizing laser pulses, biological tissue absorbs the laser energy and generates heat, resulting in transient thermoelastic expansion and subsequent wideband ultrasonic emission. The produced ultrasonic pressures can be captured by ultrasonic transducers to form photoacoustic (PA) images [21].

Recently GNS have been successfully applied as enhancing agents in PA imaging [24]. Nie and coworkers used a near-infrared pulsed laser as an excitation source and 128 ultrasonic transducers spirally distributed on a hemispherical surface to receive PA signals for the three-dimensional image reconstruction [24]. Cyclic RGD peptide-conjugated plasmonic gold nanostars were designed to specifically target over-expressed integrin $\alpha_v\beta_3$ on tumor neovasculature, enabling highly sensitive angiography by PA and simultaneous photothermal therapy. After the administration

of GNS constructs, tumor angiogenesis was clearly imaged with enhanced contrast and obtained results suggested that PA technique offers deeper imaging depth with homogeneous resolution over existing optical imaging techniques for early diagnosis of tumor angiogenesis.

The use of PAM to monitor the GNS upload kinetics in liver and spleen has been reported recently [21]. Furthermore this approach has been applied to monitor the nanoparticle extravasation to organs from bloodstream in vivo. The structure of the vessel tree and of the internal organs and their changes were clearly imaged by PAM performed at the excitation of 730 nm. The ratio of the PA signal measured in the organ to that measured in the blood vessel was used to quantify the GNS transport kinetics. In order to obtain this, PAM images were continuously acquired every 30 min from a mouse. In parallel, fluorescence images of the mouse at the same time points were acquired to validate the PAM results. The results demonstrate that PAM can potentially provide a noninvasive and semiquantitative method to monitor nanoparticle kinetics in organs and other deep imaging applications where fluorescence instrument cannot be applied.

A unique quintuple-modality theranostic nanoprobe was developed by Vo-Dinh et al. by exploiting SERS, magnetic resonance imaging (MRI), computed tomography (CT), TPL imaging, and photothermal therapy [25]. The synthesized GNS were tagged with a SERS reporter and linked with an MRI contrast agent Gd^{3+}. This nanoprobe exhibited high Gd loading density and superior tumor accumulation due to the enhanced permeability and retention (EPR) effect. These features allowed to reach much higher efficiency MRI and contrast than conventional agents [25]. The relaxivity of Gd-loaded nanoparticles is dependent on several factors, including the intrinsic relaxivity of the linked agent, its local concentration, and the residence lifetime of water protons [25, 26]. Due to the star shape, water protons may effectively interact with the gadolinium chelates and exhibit high proton relaxivity. Moreover, GNS showed extremely high two-photon action cross sections in the NIR region, which makes single-particle detection and real-time particle tracking under multiphoton microscopy feasible. Because corresponding nanoprobes accumulate preferentially in the tumor due to the EPR effect, the highly sensitive TPL optical imaging could be a promising intraoperative tool for tumor demarcation [25] to be compared to fluorescein preoperative staining. Tumor phantom experiments were also performed in this study to demonstrate the potential of GNS constructs for future in vivo applications as labels for CT and MRI. Preliminary measurements showed that the tumor phantom with GNS constructs have higher intensity than ones with GNS-free BT549 cells, therefore making possible to detect smaller tumor phantom than 0.5 cm^3 for early-stage detection [25].

The properties of GNS as excellent contrast enhancement for photoacoustic tomography were also reported by Kim et al. in 2011 [27]. The high photoacoustic sensitivity of GNS at near-infrared wavelengths enabled their in vivo detection in rat sentinel lymph nodes and vessels, with direct application toward lymphangiography.

A gold nanoparticle-Raman reporter-photosensitizer conjugate for optical diagnostic imaging and cancer therapy was reported [28]. As prepared gold nanostars

were multibranched it comprised multiply "hot spots" capable of electromagnetic radiation. GNS were coated with Raman reporter and with hypericin conjugated with denaturated BSA. In vitro studies were performed to examine the uptake of GNS and retention of hypericin's fluorescence upon uptake by the cells. Confocal fluorescence microscopy images showed that nanostars with hypericin concentration of 5 μM can be detected in cytoplasm of the cells and not inside the nucleus. The uptake of GNS within cells and its distribution in the cytoplasm can also be examined using dark-field microscopy, which makes use of the backscattering from the gold nanostars that form core.

Plasmon-resonant nanoparticles are widely used for resonant light scattering, which can be greater by orders of magnitude relative to objects of similar size [29, 30]. These nanoparticles with optical scattering in the NIR are valuable contrast agents for biophotonic imaging and may be detected at the single-particle limit against a dark background. However, their contrast is often limited in environments with high noise. For this purpose gyromagnetic imaging as a dynamic mode of optical contrast was considered, using GNS with superparamagnetic cores [29]. The nanostars exhibit polarization-sensitive NIR scattering and can produce a frequency-modulated signal in response to a rotating magnetic field gradient. This periodic "twinkling" can be converted into Fourier-domain images with a dramatic reduction in background [29]. Gyromagnetic imaging of nanostars inside of tumor cells was demonstrated, using broadband excitation: while their time-domain signals are obscured by incoherent scattering, their Fourier-domain signals can be clearly resolved in less than a second. Notably, gyromagnetically active nanostars do not cause a loss in viability, and even a mild stimulatory effect on cell growth.

Gold nanostars conjugated with cyclic RGD and anticancer drug DOX were studied in different tumor cell lines and in vivo using S180 tumor-bearing mouse model [31]. The weak red fluorescence of DOX in MCF-7 cells indicates that low amount of DOX, Au-DOX, or Au-cRGD-DOX had entered tumor cells. Similarly, the amount of DOX or Au-DOX that entered the MDA-MB-231 cells and Bel-7402 cells was so low that there was no significant difference between the fluorescence intensity from these groups of cells and MCF-7 cells treated with DOX, Au-DOX, or Au-cRGD-DOX. By contrast, Au-cRGD-DOX in MDA-MB-231 and Bel-7402 tumor cells showed obvious red fluorescence. The fluorescence intensity of the three lines incubated was compared. Significant differences appeared in MDA-MB-231 and Bel-7402 cells. All results confirmed that the presence of cRGD on the surface of the GNS increased its cellular uptake by MDA-MB-231 and Bel-7402 cells. The fluorescence images of Au-cRGD-DOX after incubating with MDA-MB-231 cells for 8 h were collected in order to understand the intracellular kinetics of the multifunctional nanoparticles. The obtained data clearly indicated that Au-cRGD-DOX 0r-released DOX entered the nucleus with only a small fraction remaining in the cytoplasm after 8 h incubation and it was confirmed by fluorescence images. In the work by Yuan et al. GNS functionalized with TAT-peptide were also observed in nucleus region by two-photon photoluminescence imaging [32]. These results suggested that the red fluorescence observed from nucleus might be contributed by free DOX released from Au-cRGD-DOX as a result of replacement of glutathione on the GNS surface by abundant intracellular glutathione.

Recent development and application of plasmonic gold nanostars fabricated in by research group led by Vo-Dinh for biomedical imaging has been recently reported [33]. The scientists demonstrated that LSPR significantly increases TPACS to more than a million GM (Göeppert-Mayer) units. TPACS of gold nanostars is greater than that of nanorods and organic fluorophores [16]. The Vo-Dinh research group demonstrated for the first time that GNS with intense NIR contrast under multiphoton microscopy can be visualized in real time [32]. The developed GNS provide a superior nanoplatform for multimodal imaging for cancer diagnostics due to their large surface area for linking other contrast agents like Gd^{3+} and ^{64}Cu, for MRI and PET imaging [25]. GNS with sizes less than 100 nm can accumulate selectively in tumors via the enhanced permeability and retention effect, which is due to the increased leakiness of blood vasculature in tumors [33, 34]. Combining this statement and ability of wide range to be linked with gold nanostars, the last are considered to be suitable platforms for multimodal imaging for cancer diagnostics.

Another promising application of GNS is brain tumor imaging [33]. GNS, as strong optical contrast agents with exceptionally high TPL signal, offer superior flexibility to investigate how drug nanocarriers and contrast agents can be delivered into brain tumor [33, 16, 35]. GNS exhibit longer serum half-life than that of commercial intravascular contrast agents that undergo significant signal decay in less then 30 min. Three hours following systemic injection of PEGylated GNS nanoparticles accumulated preferentially in the tumor than the surrounding area [33]. Moreover, GNS provide a unique nanoplatform for multimodal imaging, which can be used for combined whole-body scans with CT, MRI, or PET and high-resolution optical imaging with SERS and TPL [33, 25]. GNS have also been employed for in vivo tracking with PET imaging [33]. For this purpose GNS were radiolabeled with ^{64}Cu radioisotopes by DOTA chelators linked on the nanoparticles surface. Two-hour continuous PET scan results revealed and immediate nanoprobe uptake in liver. Further studies confirmed that GNS can be tracked in vivo dynamically with sensitive PET imaging.

Another interesting study that showed importance of GNS for biomedical application and particularly for bioimaging was published in *Nanotechnology* in 2012 [36]. PEGylated gold nanoparticles were incubated with melanoma B16-F10 cells. Dark-field microscopy showed that the biocompatible gold nanoparticles were easily internalized and most of them localized within the cells.

A novel class of multifunctional hybrid nanopatches comprised of graphene oxide and gold nanostars for enhanced photothermal effect and image-guided therapy was reported [37]. Internalization of the intact nanopatches into epithelial breast cancer cells was confirmed by Raman imaging, transmission electron microscopy, and inductively coupled plasma mass spectrometry. It appeared that the amphipathic nature and the large surface area of the graphene oxide enable it to serve as a soft, flexible, and biocompatible intracellular carrier for the in situ-grown plasmonic nanostructures and provide long-term biocompatibility with extremely low cytotoxicity. Apart from a remarkably improved photothermal effect compared to that of either of the components at very low dosages of the hybrids and using a low laser power, the hybrid nanopatches exhibit strong Raman scattering, making them excellent candidates for bioimaging, diagnostics, and image-guided therapy applications.

Gold nanostars loaded with high densities of nucleolin-specific DNA aptamer AS1411 produced anticancer effects in a panel of 12 cancer lines containing four representative subcategories [38]. It was found that the nanoconstructs could be internalized by cancer cells and trafficked to perinuclear regions. To visualize uptake by confocal fluorescence microscopy, the 5′-end of Apt was labeled with Cy5 dye prior to attaching the aptamer to the GNS. Light-triggered release further enhanced the in vitro efficacy by making available high local concentrations of Apt near the nucleus. Therefore, it was anticipated that this nanoconstruct can act as a platform for a new class of cell-type-independent agents that could address some current challenges in targeted therapy.

4.3 Interaction of Gold Nanostars with Cells

An increasing number of scientific reports have been published addressing the interactions between nanoparticles and cells as function of their size, shape, and surface chemistry [39–41]. Interactions between nanoparticles and cells should be considered first, since many applications require a strict control over nanoparticle–cell interactions [42]. As it has been already mentioned and explained in previous chapters, gold nanoparticles have attracted particular scientific and technological interest due to their unique optical properties, chemical stability, easy synthesis, and functionalization, all of which make them attractive candidates for use in biomedicine including chemical sensing, biological imaging, drug delivery, and cancer treatment [41]. Indubitably, physicochemical characteristics of gold nanoparticles as they are synthesized and decorated on the surface, significantly affect their circulation, biodistribution, cellular internalization, and trafficking in biological systems [42, 43]. Among all these factors, size and surface's effects on cell interactions have been studied most. For example, Chan et al. have shown that, for spherical gold nanoparticles stabilized by citric acid ligands, 50 nm diameter is an optimal size to maximize the rate of uptake and intracellular concentration in mammalian HeLa cells [44].

As it is discussed in previous subchapter they interaction with cells and in vivo tracking can be easily monitored by applying of various techniques. Direct visualization of interactions between drug-loaded nanoparticles and the cancer cell nucleus was reported [45]. Nanoconstructs composed of nucleolin-specific aptamers and gold nanostars were actively transported to the nucleus and induced major changes to the nuclear phenotype via nuclear envelope invaginations near the site of the construct. The nucleus is known to be the most important organelle in the growth, proliferation, and apoptosis of a cell [46]. Controlling the processes governed by the nucleus has been a primary goal for nuclear-targeted cancer therapy [47]. The number of local deformations could be increased by ultrafast, light-triggered release of the aptamers from the surface of the gold nanostars. Cancer cells with more nuclear envelope folding showed increased caspase 3 and 7 activity (apoptosis) as well as decreased cell viability. It is suggested that this newly revealed correlation between

drug-induced changes in nuclear phenotype and increased therapeutic efficacy could provide new insight for nuclear-targeted cancer therapy [45].

The two most important organelles in drug delivery are the mitochondria and the nucleus. Mitochondria are the powerhouses of cells and key regulators of apoptosis and cell death [48]. Targeting the mitochondria can result in the shutdown of cellular metabolic activities [48, 49]. The nucleus, which possesses genetic material and controls the major biological activities of the cell, unlike the mitochondria, has a membrane surrounding the nucleus—the nuclear envelope, which allows transport of biomolecules via nuclear pore complexes [48]. Small drug molecules can, therefore, enter the nucleus and potentially cause DNA damage and cell cycle arrest [48, 50]. However, the employment nanocarriers for nuclear-targeted therapy faces with main problems, namely lack of understanding on how the cancer cell nucleus and drug-loaded nanoparticles interact at the nanoscale and little control over when the drug will be released from the nanoparticles [48]. Therefore, a new two-component nanoconstruct based on aptamer-loaded gold nanostars that can solve these problems and open new possibilities for future development of nuclear-targeted therapy was reported [48]. This nanoconstruct induced major changes in the nuclear phenotype through nuclear envelope invaginations. Femtosecond, light-triggered release of the aptamers from the surface of the GNS further increased the number of nuclear envelope deformations. Cancer cells with more nuclear envelope folding showed increased apoptosis as well as decreased cell viability. The authors of this paper have revealed that correlation between drug-induced changes in nuclear phenotypes and increased therapeutic efficacy can provide new insight into nuclear-targeted cancer therapy.

In recent publication the same research group described how in vitro efficacy of aptamer-loaded gold nanostars can be enhanced by the increased loading of a G-quadruplex homodimer AS1411 on the GNS surface [51]. In a low pH buffer environment, the loading density of Apt on GNS was increased up to 2.5 times that obtained using the conventional salt-aging process. These highly loaded GNS nanoconstructs were taken up in pancreatic cancer and fibrosarcoma cells ca. two times more and at faster rates compared to normal GNS functionalized with aptamer constructs. When a similar number of GNS carriers was internalized by the cancer cells, the amount of AS1411 delivered via highly loaded GNS nanoconstructs was effectively double. This increased loading of AS1411 enhanced cellular uptake as well as in vitro efficacy of the nanoconstructs in both fibrosarcoma and pancreatic cancer cells. The obtained results suggested that increasing the loading density on GNS could provide a simple means to improve uptake as well as in vitro efficacy of the nanoconstructs in cancer cells.

Vo-Dinh et al. showed that TAT-peptide-functionalized gold nanostars enter cells significantly more than bare or PEGylated GNS [32]. The cellular uptake mechanism involves actin-driven lipid raft-mediated macropinocytosis, where particles primarily accumulate in macropinosomes but may also leak out into the cytoplasm. The results demonstrated the enhanced intracellular delivery and efficient photothermolysis of TAT-GNS constructs, making them promising agents in cancer therapy.

The preparation and properties of GNS modified with biopolymer chitosan were reported [52]. When chitosan was used as capping agent gold nanostars displayed enhanced stability in comparison with gold nanorods. Therefore, they were considered as more suitable mediators in cell photothermolysis because of the slower aggregation and more uniform cellular uptake. Flow cytometry analysis results showed a relatively non-equivalent distribution of chitosan-capped nanorods across the cells in specimen compared with gold nanostars due to highly nonuniform aggregation and cellular uptake of nanorods.

The state of the cells that were treated with chitosan-capped nanoparticles remained mostly unchanged after 72 h, which confirms the biocompatibility of chitosan-modified branched gold nanoparticles. However, the BEAS-2b cell line had a viability below 100 % when the concentration of chitosan-capped GNP was at is highest value (16 μg/mL). This result suggested a concentration limit in the safe uptake of chitosan-capped gold nanostars, which also depends on cell type. Internalization of gold nanoparticles may have an effect other then toxicity on the viability of cells or may disrupt important intracellular processes [52, 53]. The uptake and localization of chitosan-capped GNS by J5 cancer cells were verified by a three-dimensional analysis of the fluorescence distribution via confocal microscopy. The results suggested that GNS in J5 cell would accumulate in cellular organelle, lysosomes.

Shielding nanoparticles from nonspecific interactions with normal cells/tissues before they reach and after they leave tumors is crucial for the selective delivery of NPs into tumor cells. For this purpose and by utilizing the reversible protonation of weak electrolytic groups to pH changes, long-chain amine/carboxyl-terminated polyethylene glycol (PEG)-decorated gold nanostars were designed, exhibiting reversible, significant, and sensitive response in cell affinity and therapeutic efficacy to the extracellular pH gradient between normal tissues and tumors [54]. One PEGylated mixed-charge GNS with certain surface composition exhibited high cell affinity and therapeutic efficacy at pH 6.4, and low affinity and almost “zero” damage to cells at pH 7.4. Remarkably, this significant and sensitive response in cell affinity and therapeutic efficacy is reversible as local pH alternated. In vivo, these constructs showed higher accumulation in tumors and improved photothermal therapeutic efficacy than pH-insensitive GNS.

Surface-enhanced spectroscopic techniques (like SERS and SEF), which rely on local field enhancement, can strongly enhance the spectral intensity of cellular chemical constituents near the particles and serve as tools for ultra-sensitive monitoring of the intracellular distribution of various species [55]. Liz-Marzan et al. presented an effective method to distinguish intracellular from extracellular nanoparticles by selective quenching the SERS signals from dye molecules adsorbed onto star-shaped gold nanoparticles that have nor been internalized by cells [56]. This approach is expected to help understanding actual intracellular nanoparticles distributions. The authors anticipate this localization strategy would provide a means for assessing the internalization efficiency of various cargos coupled with noble metal nanoparticles, such as DNA/RNA, proteins, or drugs which are of major

relevance when studying endocytosis. As it was demonstrated in this paper, it could also prove useful way of checking cell membrane integrity.

Colloidal stable and biocompatible star-shaped SERS-encoded single nanoparticles were prepared and they can be internalized into living cells for intracellular imaging [57]. Encoded nanoparticles, of a final concentration of 6 nM, were incubated with HeLa cells for 2 h at 37 °C. During the internalization by endocytosis, both encoded nanoparticles (stars and spheres) remained separate, without any tendency toward the formation of aggregates inside the endosome. It was assumed that this colloidal stability is related to the adsorption of the cocktail of proteins secreted by the cells. However, semi-quantification of the number of particles per cell showed a higher affinity of spheres to be internalized over stars, around threefold. It was assumed that different affinity must be related with shape, which is in agreement with Cho et al. where spheres were preferentially absorbed over cubes or cages of similar size [58]. Notably, samples exposed to nanostars showed a remarkable SERS intensity while no signal was obtained from those treated with nanospheres even though the number of spheres internalized was considerably larger.

The effect gold nanostars have on the firing rate of neuronal cells have been quantified recently [59]. The evaluation if gold nanoparticles can affect the normal function of neurons, namely their activity and coding properties have been reported recently [60]. For this purpose star-shaped gold nanoparticles of 180 nm average size were synthesized. The authors applied the nanoparticles to acute mouse hippocampal slices while recording the action potentials from single neurons in the CA3 region. The results showed that CA3 hippocampal neurons increased their firing rate by 17 % after the application of gold nanostars. The increase in excitability lasted for as much as 50 min after a transient 5-min application of the nanoparticles. Further analyses of the action potential shape and computational modeling suggested that nanoparticles block potassium channels responsible for the repolarization of the action potentials, thus allowing the cell to increase its firing rate. GNS affected the coding properties of neurons by modifying their excitability.

In the cited in previous subchapter paper published in 2015 it was stated that GNS with the sizes less than 100 nm can accumulate selectively in tumor via well-known enhanced permeability and retention effect, which is due the increased leakiness of blood vasculature in tumors [33]. Therefore, it was found that 70 nm GNS can permeate into the tumor interstitial space but only in close vicinity to tumor vessels 3 h after intravenous injection [33]. Smaller nanoparticles or longer incubation time can further increase the tumor accumulation or extravasation depth [33].

Nanoparticles with one half formed of gold branches and the other of silicon oxide were designed [61]. The oxide face would be used to join the gold nanostars to specific biological receptors that would take them to the damaged cells and the metal part can exercise its therapeutic or diagnostic function.

In this chapter it has been demonstrated that GNS are suitable agents to be monitored in vivo by applying of various microscope approaches. Moreover, it has been briefly discussed the interaction of GNS with cells as this point is considered to be vitally important for successful biomedical application.

References

1. Shenoy D et al (2006) Surface functionalization of gold nanoparticles using hetero-bifunctional poly(ethylene glycol) spacer for intracellular tracking and delivery and delivery. Int J Nanomed 1(1):51–57
2. Torchilin VP, Lukyanov AN (2003) Peptide and protein drug discovery to and into tumors: challenges and solutions. Drug Discov Today 8:259–266
3. Marshall E (2000) Gene therapy on trial. Science 288:951–957
4. Nishikawa M, Hashida M (2002) Nonviral approaches satisfying various requirements for effective in vivo gene therapy. Biol Pharm Bull 25:275–283
5. Kaneda Y (2004) Biological barriers to gene transfer. In: Amiji MM (ed) Polymeric gene delivery: principles and applications. CRC Press, Boca Ranton, FL, pp 29–41
6. Huefner A et al (2014) Gold nanoparticles explore cells: cellular uptake and their use as intracellular probes. Methods 68(2):354–363. doi:10.1016/j.ymeth.2014.02.006
7. Panariti A, Miserocchi G, Rivolta I (2012) The effect of nanoparticles uptake on cellular behavior: disrupting or enabling functions? Nanotechnol Sci Appl 5:87–100
8. Tkachenko AG et al (2004) Cellular trajectories of peptide-modified gold particle complexes: comparison of nuclear localization signals and peptide transduction domains. Bioconjugate Chem 15:482–490
9. Vale RD (2003) The molecular motor toolbox for intracellular transport. Cell 112:467–480
10. Levi V, Gratton E (2007) Exploring dynamics in living cells by tracking single particles. Cell Biochem Biophys 48:1–15
11. Dykman LE, Khlebtsov NG (2014) Uptake of engineered gold nanoparticles into mammalian cells. Chem Rev 114:1258–1288
12. Rong G et al (2008) Resolving sub-diffraction limit encounters in nanoparticles tracking using live cells plasmon coupling microscopy. Nano Lett 8:3386–3393
13. Gelles J, Schnapp BJ, Sheetz MP (1988) Tracking kinesin-driven movements with nanometre-scale precision. Nature 331:450–453
14. Nan XL, Sims PA, Xie XS (2008) Organelle tracking in a living cell with microsecond resolution and nanometer precision. Chem Phys Chem 9:707–712
15. Ricles LM et al (2014) A dual gold nanoparticles system for mesenchymal stem cell tracking. J Mater Chem B 2:8220–8230
16. Yuan H et al (2012) Gold nanostars: surfactant-free synthesis, 3D modelling, and two-photon photoluminescence imaging. Nanotechnology 23:075102
17. Wang DS, Hsu FY, Lin CW (2009) Surface plasmons effects on two photon luminescence of gold nanorods. Opt Express 17:11350–11359
18. Pollnau M et al (2000) Power dependence of upconversion luminescence in lanthanide and transition-metal-ion systems. Phys Rev B 61:3337–3346
19. Huang X et al (2010) A reexamination of active and passive tumor targeting by using rod-shaped gold nanocrystals and covalently conjugated peptide ligands. ACS Nano 4:5887–5896
20. Wang H et al (2005) In vitro and in vivo two-photon luminescence imaging of single gold nanorods. Proc Natl Acad Sci U S A 102:15752–15756
21. Li W et al (2014) *In vivo* quantitative photoacoustic microscopy of gold nanostars kinetics in mouse organs. Biomed Opt Express 5:2679–2685
22. Lee CH et al (2009) Near-infrared mesoporous silica nanoparticles for optical imaging: characterization and in vivo distribution. Adv Funct Mater 19:7688–7693
23. Ye S et al (2012) Label-free imaging of zebrafish larvae in vivo by photoacoustic microscopy. Biomed Opt Express 3:360–365
24. Nie L et al (2014) Plasmonic nanostars: in vivo volumetric photoacoustic molecular angiography and therapeutic monitoring with targeted plasmonic nanostars. Small 10:1585–1593
25. Yang L et al (2013) Quintuple-modality (SERS-MRI-CT-TPL-PTT) plasmonic nanoprobe for theranostics. Nanoscale 5:12126

26. Amie S et al (2007) Gd-loaded liposomes as T1, susceptibility, and CEST agents, all in one. J Am Chem Soc 129:2430–2431
27. Kim C et al (2011) In vivo photoacoustic mapping of lymphatic systems with plasmon-resonant nanostars. J Mater Chem 21:2841–2844
28. Raghavan V et al (2014) Gold nanosensitisers for multimodal optical diagnostic imaging and therapy of cancer. J Nanomed Nanotechnol 5:238
29. Wei Q et al (2009) Gyromagnetic imaging: dynamic optical contrast using gold nanostars with magnetic cores. J Am Chem Soc 131:9728–9734
30. Yguerabide J, Yguerabide EE (1998) Light scattering submicroscopic particles as highly fluorescent analogs and their use as tracer labels in clinical and biological applications: I. Theory. Anal Biochem 262:137–156
31. Chen H et al (2013) Multifunctional gold nanostar conjugates for tumor imaging and combined photothermal and chemo-therapy. Theranostics 3:633–649
32. Yuan H et al (2012) TAT-peptide functionalized gold nanostars: enhanced intracellular delivery and efficient NIR photothermal therapy using ultralow irradiance. J Am Chem Soc 134:11358–11361
33. Liu Y et al (2015) Plasmonic gold nanostars for multi-modality sensing and diagnostics. Sensors 15:3706–3720
34. Gao ZB, Zhang LN, Sun YJ (2012) Nanotechnology applied to overcome tumor drug resistance. J Control Release 162:45–55
35. Yuan H et al (2013) Plasmonic nanoprobes for intracellular sensing and imaging. Anal Bional Chem 405:6165–6180
36. Navarro JR et al (2012) Synthesis of PEGylated gold nanostars and pyramids for intracellular uptake. Nanotechnology 23:465602
37. Nergiz SZ et al (2014) Multifunctional hybrid nanoparticles of graphene oxide and gold nanostars for ultraefficient photothermal cancer therapy. Appl Mater Interfaces 6: 16395–16402
38. Dam DHM et al (2014) Grafting aptamers onto gold nanostars increases in vitro efficacy in a wide range of cancer cell types. Mol Pharm 11:580–587
39. Zhao F et al (2011) Cellular uptake, intracellular trafficking, and cytotoxicity of nanomaterials. Small 7:1322–1337
40. Lewinski N, Colvin V, Drezek R (2008) Cytotoxicity of nanoparticles. Small 4:26–49
41. Coradeghini R et al (2013) Size-dependent toxicity and cell interaction mechanism of gold nanoparticles on mouse fibroblasts. Toxicol Lett 217:205–216
42. Liu X et al (2013) Surface and size effects on cell interaction of gold nanoparticles with both phagocytic and nonphagocytic cells. Langmuir 29:9138–9148
43. Duan X, Yaping L (2013) Physicochemical characteristics of nanoparticles affect circulation, biodistribution, cellular internalization, and trafficking. Small 9:9–10
44. Chithrani DB, Ghazani AA, Chan W (2006) Determining the size and shape of gold nanoparticles uptake into mammalian cells. Nano Lett 6:662–668
45. Dam DH et al (2012) Direct observation of nanoparticles-cancer cell nucleus interactions. ACS Nano 6:3318–3326
46. Zink D et al (2004) Nuclear structure in cancer cells. Nat Rev Cancer 4:677–687
47. Schwartz GK, Shah MA (2005) Targeting the cell cycle: a new approach of cancer therapy. J Clin Oncol 23:9408–9421
48. Dam DH et al (2012) Shining light on nuclear-targeted therapy using gold nanostars constructs. Ther Deliv 3:1263–1267
49. Fulda S, Galluzzi L, Kroemer G (2010) Targeting mitochondria for cancer therapy. Nat Rev Drug Discov 9:447–464
50. Faustino RS et al (2007) Nuclear transport: target for therapy. Clin Pharmacol Ther 81:880–886
51. Dam DH, Lee RC, Odom TW (2014) Improved in vitro efficacy of gold nanoconstructs by increased loading of G-quadruplex aptamer. Nano Lett 14:2843–2848

52. Baginskiy I et al (2013) Chitosan-modified stable colloidal gold nanostars for the thermolysis of cancer cells. J Phys Chem 117:2396–2410
53. Wang L et al (2011) Selective targeting of gold nanorods at the mitochondria of cancer cells: implications for cancer therapy. Nano Lett 11:772–780
54. Wang S et al (2015) Reversibly extracellular pH controlled cellular uptake and photothermal therapy by PEGylated mixed-charged gold nanostars. Small 11:1801–1810
55. Matiajevic E (ed) (2012) Fine particles in medicine and pharmacy. Springer, London
56. Xie N, Lin Y, Mazo M, Chiappini C et al (2014) Identification of intracellular gold nanoparticles using surface-enhanced Raman scattering. Nanoscale 6:12403–12407
57. Rodriguez-Lorenzo L et al (2011) Intracellular mapping with SERS-encoded gold nanostars. Intergr Biol 3:922–926
58. Cho EC et al (2010) The effects of size, shape and surface functional group of gold nanostructures on their adsorption and internalization by cells. Small 6:517–522
59. Kereselidze Z (2014) Interaction of gold nanostars with neuronal cells and single negative terahertz metamaterials with barium titanate resonators. Dissertation, The University of Texas at San Antonio
60. Salinas K et al (2014) Transient extracellular application of gold nanostars increases hippocampal neuronal activity. J Nanobiotechnol 14:31
61. Rodríguez-Fernández D et al (2014) A protecting group approach toward synthesis of Au–silica Janus nanostars. Chem Comm 50:79–81

Conclusions

Gold nanostars due to their unique optical properties and wide possibilities of surface functionalization are considered to be important issues for applications in diverse fields. This review briefly focuses on the main aspects connected with gold nanostars, namely their synthesis, functionalization, optical properties, and application. The emphasis has been done on the application of GNS for current and emerging needs of medicine, biology, and pharmacy. Moreover, properties of gold nanostars as contrast agents for in vivo imaging and interaction of GNS with cells are also discussed in this brief.

G. Chirico et al., *Gold Nanostars*, SpringerBriefs in Materials,
DOI 10.1007/978-3-319-20768-1

Index

G. Chirico et al., *Gold Nanostars*, SpringerBriefs in Materials,
DOI 10.1007/978-3-319-20768-1